

Optimization for Initial Design of Horizontal Axis Wind Turbines

DESIGN OF MECHANICAL SYSTEMS

MASTER THESIS

GROUP 1.121A

SPRING 2017



AALBORG UNIVERSITY

Title:

Optimization for Initial Design of
Horizontal Axis Wind Turbines

Project period:

DMS4, Spring semester 2017

Project group:

1.121A

Group members:

Halldór Albertsson
Daniel Molnar

Supervisor:

Erik Lund

Total number of pages:

109+24

Submission date:

2017-06-02

Synopsis:

This report introduces the development of a wind turbine blade optimizer tool, called BladeOpt, which is intended for early stage design of wind turbine blades. The optimizer tool is laying on the foundation of a tool called IMHAWT, developed by the authors as the previous semester project to analyse the Initial Modelling of Horizontal Axis Wind Turbines. In BladeOpt multi objective gradient based optimization algorithm is implemented and subjected to various constraints and bounds. The sensitivities for the gradient based optimization method are captured using forward difference and direct differentiation methods. The optimization is solved by using Sequential Linear Programming (SLP) algorithm. For the optimization studies a baseline turbine is defined based on published data on the National Renewable Energy Laboratory (NREL) 5MW wind turbine. 4 case studies are conducted with different aims and settings to present the capabilities of BladeOpt.

PREFACE

This master thesis is written by group 1.121A as documentation of the group work performed on the 4th semester of the master studies in 'Design of Mechanical Systems' under the Study Board of Industry and Global Business Development. This report is shaped in order to introduce the development of a wind turbine blade optimization tool, called BladeOpt. This tool aims to reduce the time of the initial modelling phase of the turbine blades. The project period was from 1st of February to the 2nd of June, and the work have been conducted under the supervision of Professor Erik Lund. The steps taken through the development of BladeOpt have been consulted with the Blades Department of Siemens Gamesa Renewable Energy, Aalborg.

The BladeOpt tool is a set of Matlab functions, capable of optimizing initial blade models with the aim of maximizing the annual energy production while minimizing the mass of the blade. In order to do that, a gradient based optimization algorithm is implemented, with several constraints both on design variables and response functions.

Attached to the report is an appendix. The appendix contains, the NREL wind turbine cross sectional properties in A; the validation of the cross sectional calculations in B; the BEM correction factors in C; additional information about the development of the beam finite elements in D; additional information about the baseline turbine used for the optimization case studies in E; cross sectional plot results from an optimization study F. The BladeOpt code and obtained study results can be found in an attached zip file.

References in the report are made using the Chicago method, meaning the authors of the reference along with the year the material is published are stated in the report in [..., XXX]. Additional information on the material is listed in the bibliography sorted by the last name of the first author.

We would like to thank our supervisor, Erik Lund for good counselling and the Blades Department of Siemens Gamesa Renewable Energy, Aalborg, for providing general feedbacks through the development of the code.

Abstract

Denne rapport introducerer et vindmølleoptimeringsværktøj kaldet BladeOpt, som er udviklet til indledende designstadier af vindmøllevinger. Optimeringsværktøjet bygger på værktøjet IMHAWT udviklet af forfatterne i forbindelse med et tidligere semesterprojekt til anvendelse ved 'Initial Modelling of Horizontal Axis Wind Turbines'. I BladeOpt er implementeret en multiobjektiv gradientbaseret optimeringsalgoritme underlagt forskellige restriktioner og grænser. Sensitiviteten af den gradientbaserede optimeringsmetode er bestemt ved brug af forward difference og direkte differentiationsmetoder. Optimeringen er udført ved brug af algoritmen; Sequential Linear Programming (SLP). Til optimeringsstudierne er en 5MW standardvindmølle defineret baseret på data udgivet af National Renewable Energy Laboratory (NREL). For at demonstrere BladeOpt's formåen er fire casestudier med forskellige målsætninger og indstillinger udført og dokumenteret.

CONTENTS

1	Introduction	1
1.1	Optimization	1
1.2	Scope of the Project	3
1.3	Summary of Previous Work	4
2	Definition of a Wind Turbine	7
2.1	General Definitions	7
2.2	Definition of NREL 5MW Wind Turbine	10
3	Optimization Problem Formulation	13
3.1	Objective Function	13
3.2	Annual Energy Production	14
3.3	Loads for structural analysis	24
3.4	Mass	25
3.5	Design Parametrization	27
3.6	Constraints	30
3.7	Design Variable Bounds	34
3.8	Safety Factors	34
3.9	Definition of the Optimization Problem	35
4	BEM	37
4.1	Blade Element Momentum Method Main Theory	37
4.2	Validation of Optimum Power Curve Computation	41
4.3	Validon of AEP Computation	42
5	Structural Analysis	45
5.1	Finite Element Analysis	45
5.2	Implementation of FEM calculations in BladeOpt	53
5.3	Validation of the FEM calculations	54
5.4	Validation of the analysis tool	59
6	Sensitivity Calculations	61
6.1	Design Sensitivity Analysis	61
6.2	Finite Difference Method	62
6.3	Discrete Approach	66

7	Optimization Scheme	73
7.1	Sequential Linear Programming	73
7.2	Implementation	78
8	Studies	81
8.1	Baseline Turbine	81
8.2	Design Variable Bounds	85
8.3	Case Study I.	87
8.4	Case Study II.	92
8.5	Case Study III.	95
8.6	Case Study IV.	98
9	Conclusion	103
10	Future Work	105

A	NREL 5 MW Wind Turbine	111
A.1	NREL Blade Cross Sectional Properties	111
B	Cross sectional Analyses	113
B.1	Cross sectional calculation	113
B.2	Cross sectional stiffness validation	115
C	BEM Corrections	119
C.1	BEM Correction Factors	119
D	FEM Formulations	123
D.1	Additional FEM formulation	123
E	Baseline turbine	129
E.1	Mass	129
E.2	Stiffness	129
E.3	Eigen Frequency	130
F	Cross sectional plots	131

CHAPTER 1

INTRODUCTION

The goal of this master project is to build an optimization algorithm with the capabilities of optimizing horizontal axis wind turbine (HAWT) blades with respect to both aerodynamic performance and structural integrity simultaneously, resulting in a fully automated initial design process for the blades. This is the second phase of a one year long project, the first phase took place on autumn semester 2016 where the HAWT analysis program IMHAWT was built. IMHAWT is an analysis tool capable of accurately computing both aerodynamic and structural responses of a HAWT for steady state conditions [Molnar and Albertsson, 2016]. Phase two is the next step in fully automating the initial design process by building an optimization algorithm on top of the foundation of IMHAWT.

This chapter consists of a quick introduction of optimization and how it is utilized for blade design, followed by defining the scope of the project and finally an overview of previous work from phase one.

1.1 Optimization

Engineers can expect to work with a great variety of tasks and one of them being design of systems. The system being designed will need to have a desired functional performance while at the same time fulfil a set of requirements and constraints.

An example of a mechanical system being designed is a high end road race bicycle. The frame of the bike will need to have all the standard functions like a seat tube for the seat post, a head tube for the front fork and a bottom bracket shell for the bottom bracket to name a few. Additionally will the frame need to be strong enough to withstand the expected use during the life time of the bike.

This can be achieved by a large variety of designs that will all fulfil the requirements of functional performance while at the same time lasting the lifetime of the product. For a high end race bike it is not enough to fulfil only the basic requirements as the bike market is a very competitive market. The user will require to have the bike as stiff as possible while at the same time being as lightweight as possible which is why all the high end bikes have high strength to weight ratio materials like carbon in the frame. Furthermore, there is a requirement that the bike frame has good aerodynamic performance such that the drag force on the frame will be as little as possible.

Designing a bike with those strict requirements requires a lot of engineering skills. The amount of design variables becomes enormous very fast as the engineer needs to design the layering of the carbon where it is needed to choose the number of layers and fibre orientation for every area of the frame while making sure that the geometry is aerodynamically efficient at the same time. Furthermore, computationally heavy methods are needed to perform analysis for each one of those designs to make sure that they fulfil the set of requirements. This process is very time consuming and it is not even certain that the best possible design has been achieved.

It can easily be seen that using intuition is not enough to make sure that the final design is the optimal design where all requirements are fulfilled while at the same time having the frame

as lightweight as possible and as aerodynamically efficient as it can be. This is where it is necessary to apply more advanced methods like optimization to efficiently solve the problem and stay competitive. In optimization the system is formulated such that a performance measure like aerodynamic efficiency and mass in this case is optimized while fulfilling all requirements at the same time.

The example above is very descriptive for highly competitive and advanced technology sectors like the car industry, the aerospace industry and the wind turbine industry.

In the wind turbine industry the design problem is almost the exact same one as in the bike frame example. The market expectations in the wind turbine industry are that new blade designs will outperform their legacy versions in terms of aerodynamic and structural design by providing more energy and simultaneously weighing and costing less. The tendency in the industry has been to launch longer and longer blades to produce as much energy as possible. The kinetic energy of the wind is defined as

$$P_{kin} = \frac{1}{2} \rho_{air} A V_0^3 \quad (1.1)$$

where P_{kin} is the kinetic energy of the wind, ρ_{air} is the density of the air and A is the swept area by the wind turbine blades while V_0 is the wind speed. The swept area of a turbine is the area swept by the blades, simply the area of a circle, $A = \pi R^2$, where R is the blade length. From the definition of the kinetic energy of the wind and the swept area of the turbine it can be seen why it is beneficial to increase the blade length as the power is proportional to the blade length squared, although, moving the turbine to a location with higher wind speed would be even more beneficial. Longer blades do have a downside though as the blade power specific cost, $(total\ blade\ cost)/P$ in $\$/MW$, has shown to be up to twice as much for a 70 m blade compared to a 30 m blade and the same goes for the blade cost share of the total turbine cost [Sandia, 2003]. Therefore is it increasingly important to make sure that aerodynamic performance and mass are the optimum for the design.

There are three main approaches that have been used in blade optimization. First is the approach of solely aerodynamic optimization by maximizing the aerodynamic efficiency of the blade [Maalawi and Badr, 2003] [Johansen et al., 2009]. This approach usually uses the Blade Element Momentum method (BEM) by Glauert to compute objective function values [Sørensen, 2016]. The second approach is a pure structural optimization that commonly uses the Finite Element Method (FEM) to obtain the objective function values. In this approach the outer shape is usually constrained by a predefined geometry that satisfies the wanted aerodynamic performance [Domnica et al., 2016] [Cai et al., 2012].

Both of the previously mentioned approaches are limited as they only consider one part of the design in the optimization scheme and do therefore allow very limited solution space. Utilizing the first two methods iteratively in blade design to find an acceptable design can be a tedious and time consuming process, thus there is an obvious advantage to be able to fully couple the first two methods in a single optimization scheme. The third and final approach improves the drawbacks of the first two methods as it includes both the aerodynamic performance and mass in the objective function and the optimized solution can be therefore the optimum compromise between the two while fulfilling the design constraints [Zhu et al., 2017] [NREL, 2010]. This third and final approach relates to the aim of this project to fully automate the initial blade design process as will be further discussed in next section.

1.2 Scope of the Project

This project takes on today's challenge of blade design, where continuous improvements of blade performance is expected by the industry. New turbines should be capable of providing more annual energy production (AEP) than its predecessors while weighing and costing less. Furthermore, the wind energy market is in a rapid growth as is clearly seen by the fact that the global annual installed wind capacity today is ten times more than in 2000 [GWEC, 2017]. Those high performance expectations together with rapid market growth put pressure on the blade manufacturers to bring better products to the market at faster pace than before. This leads to the goal of this project of automating the initial design process of the blades to shorten the time to market for high performance blades.

The initial design process or preliminary design process is the process of defining the overall system before detailed design begins. In the aerodynamic design of the blade this includes designing the blade so that the loads on the blade and the power output of the blade can be accurately predicted for the operational range of the turbine. In the structural design of the blade this includes defining the structural parameters to a level where the overall structural behaviour is captured. The preliminary design should have material, and mass distribution defined so that tip deflection and eigenfrequencies are accurately captured while simultaneously fulfilling strength requirements of the blade. Taking this initial design to the next level consists of detailed design and should not involve change in mass of the blade or overall stiffness of the blade. The detailed design process includes among other things the work of defining the laminate layup for every area of the blade, eliminate localized stress concentration and prevent localized buckling.

The first phase of this project dealt with building a program capable of accurately analyse both aerodynamic and structural steady state responses of HAWT. The final result of first phase was the HAWT analysis program IMHAWT that is described in further detail in section 1.3.

This second phase of the project deals with building an optimization scheme on the foundation of IMHAWT, where both aerodynamic and structural performance measures are included in the objective function and concurrently optimized. The blade model should be parametrized such that key parameters in the blade performance can be implemented as design variables in the optimization. Key parameters to be included are:

- Blade length
- Chord length
- Blade twist
- Inner geometry of the blade
- Positioning of airfoils

These parameters can directly be used as design variables or indirectly through other parameters in the model. Other convenient parameters can likewise be used if they can improve the outcome from the optimization.

Additionally, the program should be coded such it can handle different compositions of mass and aerodynamic performance in the objective function.

Furthermore, the program should be able to handle a set of both equality and inequality constraints on all of the most important aerodynamic and structural blade responses as well as on the design variables. The constraints can be implemented both to improve the performance or to guide the design in a wanted direction. It should be possible to activate the following constraints in the program:

- Tip displacement
- Ultimate and fatigue strains
- Structural eigenfrequencies
- Tip speed
- Design variables constraints

This is not a complete list of constraints as other constraints can be added if it helps stabilizing the optimization or improving the results. Finally, the optimization should have fast execution time.

The turbine being used for validation of the control, aerodynamic and structural calculations is the NREL 5MW wind turbine. This turbine was designed as an baseline turbine to support research in the field so the turbine design and steady state analysis of the turbine is publicly available [Jonkman et al., 2005]. The turbine is a modern three bladed horizontal axis wind turbine with 63 m long blades and rated for 5 MW power output. Based on the NREL 5MW turbine a baseline blade design is obtained and used as initial guess for the presented optimization case studies.

The NREL 5 MW was also used for validation in phase one of the project, the results from that validation along with summary of the previous work from phase one is outlined in the proceeding section.

1.3 Summary of Previous Work

In this section the previous work from phase one of the project is summarized. The main theories used for the computation along with simplifications and assumptions being made are outlined along with validation of the program. All of the work that is presented in this section is documented in detail by Molnar and Albertsson [2016].

The first phase, of the ultimate goal of the project to automate the initial design phase of HAWT, addressed the task of developing a software capable of computing the steady state responses of HAWT by coupling aerodynamic, load and structural computation using relatively simple models.

For the computation of the aerodynamic responses the Beam Element Momentum (BEM) method was implemented. The output of the BEM method is the power output of the turbine and the aerodynamic load that is then applied onto the blade in the structural model. The main theory and equations of the BEM method is described in more detailed in section 4.1.

The BEM method is limited to steady state flow and does not take any 3D effects of vortex systems in the wake into account. Hence correction factors were implemented. The three main correction factors implemented in the program are the following:

- Tip loss correction
- hub loss correction
- Correction for highly loaded rotors

Additional information about the correction factors can be found in appendix chapter C.1.

The wind field applied to the BEM model is a highly simplified version of real wind conditions. In reality the wind speed depends on height above ground, terrain roughness and other parameters as well as being turbulent on top of that. In IMHAWT the wind speed is simplified as uniform and steady wind field with constant magnitude and direction.

Discretized Bernoulli-Euler beam model was implemented in the program to compute the displacements and eigenfrequencies of the blade. The displacements are computed with an algorithm, presented by Hansen [2008], that loops through all of the discrete points computing the displacement in one point at a time.

To compute eigenfrequencies of the blade the matrix iteration method was implemented. First the mode shape and eigenfrequency are simultaneously computed for the lowest eigenfrequency, where the mode shapes are computed by utilizing the previously mentioned displacement computation algorithm. It is then assumed that the eigenfrequencies are distinct, well separated and that the eigenvectors are linearly independent. Using those assumptions the effect of the first eigenmode is subtracted from the solution space such that the solution converges to the second lowest natural frequency. The main advantage of this method is that both mode shape and eigenfrequency is simultaneously computed and the number of eigenfrequencies computed is purely up to how many needs.

In phase two of the project the aforementioned iterative structural computations are reformulated to utilize the Finite Element Method (FEM) and achieve more computational efficiency in the optimization. The computational efficiency gained by changing to FEM arises from the more efficient method of obtaining gradients as information can be reused from the analyses as is described in section 6.3. The FEM formulations are described in detail in chapter 5.

The blade cross sections are build up to imitate a real blade cross section as closely as possible by including building blocks with simple shapes that represent every component of a real cross section and make cross sectional calculations quick and simple. The outer shape of the airfoil is represented by an ellipse, furthermore, reinforcement squares are on both vertices and both co-vertices of the ellipse and finally is a shear web that connects the reinforcements on the co-vertices. The ellipse is defined by two parameters and the inner geometry of the cross section by eight parameters.

The anisotropic and orientation dependent composite materials used in the building blocks of the cross sections are limited to symmetric, balanced laminates. By setting those limitations, the laminate equivalent Young's modulus becomes thickness independent and the material is then assumed to be homogeneous and linear elastic in the spanwise blade direction and having the laminate equivalent elastic modulus. The material parameters are obtained using ESAComp material database.

Extensive validation has been performed on all of the different functions of IMHAWT. Starting with validation of tip deflection and eigenfrequencies using prismatic cantilever beam with constant material properties for both cases and additionally a uniformly distributed load for the tip deflection validation. Analytical solutions were used as baseline in both cases. The results converge to the analytical solutions with increased number of discrete points in the model. The validation of the FEM code developed during phase two is validated against a more complex Ansys model using non-prismatic beam and non-uniform load as is described in section 5.3.

To validate the computation of cross sectional stiffnesses in IMHAWT the results were compared to the advanced cross sectional analysis tool BECAS which is based on the following theory [Blasques and Stolpe, 2012], [Blasques, 2014], [Blasques and Bitsche, 2014], [Blasques et al., 2014] and [Bitsche, 2014]. The stiffness computations in IMHAWT had little to none deviation from BECAS when comparing stiffnesses of identical models. The cross sectional calculations and tables that summaries the cross sectional validation from phase one can be seen in appendix B.2.

Final validation of IMHAWT consists of a steady state response comparison with published data on the NREL 5 MW baseline turbine [Jonkman et al., 2005]. The power computation showed great correlation for most of the operational range of the turbine, still there was a small range with a deviation up to 8.8 %. Furthermore, the thrust of the turbine shows a good correlation for the whole operational range of the turbine. Moreover, out of plane and in plane tip deflection show good correlation except for increased deviation in the exact same regions as the power showed deviation. This deflection deviation is believed to be purely related to the power deviation. The deviation in power is believed to be caused by the fact that the published NREL results are obtained by more advanced model with additional correction factors than implemented in IMHAWT [Moriarty and Hansen, 2005]. Finally, eigenfrequencies of the blade are compared to the published data from NREL as well as to a replicate of the NREL 5 MW from Sandia [Resor, 2013]. The deviation from the Sandia blade was between 0-2.2% and between 2-5% for the NREL blade for the first three eigenfrequencies. Those results are as expected since the Sandia blade is modelled as cantilever beam like in IMHAWT while NREL analysis the whole turbine including the tower.

The conclusion of the phase work was that IMHAWT is capable of capturing the overall physics related to the aerodynamic performance, loads and structural response of wind turbine blade while having fast execution time.

This section concludes the summary of previous work.

CHAPTER 2

DEFINITION OF A WIND TURBINE

The aim of this chapter is to briefly introduce the general terms and phrases, that are used to describe a horizontal axis wind turbine and its operational conditions in this report, moreover to present the NREL 5MW wind turbine that has been used for validations and modified to be a baseline turbine for the optimization studies. In figure 2.1 a general three blade horizontal axis wind turbine (HAWT) is presented.

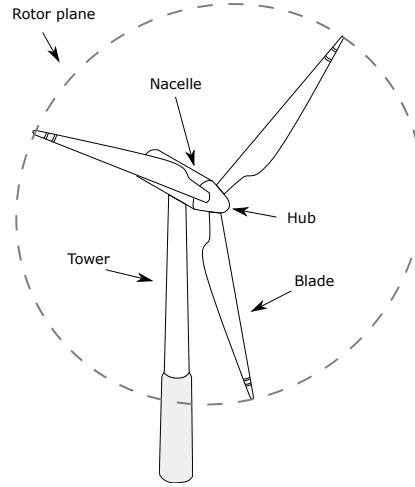


Figure 2.1: *A three blade HAWT*

2.1 General Definitions

Wind turbines extract the kinetic energy from the wind and convert it into electrical energy. As the wind passes the turbine, axial and tangential forces are generated on the blade. The tangential forces act in the plane while the axial forces act out of plane of the rotor. In figure 2.2 a general aerodynamic load distribution on a blade can be seen in the tangential direction.

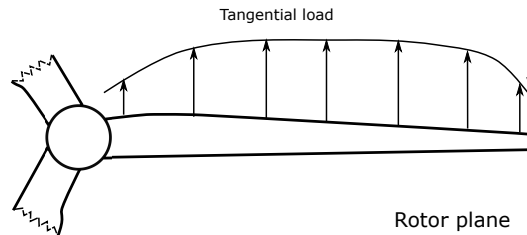


Figure 2.2: *General aerodynamic load on a wind turbine blade*

These forces create high in plane and out of plane bending moments on the blade. To utilize the in plane bending moments, the blades are connected to the rotating main shaft of the turbine through the hub of the turbine. Within the hub the control mechanism of the blades

can be implemented, depending on the control of the blades. The hub and the blades together are called the rotor of the wind turbine. The main shaft is usually connected to a gearbox within the nacelle, which is linked to a generator. In case of direct drive the main shaft is directly joined to the generator. The generator transform the mechanical energy from the shaft into electrical energy. The nacelle houses the gearing mechanism and the generator as well as connecting the rotor to the tower. The tower connecting the nacelle to the foundation of the turbine.

Wind turbines can operate in different operational conditions. The wind speed where the turbine starts to generate electricity is called cut-in wind speed and the corresponding rotational speed is called cut-in rotational speed. Together they define the cut-in conditions of the wind turbine. The wind turbines are designed for a certain rated power output. The wind speed and rotational speed where the rated power output is reached, are called rated wind and rated rotational speed, respectively. Together they define the rated conditions of the wind turbine. The cut-out conditions are defined as the wind speed and rotational speed where the wind turbine stops to produce energy. At cut out conditions, due to safety reasons, the wind turbine blades are rotated out of the wind direction, hence reducing the aerodynamic loads on the blades. To regulate the operation of the wind turbine between cut-in, rated and cut-out conditions, the turbine needs to be controlled. There are different control methods for wind turbines, one for example is called pitch control. For this regulation the blades are connected to actuators within the hub, hence they can be turned, "pitched" around their longitudinal axes, see figure 2.3. The angle of this rotation is called pitch angle.

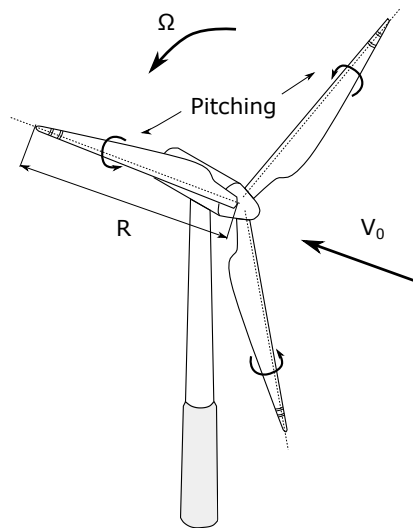


Figure 2.3: *General HAWT with parameters*

The total amount of the wind kinetic energy defined by (1.1) can not be utilized by a wind turbine, since it would mean that the speed of the wind behind the turbine would be reduced down to zero. The power output of a wind turbine can be obtained by multiplying (1.1) with a power coefficient factor C_p . C_p is defined as power produced by a wind turbine divided by the kinetic energy of the wind. The maximum value of C_p is defined as the Betz limit $\approx 59\%$. Assuming maximum efficiency and constant wind speed, only the swept area of the blades can be increased to achieve raise in the power output. The power output of the wind turbine

increases quadratically with the blade length. Increasing blade length results in a rise of the loads on the blade. Loads on a blade can be generated by aerodynamic, gravitational and inertial effects. These loads vary in time, with a frequency corresponding to the rotational speed of the rotor Ω [Hansen, 2008].

The wind turbine blades are long and slender structures, which outer geometries are designed to be aerodynamically efficient and sufficiently strong to withstand the loads generated by different load sources. A wind turbine blade outer geometry can be defined by twist and chord parameters and the type and location of the corresponding airfoils. A sketch of a wind turbine blade can be seen in figure 2.4. The coordinate system defined in figure 2.4 is referred to as global coordinate system of the blade through this report.

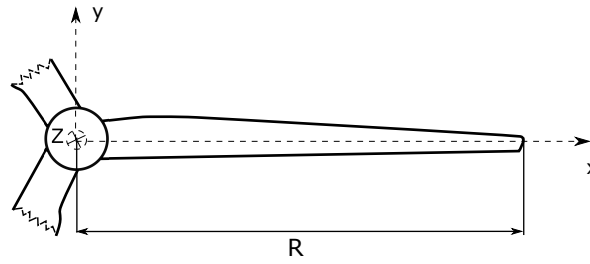


Figure 2.4: Sketch of a wind turbine blade with global coordinate system

An airfoil can be defined as a section of the blade, see figure 2.5(a). As flow passing an airfoil, interaction arises between the flow and the surface of the airfoil causing higher pressure on the pressure side of the blade, while lower on the suction side of the blade. The pressure difference generates forces on the outer structure of the airfoil. The point where the wind first interact with the airfoil is called leading edge, while the last point is defined as trailing edge. An airfoil can be described by its thickness/chord (t/c) ratio, where the chord is defined as the length of a straight line between the leading and trailing edge. The thickness/chord ratio is referred to as *ratio* through this thesis. Airfoils can have different sizes and shapes, the thinner airfoils outperform the thicker airfoils in aerodynamic performance, while the opposite of this is true for the structural performance.

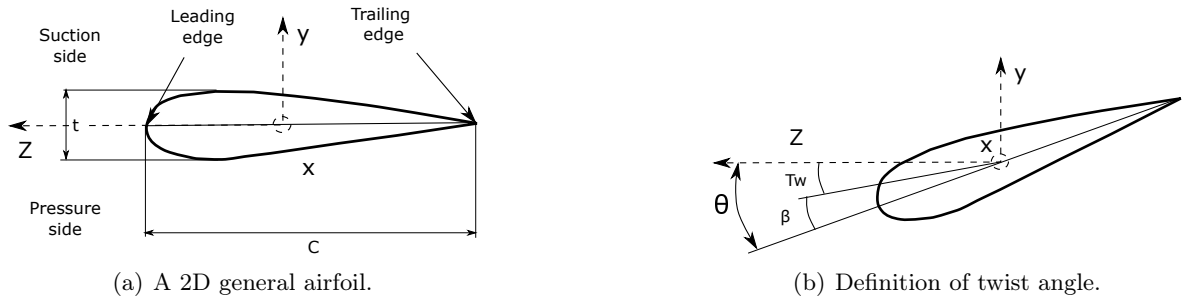


Figure 2.5: General airfoil definitions

For purely aerodynamic reasons the blades are usually twisted along their length. The twist, Tw of an airfoil is defined as the angle between the global coordinate system and the chord. In case the blade is pitched the local pitch angle θ can be defined by adding the twist Tw and

the pitch β angles, see in figure 2.5(b).

It is necessary to define directions within a cross section, to describe loads and moments. In this study flapwise and edgewise load and moment directions are defined in figure 2.6.

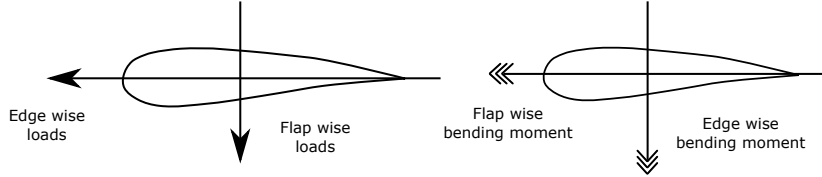


Figure 2.6: *Flapwise and edgewise directions*

The strains generated by the flapwise loads and moments are called flapwise strains, while the strains that generated by the edgewise loads and moment are called edgewise strains in the following.

The blade can be divided into different regions. In this report three regions are defined along the blade, see in figure 2.7. The first region is defined from the root of the blade, until the first non circular cross section. The second region is defined from the end of the root region until the first thinnest type of airfoil. The third region is defined from the end of the middle region until the tip of the blade. In the following these regions are referred to as root region, middle region and tip region, respectively.

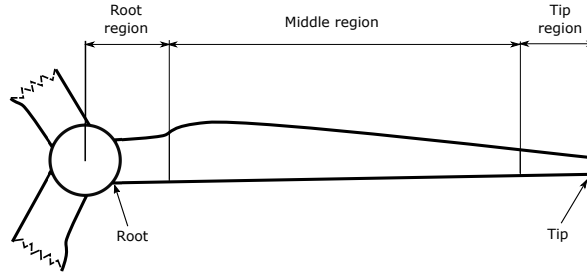


Figure 2.7: *Regions of the blade*

2.2 Definition of NREL 5MW Wind Turbine

The National Renewable Energy Laboratory has been developed a 5MW wind turbine based on available data from the wind turbine manufacturers. The turbine is a conventional three-bladed turbine and it is widely used as an input to present the capabilities of wind turbine optimization and design tools. The developed wind turbine is documented in Jonkman et al. [2005]. The general properties of the NREL 5MW wind turbine are summarized in table 2.1.

The outer geometry of the NREL 5MW turbine blade, in the following referred to as NREL blade, is defined with 17 airfoil data. The chord, twist and shape distribution of the NREL blade is presented in table 2.2.

2.2. DEFINITION OF NREL 5MW WIND TURBINE

Rated Power Output	5 MW
Rotor Diameter, Blade Length	126 m, 61.5 m
Cut-In, Rated, Cut-out Wind Speed	3 m/s, 11.4 m/s, 25 m/s
Cut-In, Rated Rotor Speed	6.9 rpm, 12.1 rpm
Pitch at Cut-In Conditions, at Rated Conditions	0°, 0°

Table 2.1: *General Properties of the NREL 5MW [Jonkman et al., 2005]*

Rotor radius (m)	Twist (°)	Chord (m)	Ratio (%)
2.87	13.308	3.542	100
5.60	13.308	3.854	100
8.33	13.308	4.167	100
11.75	13.308	4.557	40.5
15.85	11.480	4.652	35.09
19.95	10.162	4.458	35.09
24.05	9.011	4.249	30
28.15	7.795	4.007	25
32.25	6.544	3.748	25
36.35	5.361	3.502	21
40.45	4.188	3.256	21
44.55	3.125	3.010	18
48.65	2.319	2.764	18
52.75	1.526	2.518	18
56.17	0.863	2.313	18
58.90	0.370	2.086	18
61.63	0.106	1.419	18

Table 2.2: *Aerodynamic definition of NREL blade [Jonkman et al., 2005]*

In the root region of the NREL blade the shape of the airfoils is circular, the (t/c) ratio is 100 %. The mid region of the blade starts at 11.75 meter rotor radius, in the mid region the (t/c) ratio decreases from 40% to 18%. The tip region of the blade starts at 44.55 meter with airfoil ratio 18 %. In Jonkman et al. [2005] the structural properties of the NREL blade are defined through the distributed cross sectional properties in 49 cross section, which can be found in appendix A. In this report the NREL 5MW wind turbine is used for validation of different control strategies in chapter 4 and aerodynamic and structural calculations in chapter 5. Moreover, a modification of the NREL blade design is used as a baseline design for the optimization studies in chapter 8.

CHAPTER 3

OPTIMIZATION PROBLEM FORMULATION

The blade optimization problem is formulated by defining the objective function, the design parameters and the constraints. In this chapter the aforementioned topics will be further discussed, elaborating on the different possibilities and introducing the approaches taken during the development of the BladeOpt.

3.1 Objective Function

As a first step of the optimization process, the objective function needs to be defined. Several studies have been conducted to optimize wind turbines according to different optimization objectives, however, there is still not a full agreement on what can be considered as optimum design. A tendency in the wind turbine industry is to focus the developments on the reduction of the levelized cost of energy produced by a wind turbine. In wind turbine aerodynamic theory e.g. Hansen [2008] and Sørensen [2016], it is suggested to choose every variable throughout the design process to maximize the rotor power coefficient C_p . This leads to the assumption, that the most aerodynamically efficient rotor is the optimal rotor [James and Seamus, 2015]. An aerodynamically optimized turbine works at maximum efficiency for certain operational conditions. Thus, to increase the power output of a turbine at maximum efficiency the length of the blades needs to be increased. There is considerable uncertainty in the industry whether larger wind turbines will truly reduce the cost of energy [Sieros et al., 2012].

In fact, to achieve the reduction of the levelized cost of energy, the annual energy production of a wind turbine needs to be maximized, while the annual cost of the turbine needs to be kept as low as it is possible. The annual cost of the turbine can be obtained by considering the total cost of installation, operation and maintenance divided by the operation time. The capital cost i.e fixed one time cost, for an offshore turbine is around double the cost of an onshore turbine, where the turbine itself is still today the biggest part of a project owner's investment decision [Harman, 2013]. In case of an onshore turbine the turbine itself accounts for 65-84% of the capital cost but 30-50% for an offshore turbine, this difference arises from increased transportation and installation cost share for the offshore turbines [IRENA, 2012]. According to Krohn et al. [2009], around 20% of the turbine cost itself for a three bladed wind turbine is related to the cost of the blades. The cost of one blade is proportional to the amount of material used for the manufacturing.

As it can be seen, the optimization of wind turbines is a multi-discipline problem, where energy production, cost and mass are all important measures. By minimizing mass, cost is taken into account to a certain level as less weight reduces manufacturing cost, installation cost and maintenance cost. In this study, the aim of the optimization is to maximize AEP , while keeping the mass of the blade as low as possible and fulfilling several structural constraints. Hence, the objective is built from the AEP and the mass of the blade.

3.2 Annual Energy Production

When estimating the annual energy production of a wind turbine at a given location there are two main ingredients that are needed, those are the wind conditions at the location and the power that the turbine produces in those wind conditions. The wind conditions are usually described by a probability density function, $f(V)$, as a function of the wind, V , for the given location. A probability density function is a function that describes the probability of an wind speed to occur in that location. Weibull distribution is the most widely used function and is described in more details in subsection 3.2.1.

Having the before mentioned information the mean power production can be computed by integrating the product of the power, $P(V)$, and the probability density function, $f(V)$, as

$$\bar{P} = \int_0^{\infty} P(V) \cdot f(V) dV \quad (3.1)$$

Multiplying the mean power by the hours in a year gives the annual energy production in watt-hours per year. Computation of the AEP is most often done by numerical methods where the power curve is defined by the power computed at discrete wind speeds within the turbines operational range and the AEP is computed as the summation of the power contribution from each wind interval using (3.2).

Discretisation of the power curve does obviously effect the accuracy of the results, fine discretisation provides more accurate results but with the cost of higher computational power. Typical interval size for AEP computation is 1 m/s [Hansen, 2008]. AEP is computed as

$$AEP = \sum_{i=1}^{N-1} \frac{1}{2} (P(V_{i+1}) + P(V_i)) \cdot f(V_i < V_0 < V_{i+1}) \cdot (24 \cdot 365) \quad [Wh/year] \quad (3.2)$$

where N is the number of discrete wind speeds used for the computation, P_i is the power for a given wind speed and $f(V_i < V_0 < V_{i+1})$ is the probability of a wind speed V_0 occurring in the wind speed range V_i to V_{i+1} .

Figure 3.1 shows graphical representation of wind conditions, presented with probability density function and a power curve. The columns show the intervals that are used for the AEP computation and how the power within each interval is treated as the average of the interval end points when computing the AEP.

3.2.1 Weibull distributions for wind speed

The Weibull distribution is a probability density function that is capable of accurately representing wind speed measurements at wide diversity of meteorological stations as has been shown in the European Wind Atlas [Troen and Petersen, 1989]. It is a two parameter function defined as

$$f(V) = \frac{k}{A} \left(\frac{V}{A} \right)^{k-1} \exp \left(- \left(\frac{V}{A} \right)^k \right) \quad (3.3)$$

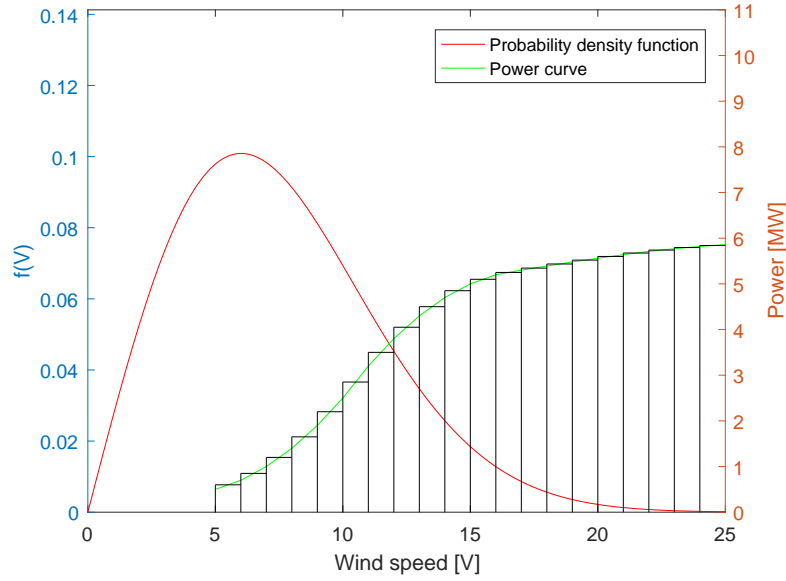
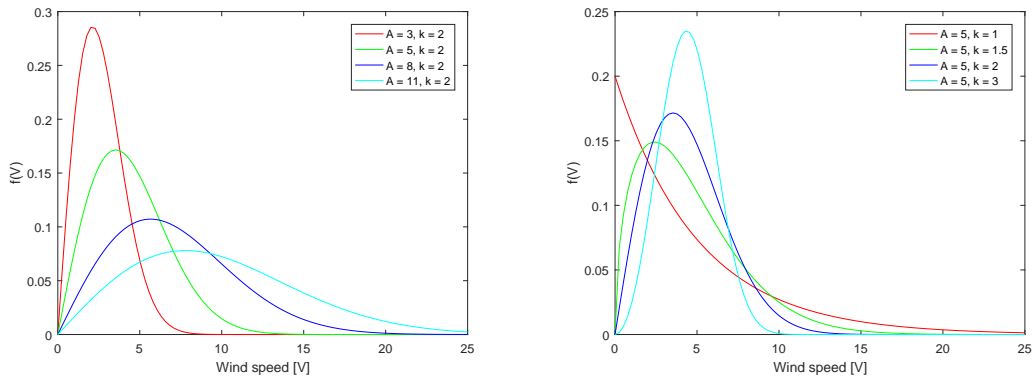


Figure 3.1: Probability density function and power curve for AEP computation

where $f(V)$ is the frequency of the occurrence of the wind speed V , A is a so called scale parameter and k is the shape parameter. The effects on the distribution when altering the shape factor, A , can be seen in figure 3.2(a) and the effects from altering the scale factor can be seen in figure 3.2(b).



(a) Weibull distribution for various scale factors. (b) Weibull distribution for various shape factors.

Figure 3.2: Weibull distributions with varying scale and shape factors

The shape factor has two specific distributions, that is an exponential distribution when $k = 1$ and Rayleigh distribution when $k = 2$. Rayleigh distribution is a one parameter function, since k is fixed at 2, that is sometimes used to describe wind data but not as widely used as Weibull.

It is helpful for one to be able to compute the average wind speed and most frequent wind

speed of the distribution, to get a better feeling of what the Weibull distribution is describing. The mean and modal values of a Weibull distributed wind data can be obtained by (3.4) and (3.5) respectively.

$$\bar{V} = A\Gamma\left(1 + \frac{1}{k}\right) \quad (3.4)$$

$$Mode(V) = A\left(\frac{k-1}{k}\right)^{\frac{1}{k}} \quad (3.5)$$

where A and k are the previously mentioned scale and shape factors and Γ is the gamma function.

When computing AEP it is necessary to know the cumulative probability of a wind speed range. The cumulative probability that the wind is above a given wind speed can be found as

$$F(V) = \exp\left(-\left(\frac{V}{A}\right)^k\right) \quad (3.6)$$

Computing the *AEP* by (3.2) requires the cumulative probability for each wind speed range. Using (3.6), the cumulative probability for a wind speed range is found by subtracting the cumulative probability of the higher wind speed from the lower wind speed in the range as

$$f(V_i < V_0 < V_{i+1}) = \exp\left(-\left(\frac{V_i}{A}\right)^k\right) - \exp\left(-\left(\frac{V_{i+1}}{A}\right)^k\right) \quad (3.7)$$

It is important to have reliable scale and shape factors when using the Weibull function to accurately estimate the energy resource of a location. The European Wind Atlas is a valuable tool to obtain reliable Weibull factors for wind resource estimations, the Atlas was published for The Commission of the European Communities to give a boost to the European wind energy sector [Troen and Petersen, 1989].

The European Wind Atlas uses data from 208 meteorological stations around Europe to provide regional wind climatologies. Furthermore, the Atlas provides methods to utilize the regional wind climatologies along with localized information like surface roughness and terrain for the specific site to obtain site specific wind climate to estimate the wind resource.

3.2.2 Power Curve Computation

The power that a wind turbine delivers during operation is a function of the blade design, blade pitch, wind speed and rotational speed of the rotor. That means that when the blade design has been decided then the power is only a function of the turbine controls and wind conditions.

As the wind conditions can not be controlled it is a matter of turbine controls to obtain the desired power for the given wind conditions. The ways of controlling a turbine to achieve the desired power output are a combination of varying or fixing rotor speed and pitch, that gives the following four combinations of controls.

- Fixed rotor speed - fixed pitch
- Variable rotor speed - fixed pitch
- Fixed rotor speed - variable pitch
- Variable rotor speed - variable pitch

All computations in BladeOpt are based on steady state conditions, even though that is the case it is necessary to implement a control strategy to imitate the turbine control settings for each steady state wind speed. That means that based on what control strategy is chosen it is needed to find what pitch and rotor speed would be used if the wind speed would have reached a steady state.

Two configurations of control methods have been implemented in BladeOpt. The first control method, hereafter referred to as setup 1, is the same control method as is used for the 5MW NREL blade. Thus variable rotor speed - fixed pitch is used during ramp up of the turbine operation and altering to fixed rotor speed - variable pitch when rated power output has been achieved. During the ramp up phase, from cut-in until rated conditions, the turbine is operated at maximum efficiency by varying the rotor speed and as the rated power output has been met the pitch is varied to keep the power at the rated power.

The purpose of the control system, among other things, is to keep the rotor speed within a certain limit. Therefore, second control method, hereafter referred to as setup 2, is implemented. The need to limit the rotor speed can for example be caused by the choice of gearbox and generator of the turbine [Hansen, 2008]. Setup 2 has three types of controls. First control method is variable rotor speed - fixed pitch during ramp up until rated rotor speed. Between rated rotor speed and rated power is the second control method, where fixed rotor speed - fixed pitch is used. Third and final control of this configuration is fixed rotor speed - variable pitch in the region above rated power. This control configuration operates at maximum efficiency until either rated power or rated rotor speed. Achieving rated rotor speed first causes the rotor speed to be fixed at rated speed until rated power output has been met, thereafter the pitch is varied to keep the power at the rated power. Note that this configuration is equivalent to setup 1 if rated power is achieved before rated rotor speed i.e. only two types of controls. Validation of the two control methods is presented in chapter 4.

Power curves, computed by IMHAWT, for the NREL 5MW turbine can be seen in figure 3.3, where each power curve is for fixed wind speed in the range of 5m/s to 19m/s.

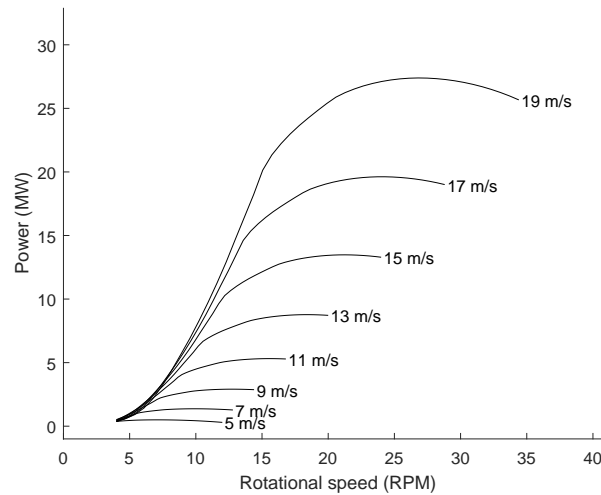


Figure 3.3: *Power curves for NREL 5MW in the range of 5 m/s to 19 m/s*

To be able to operate at maximum efficiency during ramp up it is necessary to compute at what rotor speed the maximum power can be achieved for each wind speed. As the power computation is performed through an implicit iterative numerical computation it is not possible to derive an explicit expression for the power, P , as function of the rotor speed, Ω , or $P(\Omega)$. Therefore, a numerical method is needed for the process of finding the optimum rotor speed during ramp up.

Looking at figure 3.3 it can be seen that the power curve for each wind speed is unimodal i.e has only one extrema. Furthermore, each curve is only function of the rotor speed. Therefore, 1D line search is straight forward method to use to minimize $-P(\Omega)$ for each wind speed. The Golden Section method was chosen for this process as it is a very robust and efficient method for 1D line search.

The implementation of the Golden Section method in BladeOpt requires an initial guess that is on the left side of the extrema of the lowest wind speed being used for the AEP computation. That is because the first optimum to be computed is for the lowest wind speed. When continuing to compute the optimum for the next wind speed the optimum from the previous wind speed is used as an initial guess. This method ensures robustness of the code as the power for each wind speed only has a feasible solution within certain range around the optimum.

This method is graphically shown in figure 3.4, where the blue asterisk show the starting points for each line search, the red asterisk show the optimum for each curve and the arrow show how the optimum value from the previous line search is used as an initial guess for the next one.

The final results of computing the optimal power curve for the NREL 5MW are shown in figure 3.5. Since the pitch control has not been implemented it can be seen that the power goes way above the 5MW rated power.

For both control method configurations in BladeOpt the optimum power curve computation has been implemented such that as soon as the optimum power for a certain wind speed goes

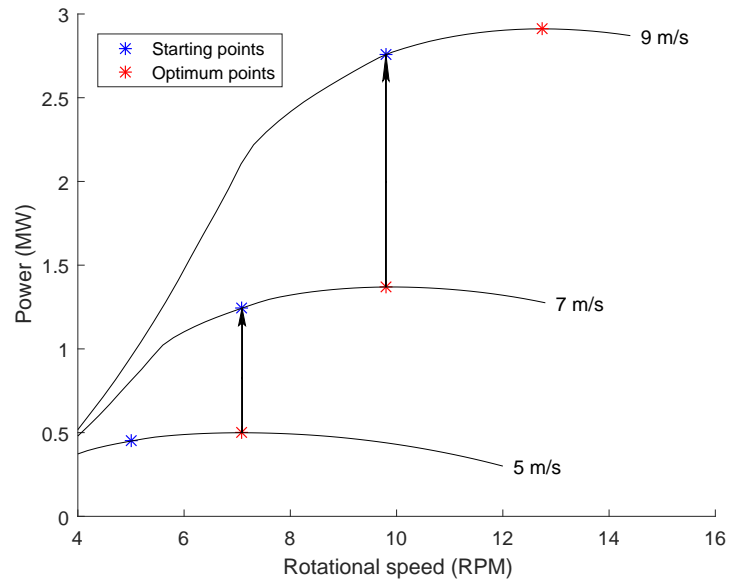


Figure 3.4: *Golden section method used to compute optimum power curve*

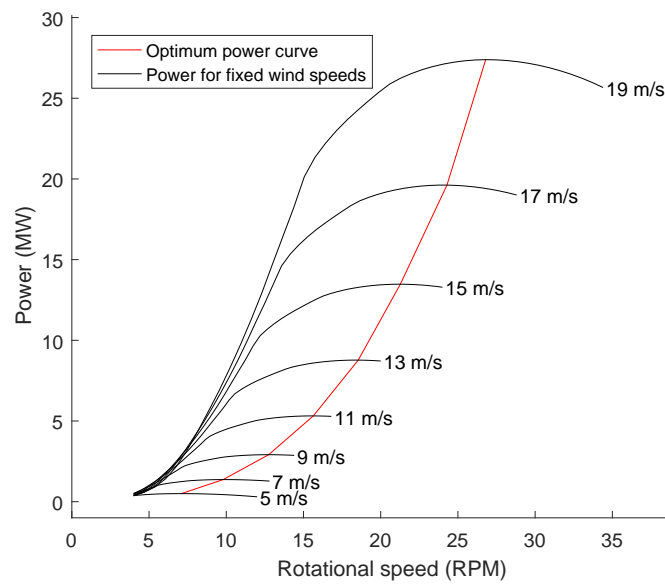


Figure 3.5: *Optimum power curve for the NREL 5 MW in the wind speed range of 5-19 m/s*

above the rated power then the necessary book keeping is done and the power computation is stopped.

The additional step taken in setup 2 is that the rotor speed is fixed at rated when the rated rotor speed has been achieved as is shown in figure 3.6.

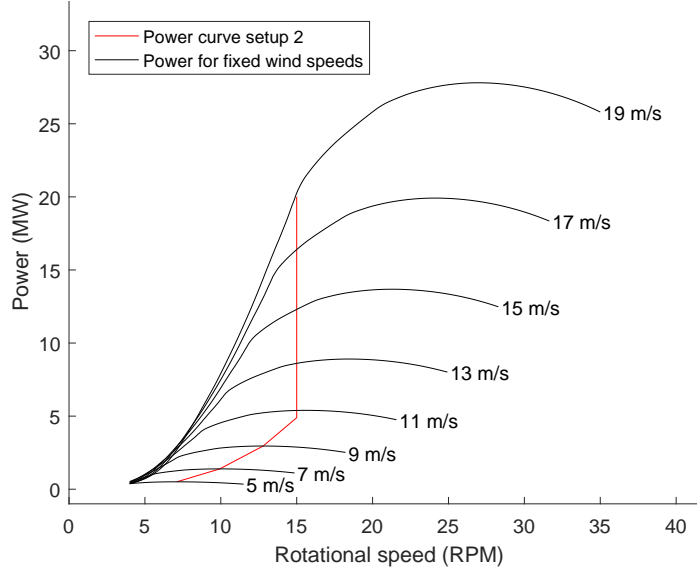


Figure 3.6: *Power curve using setup 2 control method*

The pseudo code to compute the power for a wind turbine along with the rotor speed controls for setup 1, is given in Algorithm 1.

Algorithm 1 FindOmega.m

```

1: procedure COMPUTE THE POWER CURVE USING SETUP 1
2:   for  $i = 1 : N_{WindIntervals}$  do
3:     Use golden section method to compute optimum rotor speed and power for  $V_i$ 
4:     if Power is above the rated power then
5:       Save at what wind speed power goes above rated
6:       Break out of for loop
7:     end if
8:     Set initial guess for iteration  $i+1$  to be optimum rotor speed of iteration  $i$ 
9:   end for
10: end procedure

```

The pseudo code to compute the power for a wind turbine along with the rotor speed controls for setup 2, is given in Algorithm 2.

Algorithm 2 FindOmega2.m

```
1: procedure COMPUTE THE POWER CURVE USING SETUP 2
2:   for  $i = 1 : N_{WindIntervals}$  do
3:     if Rotor speed is below the rated rotor speed then
4:       Use golden section method to compute optimum rotor speed/power for  $V_i$ 
5:     else
6:       Compute the power for  $V_i$  using rated rotor speed
7:     end if
8:     if Power is above the rated power then
9:       Save at what wind speed power goes above rated
10:      Break out of for loop
11:    end if
12:    Set initial guess for iteration  $i+1$  to be optimum rotor speed of iteration  $i$ 
13:  end for
14: end procedure
```

The procedure of finding the controls for rated wind speed as well as handling the turbine controls above rated is dealt with in the proceeding subsection.

3.2.3 AEP Computation

Having defined the Weibull distribution and how the power curve is computed up to rated power it is necessary to implement a procedure that clearly defines the point of rated rotor speed and wind speed before computing the AEP.

As described in subsection 3.2.2 the power curves for the two configurations have been defined during ramp up as well as having computed the power for one point above rated power. As the power is computed at discrete points it is necessary to interpolate to find more precisely the rated rotor and wind speed.

An example of the procedure of determining the rated rotor and wind speed for setup 1 is shown in figure 3.7. In this example the rated power is defined as 10 MW and as the optimal power at wind speeds both above and below the 10 MW power is known they are used to find the rated rotor and wind speed by linear interpolation. All power values above rated are then fixed to the rated power when the rated rotor and wind speed have been found.

An example of the procedure of determining the rated wind speed for setup 2 is shown in figure 3.8. In this example the rated power is defined as 10 MW as before but as the rotor speed is known only the rated wind speed needs to be interpolated. All power values above rated are then fixed to the rated power when the rated wind speed has been found.

Having the rated conditions for the turbine the power and rotor speed for all wind speeds above rated wind speed are then fixed to the rated values without any further computation. This method is the equivalence of a fixed rotor speed - variable pitch control.

The reason why no further computation is needed is because the information gained by that does not benefit for the optimization. Computing the pitch above rated does not change the AEP since the assumption of fixed rated power above rated wind speed is already implemented. Furthermore, the mass is not affected as the load that is applied to the blade for the structural

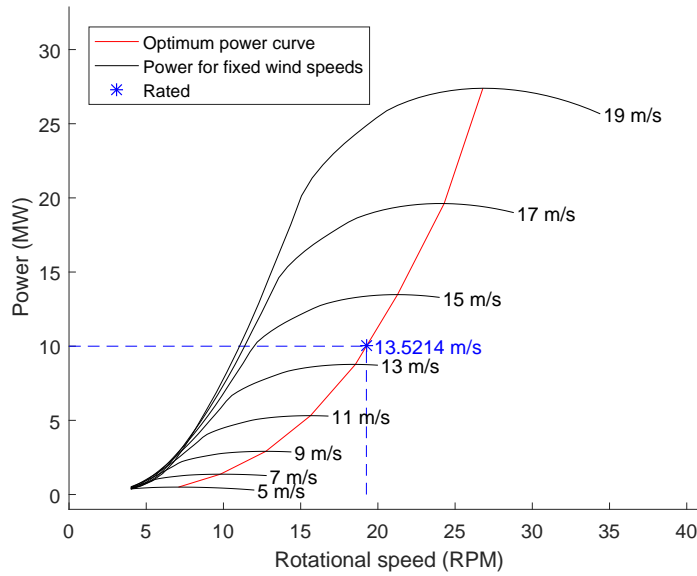


Figure 3.7: Wind speed and rotational speed are interpolated for rated power, control setup 1

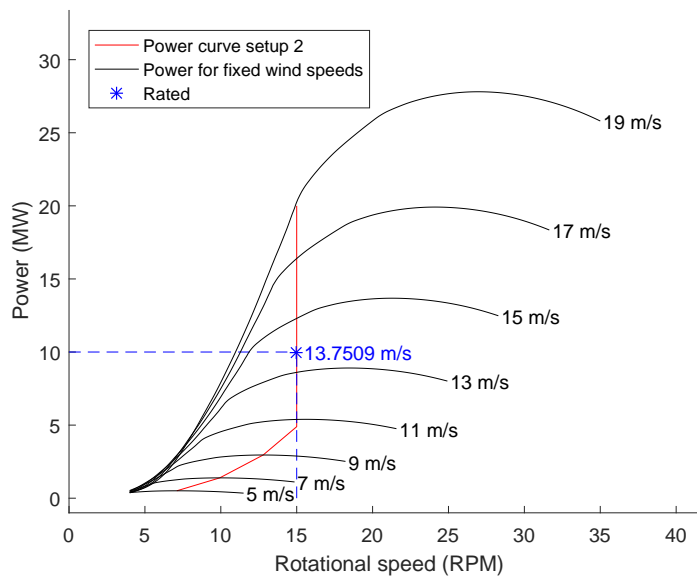


Figure 3.8: Wind speed and rotational speed are interpolated for rated power, control setup 2

analysis is already known from the computation of rated power. The method of computing loads to be applied onto the structural model is described in subsection 3.3.

The final power curves for the 10 MW turbine from the examples in figures 3.7 and 3.8 can be seen in figure 3.9. It can be seen on the figure that as the rated rotor speed is met for setup 2 then the turbine starts to provide less energy than in setup 1 as expected since setup 1 is purely operating at maximum efficiency.

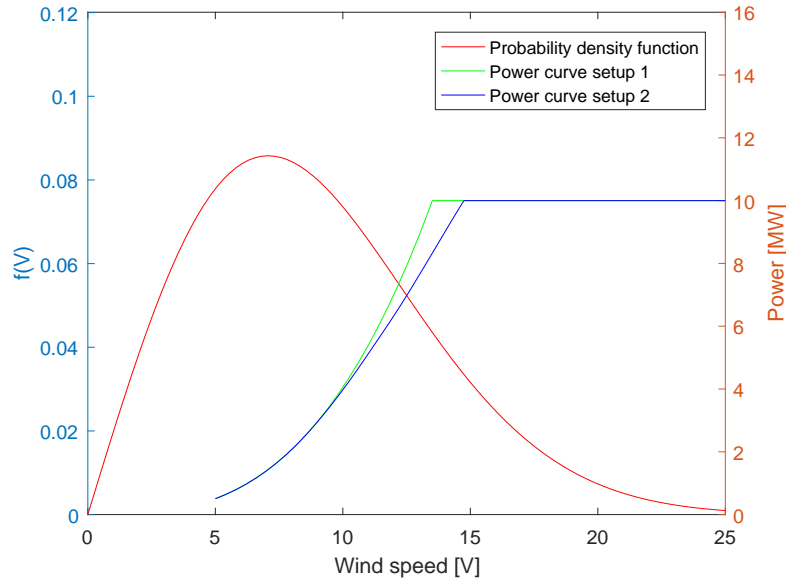


Figure 3.9: *Weibull distribution and power curves used for AEP computation*

Having the final power curves and the Weibull distribution defined the AEP is then computed by (3.2). The procedure of computing the AEP is lastly recapped by Algorithm 3.

Algorithm 3 AEPComp.m

```

1: procedure COMPUTE THE ANNUAL ENERGY PRODUCTION
2:   Compute rated wind speed using linear interpolation
3:   if Setup 1 is chosen then
4:     Compute rated rotor speed using linear interpolation
5:   end if
6:   Power production for wind speeds over rated is fixed to rated power
7:   for  $i = 1 : N_{WindIntervals}$  do
8:     Compute AEP contribution from interval  $i$  by (3.2)
9:   end for
10: end procedure

```

3.3 Loads for structural analysis

The main sources of loads on the wind turbine blades can be divided into three categories [Hansen, 2008].

- **Aerodynamic loading:** Interaction between the blades and the wind causes flapwise and edgewise loads
- **Gravitational loading:** Earth's gravity causes edgewise loads that changes direction during the rotation of the turbine
- **Inertial loading:** Caused by centrifugal forces as the turbine rotates and by acceleration as rotational speed is changed

The first two load sources are implemented in this study as they have the most effect on the design loads [Thomsen, 2009].

The gravitational loading affects the edgewise loads of the blade and is at maximum when the blade is in a horizontal position. The load is fully reversed in every cycle and the magnitude of the load depends on the weight of the blade. This load, for the case of horizontal blade, is added as a static load to the structural model in BladeOpt.

The aerodynamic loading causes both edgewise and flapwise loads on the blade and is used when computing the power of the turbine. The power is then used to compute the AEP. To compute the AEP it is necessary to compute the power for the full operational range of wind speeds. The load applied to the model to obtain the structural responses is on the other hand only necessary to be computed for a single load case i.e. single wind speed. To be conservative so that the design will not be too weak it is necessary to choose the worst load case scenario.

In the case of both control setup 1 and setup 2 then the conditions that give the biggest out of plane deflection is at the rated wind speed. The biggest in plane deflection does on the other hand occur above rated wind speed. The deflection at rated is however not that much lower than the maximum value and in the case of the NREL 5 MW turbine there is 20% difference [Jonkman et al., 2005]. The in and out of plane deflection curves for the NREL 5 MW turbine can be seen in figure 3.10.

Since the load that is applied on the model for the structural analysis is obtained from a single wind speed it can be seen that the most conservative load to choose is the load from rated wind speed. Furthermore there is a requirement by the International Electrotechnical Commission standards (IEC) for wind turbines that they should withstand an extreme operating wind gust [IEC, 2005]. BladeOpt has an input where this extreme wind gust is defined by the user, to make sure that the absolutely worst case scenario is captured. The IEC standard defines the site specific wind gust that the blade should withstand, where the magnitude of wind gust that is added to the wind speed is location specific for the intended use of the turbine.

By computing the load based on rated wind speed and adding a sudden wind gust ensures that there are no other operational conditions that are worse in terms of ultimate load, therefore constraints on both deflection and strain will be fulfilled for all steady state conditions if they fulfil this worst case. Furthermore, constraint has been added that takes edgewise fatigue loads, caused by gravitational loading, during the turbine lifetime into account. Similarly, safety factors has been added to imitate the flapwise fatigue problem. The implementation of the constraint and the safety factor are described in subsections 3.6 and 3.8 respectively.

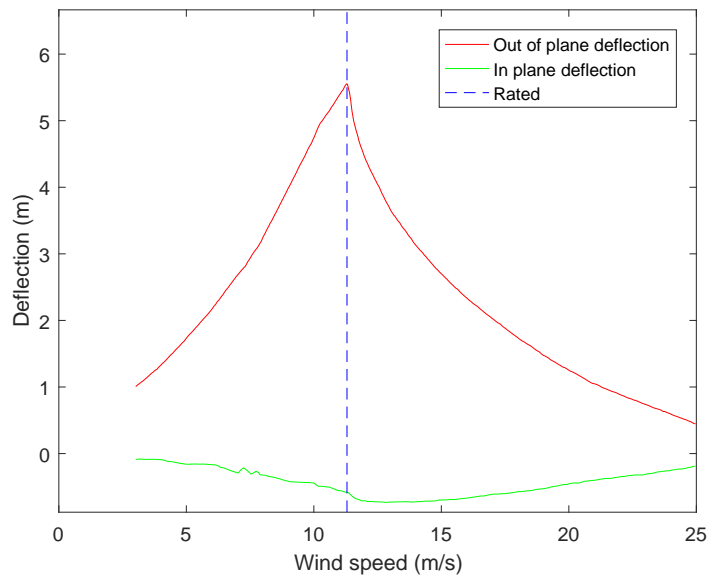


Figure 3.10: *Blade deflection of the NREL 5 MW turbine during operational range [Jonkman et al., 2005]*

3.4 Mass

To compute the mass of the blade it is necessary to define the geometry of the blade for the structural code of BladeOpt. That is done by introducing simplifications when defining the structure of the cross sections of the blade, with the aim to resemble an airfoil cross section as closely as possible using simple shapes such that the cross sectional properties can easily be computed.

Wind turbine blade cross sections are different between blade manufacturers, mainly due to different manufacturing techniques, but they are all based on the same concept [Thomsen, 2009]. The cross section on the left in figure 3.11 illustrates all the main building blocks of an airfoil cross section. The outer shape is designed to achieve a desired aerodynamic performance. The beam like structure in the middle supports the outer shell and carries the flapwise bending of the blade. The supports in the leading and trailing edge carry the edgewise bending of the blade. The main building blocks of wind turbine blade cross section are

- **Outer shell:** Designed to accomplish a desired aerodynamic performance. It usually consists of sandwich material to increase the resistance of the blade against the local buckling. The face sheets are usually biaxial (biax) composite laminates and the core material is light weight material for instance balsa wood.
- **Spar cap:** Included in the cross section to carry the flapwise bending of the blade. They serve the same purpose as the flanges of I-beam. The spar caps are usually a monolithic unidirectional (UD) composite laminate.
- **Shear web:** Supports the outer shell and acts as the web of an I beam. The shear web carries the shear forces of the blade. It is common to use sandwich material in the

web, with biax composite faces and lightweight core material, to prevent in-plane shear buckling. It differs between blade manufacturers if they use one or more webs.

- **Edge reinforcement:** Reinforcements in the leading and trailing edge of the blade to carry the edgewise loads of the blade.

The manufacturing of the blades differs between companies. The most common method is to manufacture the web and spar cap separately from the outer shell and to manufacture the shell in two parts and glue the whole assembly together. It is common to use two shear webs when using this manufacturing method.

Siemens is the only company that has a completely seamless blade as it is manufactured as a single piece using closed mould process [Siemens, 2012]. Using this seamless technology allows them to manufacture lighter and stronger blades since they have eliminated all the potential weak points caused by the normal gluing process, and the additional mass of the glue.

Figure 3.11 shows a comparison of a typical blade cross section, based on the Siemens seamless design, on the left and a simplified cross section used for the structural code of BladeOpt on the right. The outer shapes of cross sections used in the aerodynamic part of BladeOpt, are defined as airfoils like the cross section on the left while the cross sections for the structural part are defined as an ellipse.

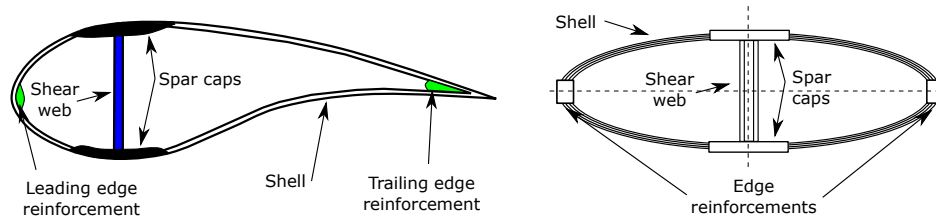


Figure 3.11: *Comparison of actual wind turbine cross section and simplified cross section*

With the intention of imitating all of the building blocks of a typical blade cross section the cross section for the structural part consists of sandwich layered outer shell, sandwich layered shear web, spar caps and reinforcements in the leading and trailing edge of the ellipse. The ellipse shaped cross section is perfectly symmetric about both of the centerlines in figure 3.11.

The material used in the structural cross section can be separately chosen for

- Ellipse face sheet
- Ellipse core
- Shear web face sheet
- Shear web core
- Spar caps
- Edge reinforcements

The materials for all of the parts of the cross section are composite materials except the core materials in the ellipse and the shear web. The usage of composite materials in the

code is limited to symmetric balanced laminates. Applying those limitations ensures that the equivalent Young's modulus of a laminate is thickness independent. The only material properties that are needed as input in this study are the laminate equivalent Youngs modulus, E , in a spanwise direction along the blade and density, ρ , moreover torsional modulus G .

Those properties are found by layering up the desired material as a symmetric balanced laminate and computing the equivalent material properties. Using this method allows the simplification that the anisotropic, orientation dependent composite is assumed to be homogeneous and linear elastic along a spanwise direction of the blade. The simplification of treating the layered composite as equivalent single layer is shown in figure 3.12.

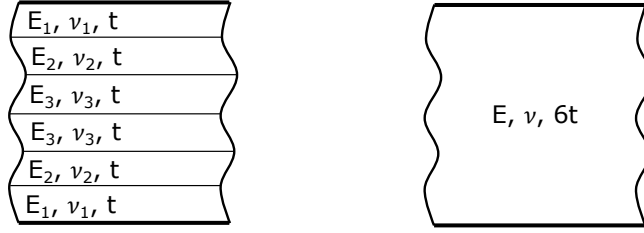


Figure 3.12: *Simplifications of material properties*

Having defined both the structure of the blade cross sections and how materials are treated in the model it is now possible to compute the mass of the blade. The mass of the blade is computed as the sum of the mass contribution from each of the building blocks of the cross section as follows

$$Mass = \sum_{i=1}^{N_{blocks}} A_i \cdot \rho_i \quad (3.8)$$

where N_{blocks} is the number of different building blocks of the cross section, A is the area of the building block and ρ is the density of the material used for the building block. The results are the mass of the blade in kg/m .

3.5 Design Parametrization

Design parametrization is very important part of the optimization formulation as the performance of optimized design is highly dependent on the parametrization. When choosing parameters as design variables it is necessary to take both the design and manufacturability into account [Choi and Kim, 2005].

In this section the choice of design variables will be presented, starting by looking at a full scale turbine and break it down into parts to identify the appropriate design parameters for the design process. Furthermore, parameters that are not used as design variables are presented and the option of including them as design parameters is discussed.

To lead up the introduction of the design parametrization a full scale turbine is presented in figure 3.13, this is modern three blade horizontal axis wind turbine as the NREL 5 MW

turbine. There are few parameters in the model at this top level and none of them is used as a design variable in BladeOpt.

First there are the wind conditions that affect the results and they are based on the local conditions at the wind turbine site as described in subsection 3.2.1. Therefore, the wind conditions are always an input in the design process. The number of blades on the turbine is also defined at the top level, BladeOpt can handle any number of blades on the turbine but since the number of blades is usually predefined it is not used as an design variable. Final two parameters at this level are control parameters of the turbine. Those are the rotor speed, Ω , which is computed for each iteration of the design as described in subsection 3.2.2 and the pitch angle, β , that is also implemented in the control strategy when obtaining the power curve.

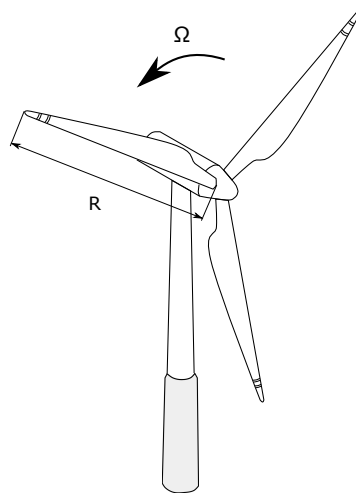


Figure 3.13: *Horizontal axis wind turbine*

Next step is to go one level deeper in the wind turbine and take a look at the turbine blade. Figure 3.14 illustrates a wind turbine blade, where the length of the blade is defined as R and the hub radius as R_{hub} . When deciding on parametrization of the blade the solution models used for the aerodynamic and structural computations of the blade need to be considered, as well as making sure to allow only feasible designs.

The loads computed in the aerodynamic part of BladeOpt are computed at cross sections along the blade and then assumed to vary linearly between those locations, each of these cross sections has a defined geometry and airfoil type, further details on the load computation are presented in section 4.1. Furthermore, the FEM model used for the structural computation in BladeOpt is based on discretizing the blade to elements, where each element represents a section of the blade. The elements used in BladeOpt are beam elements as is further described in chapter 5. Each of those elements has defined geometry and material properties that are assumed to be constant within the element. Based on how the blade is treated in the aerodynamic part and the structural part of BladeOpt it is necessary to make a relation between the two codes. This relation is achieved by aligning the cross sections in the aerodynamic part with the faces between elements in the FEM part. The vertical lines along the blade in figure 3.14 represent the cross sections used for load calculation and the faces between elements in the FEM part. Furthermore, cross sectional properties for each element in the FEM code

are computed in the element face closer to the blade root and then taken as constant for the whole element.

To parametrize the blade, the length of element, L_e , is chosen as a design variable type in the optimization where $e = 1, \dots, N_{elem}$. This design variable type affects the outcome of both the AEP in the aerodynamic part and the mass in the structural part. The element length is a unique value for each element so the number of design variables that arises from this variable type depends on how many elements the user defines in the initial model. The blade length is not chosen as a design variable but it is directly related to the element lengths as the sum of them and does therefore vary in the optimization process as the element lengths vary. The hub radius is not used as design variable either as it is constrained by the nacelle design of the turbine and just taken as input into the model.

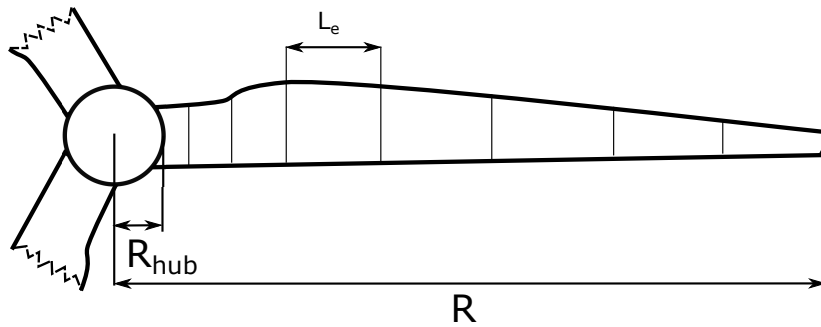


Figure 3.14: *Blade of a wind turbine*

The cross sections between the previously described elements are the next steps of the full parametrization of the design. Those cross sections are defined differently for the aerodynamic and the structural code as described in section 3.4.

There are two parameters used to define the outer geometry of those two cross section types, the thickness, t , and the chord, c , both variables affect the AEP and the mass. The chord is a design variable in BladeOpt while the thickness is defined by the thickness ratio t/c of the selected airfoil which is user input. The relation between how the outer geometry is defined for the two types of cross sections can be seen in figure 3.15. Additionally, the twist, Tw , at each cross section is a design variable that affects both the AEP and the mass.

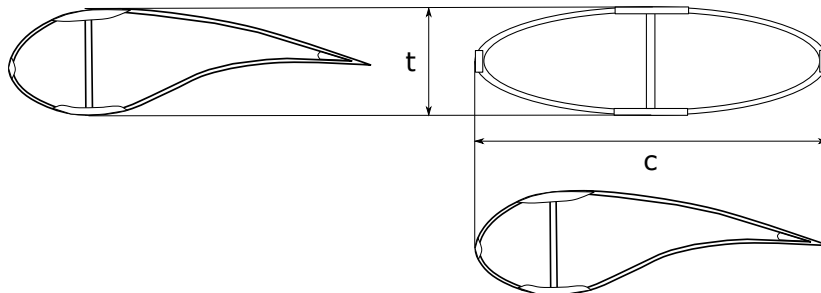


Figure 3.15: *Outer geometry of cross sections*

All the design variables that are used for the AEP computation in the aerodynamic code

have now been defined. The inner geometry parametrization is defined in the following. Cross section used for the structural computation can be seen in figure 3.16, where it can be seen that there are eight design variables that define the inner geometry of the cross section. All of those variables do only affect the mass but not the AEP computation.

The first two design variables define the thicknesses of the sandwich structure in the ellipse, the thicknesses of the face sheets are defined by TF_e and the thickness of the core is defined as TC_e . The shear web thicknesses are defined by two variables as well, where the thickness of the face sheets is defined as TF_{sw} and the thickness of the core is defined as TC_{sw} . Furthermore, the spar cap is defined by two design variables, those are W_{sc} and H_{sc} that define the width and height of the spar caps respectively. Finally, two design variables are defined for the edge reinforcement geometry, those are W_{re} and H_{re} that define the height and width of the reinforcements respectively.

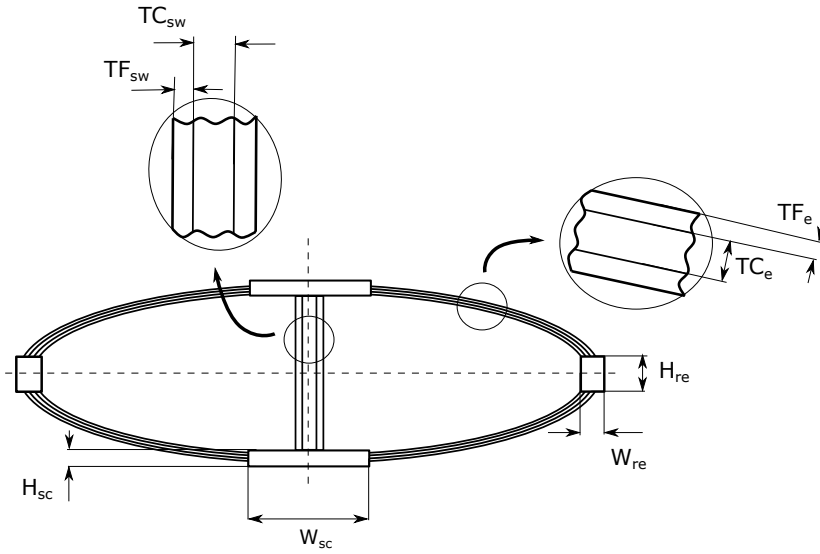


Figure 3.16: *Inner geometry of cross sections*

Composite material thicknesses in BladeOpt are treated as continuous variables that can have any thickness. That means that the results might not always be feasible for manufacturing since the thickness is controlled by the laminae thicknesses in reality so the design will need to be altered such that it is feasible before realization.

All of the parameters that have been implemented as design variables in BladeOpt have now been introduced. Those are eleven types of design variables and are summarized in table 3.1 along with information on what part of the objective function they affect.

For the design variables that describes the cross sectional geometry q is defined as the number of cross sections $q = 1, \dots, N_{crosssection}$.

3.6 Constraints

To obtain a physically acceptable design, constraints are set on the optimization problem. Constraints can be defined on both response functions, e.g. maximum strain, eigenfrequencies,

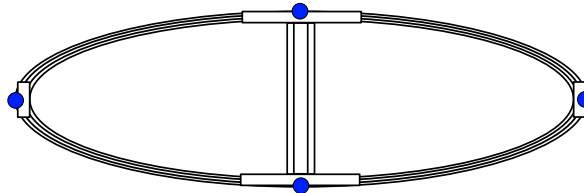
Design variables	Description	AEP	Mass
L_e	Element length	x	x
c_q	Chord	x	x
Tw_q	Twist	x	x
TF_{eq}	Ellipse face thickness		x
TC_{eq}	Ellipse core tickness		x
TF_{swq}	Shear web face thickness		x
TC_{swq}	Shear web core tickness		x
W_{scq}	Spar cap width		x
H_{scq}	Spar cap height		x
W_{req}	Edge reinforcement width		x
H_{req}	Edge reinforcement height		x

Table 3.1: *Design variables in BladeOpt*

cies, and design variables of the wind turbine blade. Using appropriately defined constraints, feasible design can be established with respect to the operational conditions and the manufacturability of the blade.

Deflection To prevent the collision between the blade and the tower for any operational conditions, a constraint needs to be set on the out of plane tip displacement. To perform that, the maximum distance between the tower and the rotor plane is necessary to be known, which typically depends on the size of other components of the wind turbine e.g. hub, nacelle, drive train etc.

Strains To avoid the ultimate and fatigue failure of the composite material, constraints need to be defined based on a failure criteria. Although several criterion have been developed to predict the failure of the composite materials, none of the available one has demonstrated the capability of convincingly matching experimentally determined failure envelopes [Overgaard, 2016]. A simple approach is to apply the maximum strain criteria and set a constrain on the maximum strain values. Using the simplified cross sections, maximum/minimum strains occur at the vertices and co-vertices of the cross section, figure 3.17. The material used in these locations are UD composites where the fibres are aligned with the longitudinal axis of the blade, hence the maximum allowable strain values can be set to e.g. the ultimate material parameters.

Figure 3.17: *Maximum strain locations in a cross section*

The displacements and strains are calculated using the loading condition defined in subsection 3.3.

Eigen frequencies To avoid resonance during the operation of the wind turbine, constraints on the eigen frequencies of the blade need to be set. Vibrations can be generated by the wind, and by the components of the wind turbine. One main source of vibration is the rotation of the rotor. As the rotor rotates vibration is generated by e.g. shading effect of the tower, wind shear, gravitational loads, these phenomena are proportional with the rotor speed and the number of blades. For a three bladed wind turbine, typically the third rotational frequency is in main interest. The rotational frequency ψ is defined as: $\psi = \frac{\Omega}{2}\pi$. To avoid resonance the three lowest eigen frequencies of the blade are constrained. The first three eigen frequencies is usually set to be larger than the third rotational frequency.

Fatigue The edgewise and flapwise loads on the wind turbine blades, originating from e.g. gravitational loads, wind shear, tower shading, vary in time with a frequency correspondint to the rotational speed of the rotor. These flapwise and edgewise altering loads develop fatigue damage in the blade materials, which can lead to failure of the blade. To design a blade that can withstand at least 20 years of operational life for onshore or 25 years for offshore blades, the fatigue problem needs to be investigated during the design process of the blade. Several researches have been conducted to develop methods, that can estimate the fatigue damage in a blade for the whole operational life of the wind turbine. The approach presented in Fuglsang et al. [2002], requires time-domain simulations with turbulence models, which is not suitable for gradient based optimization, since the stochastic nature of these simulations does not allow for accurate evaluation of gradients of objectives and constraints with respect to design variables [Zahle et al., 2015]. Linear, frequency based approach has been developed in Tibaldi et al. [2016], to compute wind turbine fatigue loads efficiently, thus providing an efficient evaluation of gradients. The method requires high-order linear aeroservoelastic wind turbine model to compute the frequency response of loads due to a turbulent wind input [Tibaldi et al., 2016], hence it is out of the scope of this study.

To deal with the edgewise fatigue problem and prevent unrealistic results a simple approach is implemented in the optimization process. The edgewise fatigue loads, originating from gravity, are fully reversed in every blade rotation. Although edgewise gravitational loads are not always the dominant load condition, they can be more significant than flapwise aerodynamic loads in determining the fatigue strength of very large blades [Ning et al., 2013]. It is assumed that the $S - N$ curve can be described as:

$$\frac{\epsilon_c}{\epsilon_{ult}} = CN_{cycles}^{-\frac{1}{m}} \quad (3.9)$$

where ϵ_{ult} is the ultimate tensile or compressive strain of the material and ϵ_c denotes the highest tensile or compressive strain of the material in the fatigue cycle. C and m coefficients are obtained from Mandell and Samborsky [1997], using that the load is fully reversed $C = 1$ and $m = 14.9$. N_{cycles} denotes the total number of cycles for the designed life time, which can be estimated by calculating the expected number of cycles in a year using the probability of

the wind speeds and the related rotational speeds obtained by the control set ups presented in section 3.2. The time of one rotation can be calculated as:

$$t = \frac{2\pi}{\Omega} \quad (3.10)$$

where Ω is the rotational speed for a given wind speed in radian per second at V wind speed. Knowing the probability for the wind intervals N_{cycles} can be calculated in similar way as the AEP is computed in section 3.2.

$$N_{cycles} = \frac{3600}{t} \cdot f(V_i < V_0 < V_{i+1}) \cdot 24 \cdot 365 \cdot N_{years} \quad (3.11)$$

Thus the allowable fatigue strain can be obtained by (3.9). Setting fatigue strain as allowable strain for the steady state response of the blade can lead to a blade design where the edgewise fatigue is considered. Flapwise fatigue calculations are not implemented, however, using the ultimate strain values as constraints would lead to a blade design that can not withstand its operational conditions, hence strict safety factor is set on the ultimate strain values of the spar cap material. These constraints do not replace the full fatigue analyses, hence more detailed fatigue analysis of the blade is suggested to be done in the next steps of the blade design.

Tip speed Due to aero-acoustic noise generation, onshore wind turbines are usually constrained to operate at blade tip speed in the range of 75-80 meter per second [Dykes et al., 2014]. In case of offshore turbines this limit can be increased around 100-110 meter per second. The tip speed can be obtained as:

$$V_{tip} = R\Omega \quad (3.12)$$

The effects of the different tip speed constraints on the turbine design have been investigated in Dykes et al. [2014]. Results shows that allowing higher tip speed can reduce the cost of other wind turbine components.

Buckling Wind turbine blades experience high bending loads under operational conditions due to the aerodynamic and gravitational effects, which result compression and tension in the shell material of the blade. Under compression, buckling of the composite panels can occur, which can lead to delamination failure in the composite material. The local buckling-driven delamination can cause structural collapse in the wind turbine blade [Haselbach et al., 2016]. Although it is desired to fit buckling analyses into the optimization process to overcome the problem, the evaluation of buckling loads would require detailed finite element model of the blade, resulting increase in computational time. Buckling is primarily overcome by adjusting the core thickness in the panels [Zahle et al., 2015]. Within this study, constraints are not implemented on buckling of the composite surface panels, thus they will have to be investigated as a further step of the blade design.

Design variable constraints To ensure a continuous, manufacturable design, constraints need to be set on the design variables. The implemented design variable constraints will be described in chapter 8.

Summary of Implemented constraints In this study, constraints are implemented on the

- out of plane displacement of the blade tip
- maximum strains
- three lowest eigen frequencies
- tip speed of the blade
- edgewise fatigue problem
- design variables

In this study, constraints are not implemented on the

- flapwise fatigue problem
- buckling

3.7 Design Variable Bounds

To restrict the design space and ensure a feasible design, bounds can be defined on each design variable. These bounds are dependent on the available manufacturing equipments, methods and transportation boundaries. The implemented bounds will be described in chapter 8.

3.8 Safety Factors

IEC [2005] standard requires to introduce partial safety factors to deal with the uncertainties and variability in loads and materials, the uncertainties in the analysis methods and the importance of structural components with respect to the consequences of failure. In BladeOpt, it is possible to define the following safety factors:

- partial safety factor for loads - γ_f
- partial safety factor for materials - γ_m
- partial safety factor for failure - γ_n

The IEC [2005] standard defines the values for these safety factors based on analysis type, such as ultimate strength, fatigue failure, stability and critical deflection analyses. The safety factor for loads is applied, as:

$$F_d = \gamma_f F_k \tag{3.13}$$

where F_d represents the design value of the loads for a given load case, while F_k denotes the characteristic value for the load. The safety factor for materials is applied as:

$$f_d = \frac{1}{\gamma_m} f_k \quad (3.14)$$

where f_d represents the design values for materials, while f_k denotes the characteristic values of material properties. The safety factor for the analysis γ_n can be implemented, as:

$$F_{ad} = \gamma_n F_{ak} \quad (3.15)$$

where, F_{ad} represents the design value of the analysis result, while F_{ak} denotes the obtained analysis result. In BladeOpt, γ_n is used on the displacement; strain; and eigen frequency analyses.

The values of the safety factors depend on different circumstances and design situations. Assuming normal design situations, the common range of the safety factors are presented based on IEC [2005] in table 3.2.

Analysis	γ_f	γ_m	γ_n
Ultimate strength analysis	1.25 - 1.35	≥ 1.1	0.9 - 1.3
Fatigue analysis	1	1.2 - 1.7	1 - 1.3
Critical deflection analysis	1.25 - 1.35	1.1	1 - 1.3

Table 3.2: *Safety factors for different type of blade analyses*

In BladeOpt, one value can be defined for each type of safety factor. The applied values are presented in chapter 8.

3.9 Definition of the Optimization Problem

The two performance measures that build up the objective function of the study are as previously mentioned the *AEP* and *Mass*. Having those two performance measures makes the the problem a multi objective problem, where the aim is to minimize the *Mass* and maximize the *AEP*. To combine those measures in the same objective a summation of the *Mass* and $-AEP$ is to be minimized. It is a good practice to normalize the measures, to balance the importance of them, as they are of different magnitudes. That is done by dividing the *Mass* by the mass of the initial guess, $Mass_0$, and by dividing the *AEP* by the AEP of the initial guess, AEP_0 . Finally, weight factors are added for both measures such that the importance of them can be adjusted according to the goal of the optimization.

The optimization problem can be symbolically defined as:
Minimise:

$$-w_1 \frac{AEP}{AEP_0} + w_2 \frac{Mass}{Mass_0} \quad (3.16a)$$

subjected to constraints:

$$\begin{aligned}
 u_{tip} &\leq \bar{u}_{tip}, & (\text{Tip displacement}) & (3.16b) \\
 \epsilon_c - \epsilon_{q_m} &\leq 0, & (\text{Edgewise fatigue strain}) & (3.16c) \\
 \epsilon_{q_m} &\leq \epsilon_{ult}, & (\text{Flapwise strain}) & (3.16d) \\
 V_{tip} &\leq \bar{V}_{tip}, & (\text{Tip speed}) & (3.16e) \\
 (3 \cdot \psi)^2 - \lambda_n &\leq 0, & (\text{Eigen frequency 1-3}) & (3.16f) \\
 x_{i-1} &\leq x_i \leq x_{i+1}, & (\text{Design variable constraints}) & (3.16g)
 \end{aligned}$$

and bounds:

$$\underline{x}_i \leq x_i \leq \bar{x}_i, \quad (\text{Design variable bounds}) \quad (3.16h)$$

In (3.16a) w_1 represents the weight factor for the *AEP* and w_2 represents the weight factor on the *Mass*. Changing the value of the weight factors changes the importance of the performance measures e.g. by setting w_1 to zero and w_2 to one leads to purely structural optimization while increasing w_1 will put higher importance on the *AEP*, similarly can purely aerodynamic optimization be executed by setting w_2 to zero and w_1 to one.

In (3.16b) - (3.16g); \bar{u}_{tip} is the maximum tip displacement and u_{tip} is the tip displacement of the design, ϵ_{q_m} denotes the strain at point m , in cross section q . \bar{V}_{tip} represents the maximum tip speed, λ_n the eigen values where $n = [1,2,3]$, \bar{x}_i and \underline{x}_i are the maximum and minimum bounds of the design variables.

In chapter 8, the effects of the different weight factors will be evaluated through case studies. The design independent constraints, the design variable bounds and constraints that are used for the optimization studies are presented in chapter 8.

CHAPTER 4

BEM

In this chapter the main theory for the aerodynamic part of BladeOpt is introduced, where the BEM method is used to compute the loads on the blade as well as the turbine power. Furthermore, the method of using golden section line search to compute the optimum power curve for a set of wind speeds is validated. Finally, the AEP computations for both of the implemented control strategies are validated.

4.1 Blade Element Momentum Method Main Theory

The Blade Element Momentum method is the most common method used for computing induced velocities for wind turbines [Moriarty and Hansen, 2005]. Utilization of the method allows one to compute the steady state loads, thrust and power of a wind turbine [Hansen, 2008]. The loads on the turbine blades are caused by interaction between the body of the blades and the wind flow, purely due to viscosity of the air. As if there would be an inviscid fluid available it could flow past the turbine blades without causing any load on them.

This interaction causes two types of stresses on the blade surface, those are normal stresses, P , and shear stresses, τ . Integrating those stresses over the blade surface gives the loads on the blades. The total load is usually split to lift and drag as is seen in figure 4.1, where the lift, L , is always perpendicular to the wind direction and the drag, D , is always parallel to the wind direction.

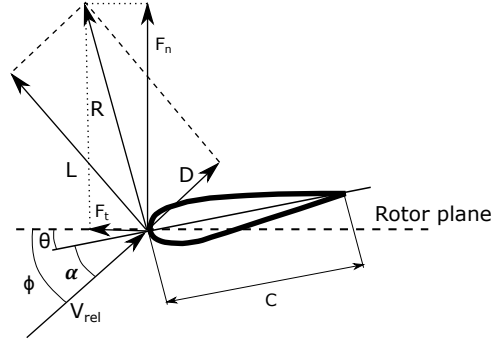


Figure 4.1: *Forces acting on airfoil from interaction with air flow*

Lift and drag properties of airfoils are generally obtained by load measurements on airfoils in wind tunnels [Munson et al., 2015]. They are presented by lift coefficient, C_L , and drag coefficient, C_D , as a function of the angle of attack, α . The angle of attack is defined as the angle between the airfoil chord C , and the relative direction of the wind speed, V_{rel} , where the chord is defined as the length of a straight line between the leading and trailing edge of the cross section. All results for comparisons and validations against the NREL blade in this report are generated by using published lift and drag coefficient data for the airfoils that are used in the blade [Jonkman et al., 2005].

In BEM the swept area of the turbine is discretized to N annular elements of width dr as can

be seen in figure 4.2. In the BEM method there are two assumptions made for those annular elements, those are

1. The annular elements are defined by streamlines, therefore, air does not flow between any two elements, i.e the elements are radially independent.
2. The flow within each annular element is constant, which is the same as assuming infinite number of blades.

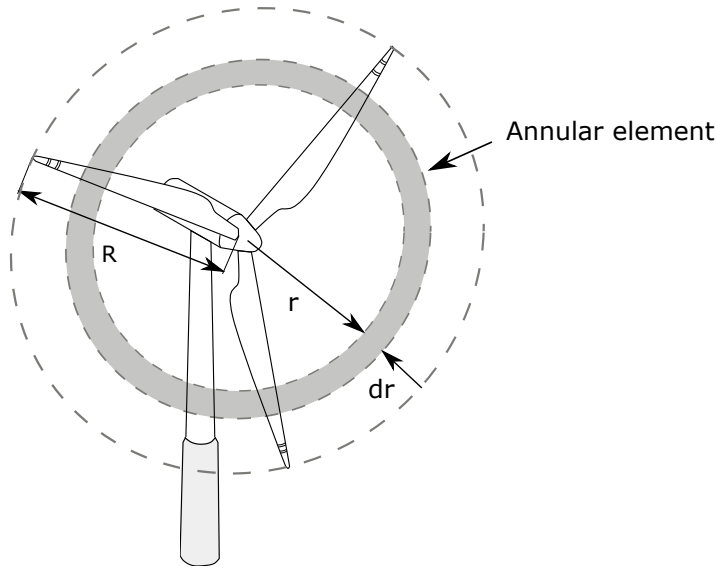


Figure 4.2: *Annular elements used for BEM method*

The load on the blade is computed for each of the annular elements using the local conditions of the element. The velocities used in the computations can be seen in figure 4.3. Here the tangential velocity is $\omega(1 + a')$ and the axial velocity is $V_0(1 - a)$, where ω is the rotor speed, a is the induced axial velocity, a' is the induced tangential velocity and V_0 is the steady state wind speed ahead of the turbine. Furthermore, V_{rel} is the wind speed relative to the rotating turbine blade and is defined as

$$V_{rel} = \frac{V_0(1 - a)}{\sin(\phi)} \quad \text{and} \quad V_{rel} = \frac{\omega r(1 + a')}{\cos(\phi)} \quad (4.1)$$

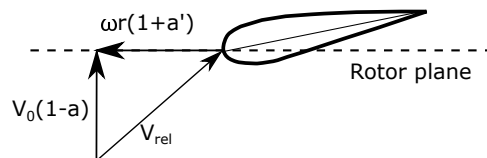


Figure 4.3: *Velocities*

Looking at figure 4.3 it can be seen that the flow angle, ϕ , in figure 4.1 can be described as

$$\phi = \tan^{-1} \left(\frac{(1-a)V_0}{(1+a')\omega r} \right) \quad (4.2)$$

Additionally, the angle of attack, α in figure 4.1, can be described as the difference between the flow angle and the local pitch, θ .

$$\alpha = \phi - \theta \quad (4.3)$$

The forces acting on the blade can be seen in figure 4.1 and are denoted as F_n in the axial or the normal direction of the blade and F_t in the tangential direction of the blade. Those forces are the projection of the lift and drag forces and are defined as

$$F_n = C_n \frac{1}{2} \rho_{air} C V_{rel}^2 \quad (4.4)$$

$$F_t = C_t \frac{1}{2} \rho_{air} C V_{rel}^2 \quad (4.5)$$

where C_n and C_t are found by projecting the lift and drag coefficients in normal and tangential direction as

$$C_n = C_L \cos(\phi) + C_D \sin(\phi) \quad (4.6)$$

$$C_t = C_L \sin(\phi) - C_D \cos(\phi) \quad (4.7)$$

Both the lift and drag coefficients are functions of α as mentioned before and are found from force measurements on airfoils in wind tunnels.

The final variables still to be defined are the axial and tangential induction factors. The induction factors for the standard BEM method are as follows

$$a = \frac{1}{\frac{4F \sin^2(\phi)}{\sigma C_n} + 1} \quad (4.8)$$

$$a' = \frac{1}{\frac{4F \sin(\phi) \cos(\phi)}{\sigma C_t} - 1} \quad (4.9)$$

where F is the correction factor and σ is the solidity of the turbine or how big fraction of the annular area is covered by blades. The solidity is defined as $\sigma = (CN_B)/(1\pi r)$ where N_B is the number of blades on the turbine.

There are multiple correction factors available for the induction factors in the standard BEM method [Hansen, 2008] [Moriarty and Hansen, 2005]. The most common correction factors have been implemented in BladeOpt.

First correction factor to be implemented is the Prandtl tip loss factor to correct for assumption number 2 in BEM as there are finite numbers of blades in reality. Furthermore, the hub loss correction has been implemented to correct for a vortex forming in the wake near the hub. Finally, correction has been implemented to correct for heavily loaded rotors when the axial induction factor is above 0.4 as that causes high pressure gradients across the span of the blade which causes flow between annular elements which is not taken into account in the standard BEM method and corrects for assumption 1. Further description of the correction factors is in appendix C.1.

A pseudo code of the BEM method used to compute the loads is given in Algorithm 4. This algorithm is based on algorithm presented by Hansen [2008].

Algorithm 4 BEM.m

```

1: procedure COMPUTE THE LOADS ON THE BLADE
2:   Initialize convergence criteria
3:   while Diffa > tolerance || Diffat > tolerance do
4:     Compute flow angle by (4.2)
5:     Compute angle of attack by (4.3)
6:     Interpolate  $C_L$  and  $C_D$ 
7:     Compute  $C_n$  by (4.6)
8:     Compute  $C_t$  by (4.7)
9:     Compute Tip loss correction
10:    Compute Hub loss correction
11:    Compute correction for heavily loaded rotors
12:    Compute Diff
13:    Compute Diffat
14:  end while
15:  Compute the loads,  $F_n$  and  $F_t$ 
16: end procedure

```

This algorithm has shown to be very robust when computing loads on blades with aerodynamically efficient design and operated within normal operational conditions. However, the algorithm has shown convergence issues for aerodynamically inefficient designs and when using control values outside normal operational procedure, which is not a problem as those designs are not of interest to this study.

Having the loads on the blade at each annular element allows to compute the power output of the blade. It is assumed that the load varies linearly between the centres of the annular elements. The shear forces, V , acting on the blade are defined as

$$\frac{dV_n}{dr} = -F_n \quad \text{and} \quad \frac{dV_t}{dr} = -F_t \quad (4.10)$$

Using the shear forces the moment, M , on the blade is found as

$$\frac{dM_n}{dr} = -F_n \quad \text{and} \quad \frac{dM_t}{dr} = -F_t \quad (4.11)$$

As the moment acting on the blade has been defined it is possible to compute the power output, P , as

$$P = N_B \Omega M_t \quad (4.12)$$

A pseudo code of the power computation for a given turbine design is given in Algorithm 5

Algorithm 5 BEMPower.m

- 1: **procedure** COMPUTE THE POWER OF THE TURBINE
 - 2: Compute the moment by 4.11
 - 3: Compute the power by 4.12
 - 4: **end procedure**
-

The main concept and theory of the BEM method has been presented above, for more detailed information on the derivation see [Hansen, 2008], [Sørensen, 2016] and [Molnar and Albertsson, 2016].

4.2 Validation of Optimum Power Curve Computation

The optimum power curve during ramp up is computed by using a 1D line search method, the golden section method, to compute the optimum power on all wind interval boundaries. The method of computing the optimum power curve is described in further detail in subsection 3.2.2. To validate that the implemented method is providing the true optimum power curve a comparison is made with the whole solution space of the power of the NREL 5MW turbine. Thus for a baseline the power curves have been computed for a set of wind speeds using fine discretisation and the optimum power curve then found by connecting the maximum power of the computed wind speeds. Comparison of the optimum curve found from the full solution space versus the optimum curve found by the implemented method is shown in figure 4.4. The black lines on the figure are the power curves for fixed wind speeds, the red line is the baseline optimum power curve found by taking the maximum value for each of the fixed wind speed power curves and the blue asterisks are the points of optimum power for each wind speed computed by the implemented method.

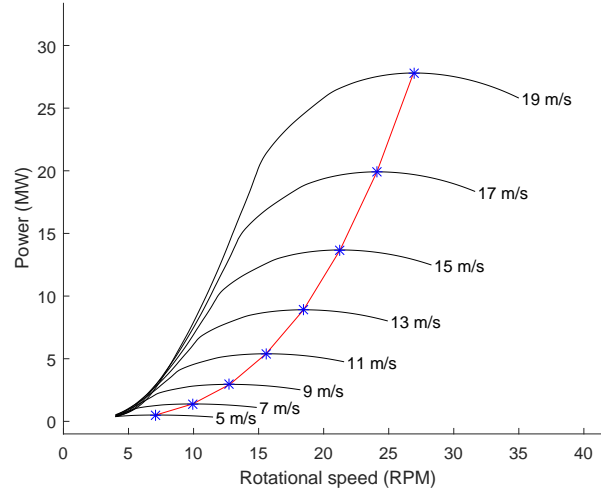


Figure 4.4: *Validation of optimum power computation*

There is excellent correlation between the baseline optimum power curve as can be seen on the figure. Those results show that the implemented method is capable of providing valid results for the optimum power curve that is used for the AEP computation in the following computations.

4.3 Validion of AEP Computation

It is necessary for good optimization results that the AEP computation gives reliable results, thus the BladeOpt results will be validated against verified results.

The AEP for both the baseline and for BladeOpt is computed by (3.2). Power data used for the baseline AEP is published power data of steady state response of the 5 MW NREL turbine [Jonkman et al., 2005], whereas the method of computing the power curve in BladeOpt is described in detail in subsections 3.2.2.

The same Weibull distribution is used for the baseline case and in BladeOpt. The shape factor, k , used in the Weibull distribution is 2 and the scale factor, A , is 8.5. Those Weibull factors are equivalent to Weibull factors from Horns Rev Fyrskib in Denmark [Troen and Petersen, 1989].

The red line in figure 4.5 shows the Weibull distribution used for the computation, the cyan line shows the published power curve for the NREL blade, the power curve computed by BladeOpt using control setup 1 is shown in green and finally, the power curve computed by BladeOpt using control setup 2 is shown in blue.

Close-up of the difference between the power curves in Figure 4.5 is shown in Figure 4.6.

From the figures above it can be seen that there is slightly higher power output from both BladeOpt control setups during ramp up. Those results are in full agreement with what has previously been documented in phase one of this work where the power during ramp up was up to 5% more in BladeOpt [Molnar and Albertsson, 2016]. This deviation originates from the fact that the NREL turbine response is computed with Aerodyn, which uses more advanced

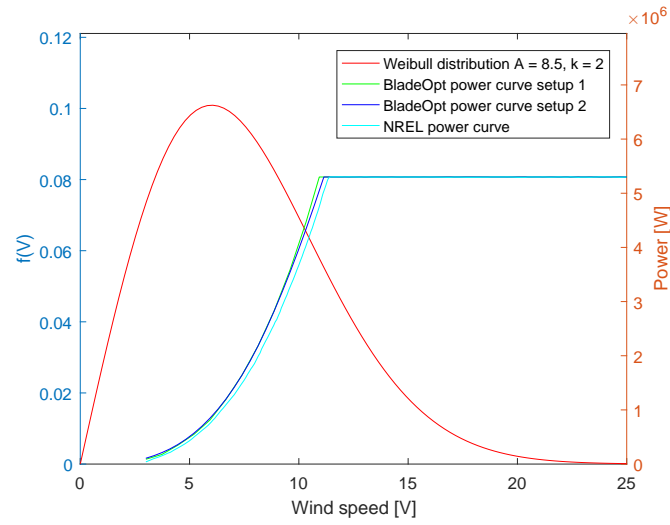


Figure 4.5: *Power curves and Weibull distribution used for validation of AEP computation*

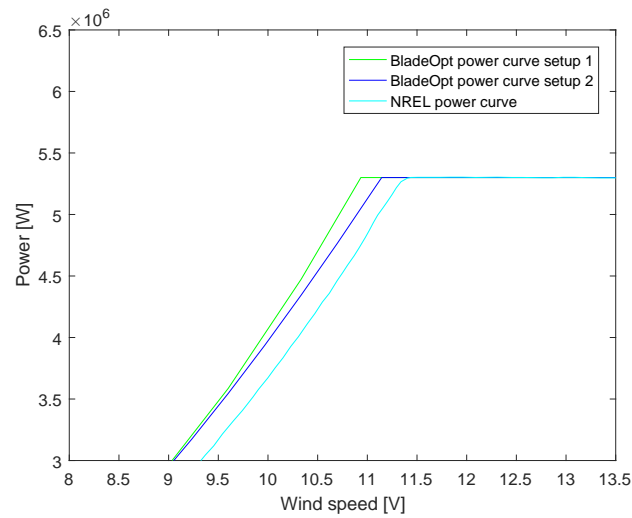


Figure 4.6: *Close up of power curves for comparison*

model and takes more flow states into account [Moriarty and Hansen, 2005].

AEP computed using the power curves and the Weibull distribution presented in figure 4.5 is listed in table 4.1.

	NREL	BladeOpt setup 1	BladeOpt setup 2
AEP (GWh)	17.846	18.887	18.794
Deviation (%)		5.83	5.31

Table 4.1: *Comparison of AEP between baseline data and BladeOpt*

It can be seen in the table above that the AEP computed by BladeOpt is close to 6% higher for control setup 1 then the baseline data and just over 5% for control setup 2. Seeing this deviation is very understandable based on the previously mentioned differences in the codes that compute the loads on the blade. This deviation is therefore in accordance with what is expected of the implemented model in this case.

CHAPTER 5

STRUCTURAL ANALYSIS

During the development of BladeOpt, the structural computation from phase one was changed over to finite element analysis. In FEM the structure is discretised into small segments, called elements. These elements are defined by nodes and specific interpolation functions. The fully continuous field quantities are approximated by finite number of nodal quantities and piecewise interpolation within elements. For each element, characteristic matrices and vectors are formulated, based on the problem specific governing equations and the element type. These matrices are assembled into global matrices, which represent the whole structure. Applying the appropriate boundary conditions, the algebraic system of equations for the whole system can be solved. Thus, the approximated field quantities are obtained. Although, a FEM analysis does not provide exact solution to the problem, the results converge, as the discretized model represents the structure more accurately. There are many available element types, which are specialized for different applications. Thus, it is necessary to fully understand the investigated problem, before the element type is chosen. The primary task of the structural analysis is to efficiently obtain the deflections, strains and eigen-frequencies of the blade. Although a full scale solid or shell finite element model of the blade could provide detailed information about the blade's structural behaviour, it is computationally inefficient to implement for the defined optimization problem. 3-D beam elements are convenient to apply, since the necessary structural responses can be captured and the sensitivities can be computed efficiently. The 3-D beam elements are based on the assumptions of linear elasticity, which assumes small rotations and displacements in the structure. Due to the small deformations the axial, bending, and torsional problems can be decoupled and looked separately [Cook et al., 2002].

5.1 Finite Element Analysis

The classical two node beam element is chosen for the analysis of the wind turbine blade, since the implementation of this element is straightforward and the analysis is computationally efficient. Considering that the blade is a long and slender structure, the transverse shear deformation can be neglected. Thus, the Bernoulli-Euler beam theory is applicable to use to describe the bending of the beam. The Bernoulli-Euler beam theory assumes, that; the straight cross sections remain straight after deformation, the transverse normals do not elongate, transverse normals rotate such that they remain perpendicular to the center line, moreover the internal energy of beam member is only due to bending strains and stresses. The torsional deformation of the elements is assumed to be governed by Saint-Venant torsional principle, which assumes that every cross section rotates as rigid body and cross sections are free to extend in the direction of the axis where the torque is applied. Moreover, the warping is assumed to be constant along the length of the element.

5.1.1 3-D Beam Elements

The development of the element is based on Olesen [2009]. A general beam section is presented, with the used coordinate system and the components of the internal force and moment vectors, in figure 5.1. The internal axial force is denoted as F_x and the shear forces are denoted as F_y

and F_z , respectively. The internal torsional moment and bending moments are represented as M_x , M_y and M_z , respectively.

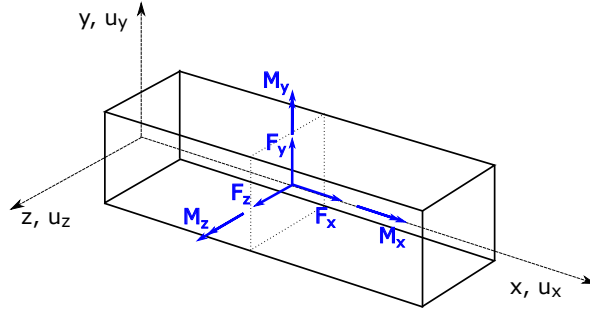


Figure 5.1: A general beam section

Generalized stresses and generalized strains can be introduced, as the quantities that are conjugate terms in the determination of the internal work of deformation [Olesen, 2009]. The generalized stresses $\{\tilde{\sigma}\}$ are collected in a vector, as:

$$\{\tilde{\sigma}\} = \{F_x \ M_x \ M_y \ M_z\}^T \quad (5.1)$$

The generalized strains $\{\tilde{\epsilon}\}$ can be expressed, as:

$$\{\tilde{\epsilon}\} = \{\epsilon_x \ \kappa_x \ \kappa_y \ \kappa_z\}^T \quad (5.2)$$

where ϵ_x represents the longitudinal strain of the beam axis, κ_x represents the twist of the beam, κ_y and κ_z represents the curvature of the beam axis in the (x,z) and (x,y) planes, respectively. The generalized displacements of the beam section are expressed, as:

$$\{\tilde{u}\} = \{u_x \ u_y \ u_z \ \theta_x \ \theta_y \ \theta_z\}^T \quad (5.3)$$

where θ_x is the angle of twist of the beam axis, θ_y and θ_z are the rate of deflections defined, as:

$$\theta_y = \frac{-du_z}{dx}, \quad \theta_z = \frac{du_y}{dx} \quad (5.4)$$

Using that the strains are related to the displacements as $\{\tilde{\epsilon}\} = [\partial] \{\tilde{u}\}$, the generalized strains can be expressed from the displacements:

$$\{\tilde{\epsilon}\} = \left\{ \frac{du_x}{dx} \quad \frac{d\theta_x}{dx} \quad -\frac{d^2u_z}{dx^2} \quad \frac{d^2u_y}{dx^2} \right\}^T \quad (5.5)$$

The relation between the stresses and strains can be expressed for linear elastic materials as:

$$\{\tilde{\sigma}\} = [E] \{\tilde{\epsilon}\} \quad (5.6)$$

where $[E]$ denotes the material stiffness matrix, which can be expressed, as:

$$[E] = \begin{bmatrix} EA & 0 & 0 & 0 \\ 0 & GI_x & 0 & 0 \\ 0 & 0 & EI_y & 0 \\ 0 & 0 & 0 & EI_z \end{bmatrix} \quad (5.7)$$

where E represents the elastic modulus of the material and G the shear modulus. I_x is the torsional moment of inertia of the beam cross section, I_y and I_z the principal moment of inertia of the cross section around y and z axes, respectively. The torsional moment of inertia for circular cross sections is equal with the polar moment of inertia J .

The beam can be exposed to generalized loads, which can be introduced as the quantities that are conjugate terms in the determination of the external work. The generalized loads can be expressed as:

$$\{\tilde{q}\} = \begin{Bmatrix} q_x \\ q_y \\ q_z \\ m \end{Bmatrix} \quad (5.8)$$

where q_x , q_y and q_z represent the distributed loads in x , y and z directions, respectively, while m_x denotes the distributed moment around the x axis of the beam. The relation between the generalized loads $\{\tilde{q}\}$ and the generalized stresses $\{\tilde{\sigma}\}$ can be found by writing the equilibrium equations for an infinitely small part of the beam for the axial, bending, and torsional problems separately. The field quantities $\{\tilde{u}\}$, $\{\tilde{\epsilon}\}$ can be interpolated within an element using interpolation (shape) functions. These interpolation functions are polynomial in order to provide a continuous field over the element.

The 3-D beam element, figure 5.2, has 2 nodes at each end of the element, each with 6 degrees of freedom, 3 degrees of freedom describes the translational and 3 the rotational movements. The twelve degrees of freedom's of the element are collected in the element degrees of freedom vector as:

$$\{d_e\} = [d_1 \ d_2 \ d_3 \ d_4 \ d_5 \ d_6 \ d_7 \ d_8 \ d_9 \ d_{10} \ d_{11} \ d_{12}]^T \quad (5.9)$$

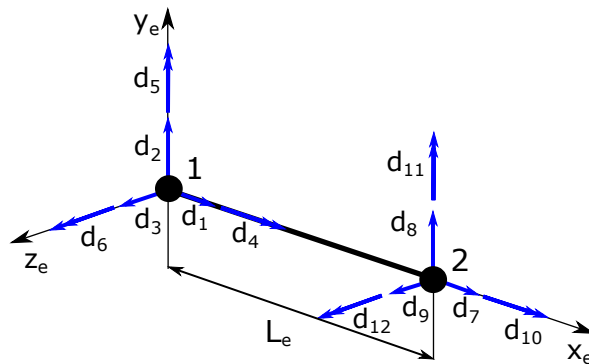


Figure 5.2: Degrees of freedom of the 3-D beam element

The shape functions, $[N]$, for the two node 3-D beam element, can be seen in the appendix D, (D.3) - (D.8). Using these functions the displacement field, $\{\tilde{u}\}$, can be approximated at any arbitrary point within the element volume from the element degrees of freedom, $\{d_e\}$, as:

$$\{\tilde{u}\} = [N] \{d_e\} \quad (5.10)$$

Introducing deflection and rotation field approximations into (5.5), the following relation is obtained:

$$\{\tilde{\epsilon}\} = \left[\frac{d}{dx} [N_{u_x}] \quad \frac{d}{dx} [N_{\theta_x}] \quad -\frac{d^2}{dx^2} [N_{u_z}] \quad \frac{d^2}{dx^2} [N_{u_y}] \right]^T \{d_e\} = [B] \{d_e\} \quad (5.11)$$

where the $[B]$ is called the strain - displacement matrix. The expressions for $[N_{u_x}]$, $[N_{\theta_x}]$, $[N_{u_z}]$ and $[N_{u_y}]$, as well as, for the strain-displacement matrix for the 3-D beam element can be seen in appendix D, (D.11) - (D.14). Similarly to the displacement field, velocity $\{\dot{u}\}$ and acceleration $\{\ddot{u}\}$ fields can be approximated at any arbitrary point within the element volume, by the shape functions and the velocity and acceleration values of the degrees of freedom.

5.1.2 Element Matrices

The governing equation of the static problem can be derived from the principle of virtual work, see appendix D. The equilibrium equation of a static structural problem in matrix form is expressed for the elements as:

$$[k_e] \{d_e\} = \{r_e\} \quad (5.12)$$

where $[k_e]$ is the element stiffness matrix, $\{r_e\}$ is the element load vector and $\{d_e\}$ is the nodal degrees of freedom in the element coordinate system (x_e, y_e, z_e) . The algebraic equations for the stiffness matrix and consistent load vector can be found in appendix D, (D.19) and (D.20). Solving the algebraic equation of the stiffness matrix for the 3-D beam element, the following expression is obtained:

$$[k_e] = \begin{bmatrix} X & 0 & 0 & 0 & 0 & 0 & -X & 0 & 0 & 0 & 0 & 0 \\ & Y_1 & 0 & 0 & 0 & Y_2 & 0 & -Y_1 & 0 & 0 & 0 & Y_2 \\ & & Z_1 & 0 & -Z_2 & 0 & 0 & 0 & -Z_1 & 0 & -Z_2 & 0 \\ & & & S & 0 & 0 & 0 & 0 & 0 & -S & 0 & 0 \\ & & & & Z_3 & 0 & 0 & 0 & Z_2 & 0 & Z_4 & 0 \\ & & & & & Y_3 & 0 & -Y_2 & 0 & 0 & 0 & Y_4 \\ & & & & & & X & 0 & 0 & 0 & 0 & 0 \\ & & & & & & & Y_1 & 0 & 0 & 0 & -Y_2 \\ & & & & & & & & Z_1 & 0 & Z_2 & 0 \\ & & & & & & & & & S & 0 & 0 \\ & & & & & & & & & & Z_3 & 0 \\ & & & & & & & & & & & Y_3 \end{bmatrix} \quad (5.13)$$

sym.

where

$$X = \frac{EA}{L_e} \quad Y_1 = \frac{12EI_z}{L_e^3} \quad Y_2 = \frac{6EI_z}{L_e^2} \quad Y_3 = \frac{4EI_z}{L_e} \quad Y_4 = \frac{2EI_z}{L_e} \quad (5.14)$$

$$S = \frac{GJ}{L_e} \quad Z_1 = \frac{12EI_y}{L_e^3} \quad Z_2 = \frac{6EI_y}{L_e^2} \quad Z_3 = \frac{4EI_y}{L_e} \quad Z_4 = \frac{2EI_y}{L_e} \quad (5.15)$$

A is the cross sectional area and J is the polar moment of inertia. L_e is the length of the element. An element with non-uniform, linearly changing, distributed loads can be seen in figure 5.3.

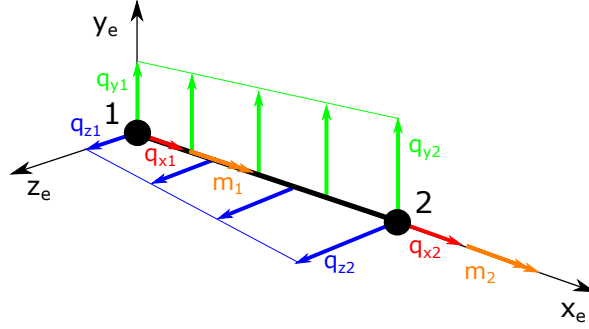


Figure 5.3: *Non-uniform linearly changing distributed loads on a 3-D beam element*

where q_{x1} , q_{y1} , q_{z1} , m_1 are the values of the distributed axial, bending and torsional loads at node 1, while q_{x2} , q_{y2} , q_{z2} , m_2 are the values of the distributed axial, bending and torsional loads at node 2. The consistent element load vector is obtained, as:

$$\{r_e\} = \left\{ \begin{array}{l} \frac{2q_{x1} + q_{x2}}{6} L_e \\ \frac{7q_{y1} + 3q_{y2}}{6} L_e \\ \frac{7q_{z1} + 3q_{z2}}{6} L_e \\ \frac{2m_1 + m_2}{6} L_e \\ -\left(\frac{q_{z1}}{20} + \frac{q_{z2}}{30}\right) L_e^2 \\ \left(\frac{q_{y1}}{20} + \frac{q_{y2}}{30}\right) L_e^2 \\ \frac{q_{x1} + 2q_{x2}}{6} L_e \\ \frac{3q_{y1} + 7q_{y2}}{6} L_e \\ \frac{3q_{z1} + 7q_{z2}}{6} L_e \\ \frac{m_1 + 2m_2}{6} L_e \\ \left(\frac{q_{z1}}{30} + \frac{q_{z2}}{20}\right) L_e^2 \\ -\left(\frac{q_{y1}}{30} + \frac{q_{y2}}{20}\right) L_e^2 \end{array} \right\} \quad (5.16)$$

The governing equation of a linear structural dynamics problem can be derived from the equation of motion, see appendix D. For a free undamped system, it is expressed for each

element in matrix form, as:

$$[m_e] \{\ddot{d}_e\} + [k_e] \{d_e\} = \{0\} \quad (5.17)$$

where $[m_e]$ is the mass matrix and $\{\ddot{d}_e\}$ is the acceleration of the nodal degrees of freedom. To accurately represent the continuous mass distribution of the elements at the discrete points, consistent mass matrix formulation, (D.28), is used. The consistent mass matrix for the 3-D beam element is calculated as:

$$[m_e] = m \begin{bmatrix} \frac{1}{3} & 0 & 0 & 0 & 0 & 0 & \frac{1}{6} & 0 & 0 & 0 & 0 & 0 \\ \frac{13}{35} & 0 & 0 & 0 & \frac{11L_e}{210} & 0 & \frac{9}{70} & 0 & 0 & 0 & \frac{-13L_e}{420} \\ \frac{13}{35} & 0 & 0 & \frac{-11L_e}{210} & 0 & 0 & \frac{9}{70} & 0 & \frac{-13L_e}{420} & 0 & 0 \\ \frac{I_y + I_z}{3A} & 0 & 0 & 0 & 0 & 0 & 0 & \frac{I_y + I_z}{6A} & 0 & 0 & 0 \\ \frac{L_e^2}{105} & 0 & 0 & 0 & \frac{-13L_e}{420} & 0 & \frac{-L_e^2}{140} & 0 & 0 & 0 & 0 \\ \frac{L_e^2}{105} & 0 & \frac{13L_e}{420} & 0 & 0 & 0 & 0 & 0 & \frac{-L_e^2}{140} & 0 & 0 \\ \frac{1}{3} & 0 & 0 & 0 & 0 & 0 & 0 & 0 & 0 & 0 & 0 \\ \frac{13}{35} & 0 & 0 & 0 & 0 & 0 & 0 & 0 & 0 & \frac{-11L_e}{210} & 0 \\ \frac{13}{35} & 0 & 0 & 0 & 0 & 0 & 0 & 0 & \frac{11L_e}{210} & 0 & 0 \\ \frac{I_y + I_z}{3A} & 0 & 0 & 0 & 0 & 0 & 0 & 0 & 0 & 0 & 0 \\ \frac{L_e^2}{105} & 0 & 0 & 0 & 0 & 0 & 0 & 0 & 0 & 0 & 0 \\ \frac{L_e^2}{105} & 0 & 0 & 0 & 0 & 0 & 0 & 0 & 0 & 0 & 0 \end{bmatrix} \quad (5.18)$$

sym.

where m is the mass of the element.

5.1.3 Coordinate Transformation

The matrices and vectors presented above are applicable in the local coordinate system (x_e, y_e, z_e) of the element, figure 5.4. To build the structure size matrices, first, these element matrices need to be transformed to the global coordinate system (x, y, z) .

The transformation is performed, by applying coordinate transformation, on the element matrices and vectors. The transformation matrix is constructed as:

$$[T]_{12 \times 12} = \begin{bmatrix} [\Lambda] & 0 & 0 & 0 \\ 0 & [\Lambda] & 0 & 0 \\ 0 & 0 & [\Lambda] & 0 \\ 0 & 0 & 0 & [\Lambda] \end{bmatrix} \quad (5.19)$$

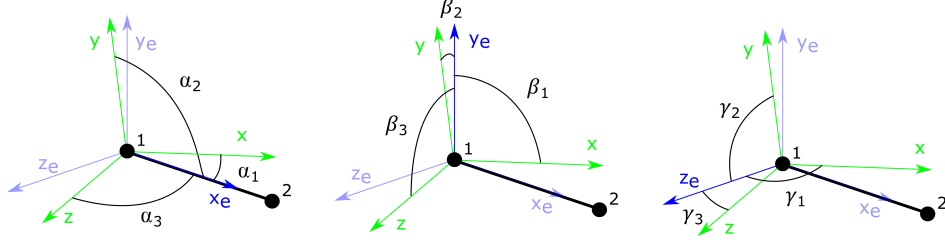


Figure 5.4: Global and element coordinate systems

where the transformation matrix $[\Lambda]$ is:

$$[\Lambda] = \begin{bmatrix} l_1 & m_1 & n_1 \\ l_2 & m_2 & n_2 \\ l_3 & m_3 & n_3 \end{bmatrix} = \begin{bmatrix} \cos\alpha_1 & \cos\alpha_2 & \cos\alpha_3 \\ \cos\beta_1 & \cos\beta_2 & \cos\beta_3 \\ \cos\gamma_1 & \cos\gamma_2 & \cos\gamma_3 \end{bmatrix} \quad (5.20)$$

where l_1, m_1, n_1 are the cosines of the angles between x_e and x, y, z , respectively. l_2, m_2, n_2 are the cosines of the angles between y_e and x, y, z and l_3, m_3, n_3 are the cosines of the angles between z_e and x, y, z . For the blade analysis the element axis x_e and the global axis x are aligned, hence (5.20) can be simplified, as:

$$\Lambda = \begin{bmatrix} 1 & 0 & 0 \\ 0 & m_2 & n_2 \\ 0 & m_3 & n_3 \end{bmatrix} \quad (5.21)$$

The element matrices and vectors are calculated in the global coordinate system as:

$$[k] = [T]^T [k_e] [T] \quad (5.22)$$

$$\{r\} = [T]^T \{r_e\} \quad (5.23)$$

$$\{d\} = [T]^T \{d_e\} \quad (5.24)$$

$$[m] = [T]^T [m_e] [T] \quad (5.25)$$

5.1.4 Assembly of the Elements

To represent the whole structure, it is necessary to appropriately assemble the element matrices and vectors, taking into account that each node is a connector to which elements are attached. Assembly of elements and load terms produces a set of equations, stating that each node within the structure is in equilibrium [Cook et al., 2002]. The description of the assembly procedure can be seen in appendix D.

5.1.5 Solution Procedure

Static displacement Analysis The governing equation for static equilibrium of the structure is expressed as:

$$[K] \{D\} = \{R\} \quad (5.26)$$

where $[K]$ is the global stiffness matrix, $\{R\}$ is the global load vector and $\{D\}$ contains the degrees of freedom of the entire structure. Once the global matrices and vectors are fully assembled, the boundary conditions are necessary to be defined. (5.26) can be partitioned, as:

$$\begin{bmatrix} [K_{11}] & [K_{12}] \\ [K_{21}] & [K_{22}] \end{bmatrix} \begin{Bmatrix} \{D_x\} \\ \{D_c\} \end{Bmatrix} = \begin{Bmatrix} \{R_c\} \\ \{R_x\} \end{Bmatrix} \quad (5.27)$$

where subscript x represents the unknown quantities while c represents prescribed quantities. For a cantilever beam the degrees of freedoms of the supported node $\{D_c\}$ are zero. Hence, knowing the loading condition of the beam $\{R_c\}$ the global displacements $\{D_x\}$ can be obtained, as

$$[K_{11}] \{D_x\} = \{R_c\} \quad (5.28)$$

where $[K_{11}]$ is a sub-matrix of the stiffness matrix $[K]$, which corresponds to the unknown degrees of freedoms. To solve (5.28) directly for $\{D_x\}$, the stiffness matrix $[K_{11}]$ needs to be factorized. Using LU factorization $[K_{11}]$ is decomposed to the product of $[L]$ and $[U]$, as:

$$[K_{11}] = \begin{bmatrix} \nearrow & 0 \\ L & \searrow \end{bmatrix} \begin{bmatrix} \nearrow & U \\ 0 & \searrow \end{bmatrix} = [L][U] \quad (5.29)$$

Substituting (5.29) into (5.26) and defining a helping vector $\{V\}$, as $\{V\} = [U] \{D_x\}$ the following expression is obtained:

$$[L] \{V\} = \{R_c\} \quad (5.30)$$

By forward substitution the helping vector $\{V\}$ can be determined. Knowing $\{V\}$ the displacement vector $\{D_x\}$ can be obtained by backward substitution. Thus, the global displacement vector $\{D\}$ is known.

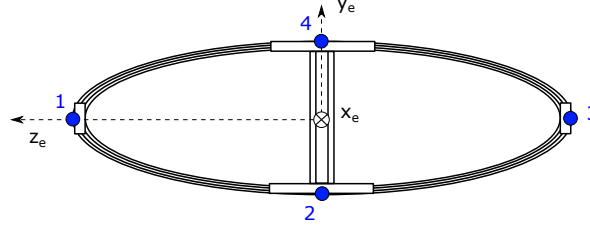
Strain Analysis To obtain the strains, first the element displacement vectors are extracted from $\{D\}$. The element vectors are transformed back into the element coordinate systems, using that:

$$\{d_e\} = [T] \{d\} \quad (5.31)$$

The strain field $\{\tilde{\epsilon}\}$ is obtained by (5.11), at the nodes. The maximum strain values are located at the maximum distances from the center, figure 5.5. To calculate the local strains at these points, the following expression is used:

$$\epsilon_{q_m} = \epsilon_{x_{q_m}} + \kappa_{z_{q_m}} y_{q_m} + \kappa_{y_{q_m}} z_{q_m}, \quad \text{where } m = (1, 2, 3, 4) \quad (5.32)$$

where y_{q_m} and z_{q_m} are the corresponding coordinate values of point 1, 2, 3, 4 in figure 5.5 at cross section q where the strain is evaluated. $m = [1,3]$ denotes the edgewise strains and $m = [2,4]$ denotes the flapwise strains.


 Figure 5.5: *Maximum strain locations in the cross section*

Free Vibration Analysis The governing equation for a free undamped, linear vibration problem is expressed as:

$$[M] \{\ddot{D}\} + [K] \{D\} = \{0\} \quad (5.33)$$

where $[M]$ is the global mass matrix, $[K]$ is the global stiffness matrix and $\{\ddot{D}\}$ is the global acceleration vector, $\{D\}$ is the global displacement vector. The solution for such a system of equations is given by the harmonic vibrations:

$$\{D\} = \{\phi\} \sin \omega t \quad (5.34)$$

$$\{\ddot{D}\} = -\omega^2 \{\phi\} \sin \omega t \quad (5.35)$$

where $\{\phi\}$ is the nodal amplitudes and ω is the angular frequency. Substituting (5.34) and (5.35) into (5.33), the generalized eigenvalue problem is obtained:

$$([K] - \lambda_n [M]) \{\phi_n\} = \{0\} \quad (5.36)$$

where $\lambda_n = \omega_n^2$. The number of eigenvalues n is equal to the number of degrees of freedom of the system. Hence, for a structure having a large number of degrees of freedom solving $\det([K] - \lambda_n [M]) = 0$ is inefficient or even impossible. For structural analysis, usually a set of the lowest eigen frequencies is important. A subset of eigenvalues can be extracted in case of symmetric $[K]$ and $[M]$ matrices using, e.g. Lanczos Algorithm.

The eigenvectors, $\{\phi\}$, that correspond to different eigenfrequencies ω_i and ω_j are orthogonal w.r.t. both stiffness and mass matrices. This orthogonality can be expressed, as:

$$\{\phi\}_i^T [K] \{\phi\}_j = 0, \quad i \neq j \quad (5.37)$$

$$\{\phi\}_i^T [M] \{\phi\}_j = 0, \quad i \neq j \quad (5.38)$$

5.2 Implementation of FEM calculations in BladeOpt

The Finite Element calculations in BladeOpt are implemented based on the above presented theory. The stiffness, mass and transformation matrices are coded using the symbolic tool in

Matlab. Substituting the cross sectional properties of each element, the element matrices in global coordinate system are computed. Since the loads obtained by the BEM calculations are already defined in the global coordinate system, the global load vectors are directly obtained. The element matrices and load vectors are constructed and the global matrices and vector are assembled. Applying the boundary conditions of a cantilever beam, the deformation field is obtained. From the deformation field, the strains are evaluated. To extract the subset of eigenvalues, the Matlab in built function *eigs* is used. The *eigs* function uses a variant of the Lanczos Algorithm, see more Matlab [2017].

Algorithm 6 FEMStructural.m

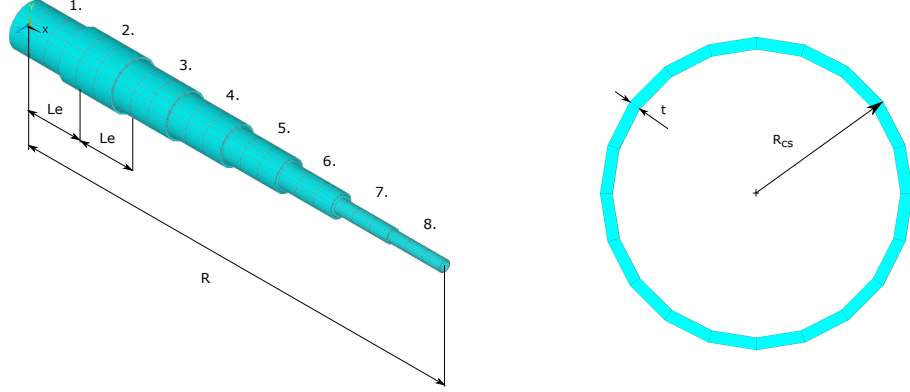
```

1: procedure CALCULATE THE STRUCTURAL RESPONSES OF THE BLADE
2:   for  $i = 1 : N_{element}$  do
3:     Evaluate  $[k]$  by (5.13) and (5.22).
4:   end for
5:   Assemble  $[K]$ .
6:   for  $i = 1 : N_{element}$  do
7:     Evaluate  $\{r\}$  using (5.16).
8:   end for
9:   Assemble  $\{R\}$ .
10:  Apply boundary conditions to obtain  $\{D_x\}$ ,  $[K_{11}]$ ,  $\{R_c\}$ .
11:  Compute  $\{D_x\}$  by using backslash operator in Matlab, as  $[K_{11}] \setminus \{R_c\}$ .
12:  Subtract  $\{d\}$  from  $\{D\}$  and obtain  $\{d_e\}$  using (5.31).
13:  for  $i = 1 : N_{element}$  do
14:    Evaluate  $[B]$  by (D.15).
15:  end for
16:  for  $i = 1 : N_{element}$  do
17:    Obtain  $\{\tilde{e}\}$  using (5.11).
18:    Compute  $\epsilon_{q_m}$  at the cross sections, (5.32).
19:  end for
20:  for  $i = 1 : N_{element}$  do
21:    Evaluate  $[m]$  by (5.18) and (5.25).
22:  end for
23:  Assemble  $[M]$ .
24:  Obtain 3 lowest eigenvalues  $\lambda_n$  and corresponding eigenvectors  $\{\phi_n\}$  using eigs.
25:  Sort  $\lambda_n$  in descendent order.
26: end procedure

```

5.3 Validation of the FEM calculations

To validate the Finite Element calculations, a validation study is conducted. A cantilever beam model, figure 5.6, is implemented in ANSYS APDL and in BladeOpt.

Figure 5.6: *Model for validation*

In ANSYS, BEAM188 element is selected to construct the model. This element is a two node beam element based on Timoshenko beam theory, thus includes the effects of transverse shear deformation. Every node on the beam is associated with circular cross section that are varying both in radius R_{cs} and thickness t . In ANSYS the circular shapes are approximated with 20 points, figure 5.6 to calculate the cross sectional properties, while in BladeOpt analytical expressions are used. 8 different sections are defined on 8 line segments with equal length $L_e = 10 \text{ m}$, where $e = 1, \dots, 8$. Each segment has piecewise constant properties. The segments are divided into 3 equal elements along the length, thus the models are constructed in total 24 elements. The dimensions of the implemented models are summarized in table 5.1.

Section ID	R_{cs} [m]	t [m]
1.	3.8	0.3
2.	4.3	0.3
3.	3.8	0.3
4.	3.3	0.3
5.	2.7	0.2
6.	2	0.2
7.	1.2	0.2
8.	1	0.1
R	80 [m]	

Table 5.1: *Dimensions of the model*

In BladeOpt the materials are assumed to be homogeneous and linear elastic along the spanwise direction of the blade. Thus, for the validation example Aluminium 6061-T6 material is applied, the material properties are summarized in table 5.2.

	Modulus of Elasticity	Shear Modulus	Density	Poisson's Ratio
Aluminium 6061-T6	69 GPa	26 GPa	2700 kg/m ³	0.33

Table 5.2: *Aluminium material properties*

The loading condition is defined to imitate the actual axial load on a wind turbine blade. The equation of the distributed applied load can be described as:

$$q_y(x) = \frac{-2000000}{R}x \quad (5.39)$$

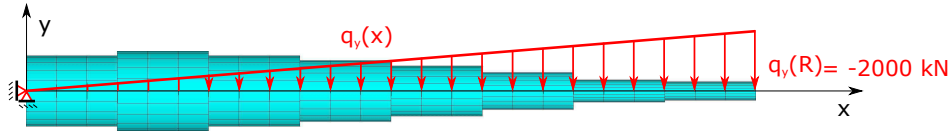


Figure 5.7: *Model for validation*

Due to the fact, that the Timoshenko beam includes the effect of transverse shear deformation the element is expected to behave softer, than the Bernoulli-Euler beam, in BladeOpt. The displacements results, obtained from ANSYS and BladeOpt, are plotted in figure 5.8.

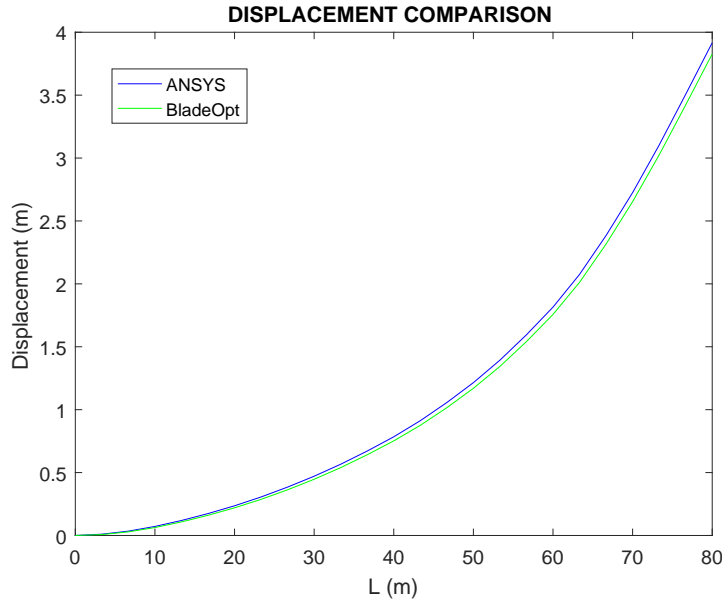


Figure 5.8: *Displacement curves*

The displacements are summarized in table 5.3.

It can be seen that, the displacement results from ANSYS are larger, than the results from BladeOpt, as it is expected. The absolute error is large at the first elements and decreases along the blade, which shows that the transverse shear deformation can be neglected in case of long and slender beams. The maximum strain values, in BladeOpt, are obtained at the middle of the elements and compared to ANSYS element strains, in table 5.4.

Node number	ANSYS [m]	BladeOpt [m]	Absolute Error [%]
1.	0	0	0
2.	0.0103	0.0073	28.5422
3.	0.0345	0.0287	16.9260
4.	0.0719	0.0631	12.1623
5.	0.1192	0.1079	9.4619
6.	0.1741	0.1603	7.9170
7.	0.2360	0.2197	6.8809
8.	0.3061	0.2871	6.1949
9.	0.3847	0.3631	5.6170
10.	0.4710	0.4468	5.1343
11.	0.5664	0.5393	4.7741
12.	0.6712	0.6415	4.4373
13.	0.7844	0.7520	4.1311
14.	0.9124	0.8755	4.0403
15.	1.0567	1.0157	3.8840
16.	1.2147	1.1698	3.7002
17.	1.3934	1.3437	3.5689
18.	1.5953	1.5412	3.3920
19.	1.8151	1.7571	3.1972
20.	2.0752	2.0120	3.0473
21.	2.3844	2.3165	2.8477
22.	2.7254	2.6534	2.6419
23.	3.1031	3.0244	2.5350
24.	3.5065	3.4222	2.4028
25.	3.9166	3.8276	2.2712

Table 5.3: *Comparison of displacement results*

Element number	ANSYS [10^{-2}]	BladeOpt [10^{-2}]	Absolute Error [%]
1.	0.4959	0.4958	0.0202
2.	0.4639	0.4639	0
3.	0.4322	0.4321	0.0231
4.	0.3086	0.3085	0.0324
5.	0.2847	0.2846	0.0351
6.	0.2611	0.2610	0.0383
7.	0.3091	0.3090	0.0324
8.	0.2798	0.2797	0.0357
9.	0.2514	0.2513	0.0398
10.	0.3024	0.3022	0.0661
11.	0.2667	0.2665	0.0750
12.	0.2326	0.2324	0.0860
13.	0.4374	0.4370	0.0914
14.	0.3707	0.3703	0.1079
15.	0.3085	0.3081	0.1297
16.	0.4761	0.4752	0.1890
17.	0.3768	0.3759	0.2389
18.	0.2878	0.2868	0.3475
19.	0.6447	0.6417	0.4633
20.	0.4397	0.4366	0.7050
21.	0.2719	0.2687	1.1769
22.	0.3730	0.3641	2.3861
23.	0.1453	0.1360	6.4006
24.	0.0293	0.0196	33.1058

Table 5.4: *Comparison of maximum strain results per elements*

The strain results shows good correlation at the beginning of the beam, while towards the end the relative error increases rapidly. This difference can be due to the differences in the Timoshenko and Bernoulli-Euler beam formulations.

To validate the frequency calculations, the five lowest eigen frequencies are compared in table 5.5.

Frequency	ANSYS [Hz]	BladeOpt [Hz]	Absolute Difference [%]
1.	2.2136	2.2637	2.2645
2.	2.2136	2.2637	2.2645
3.	5.8054	6.0583	4.3569
4.	5.8054	6.0583	4.3569
5.	11.864	12.9756	9.3694

Table 5.5: *Comparison of frequency results*

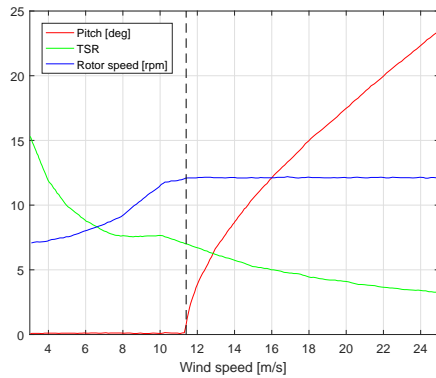
The frequencies from ANSYS are slightly smaller, than the results obtained from BladeOpt. This phenomena can be explained by the different assumptions for the elements.

It can be concluded from the above presented results that the FE calculations in BladeOpt are valid in case of long and slender structures.

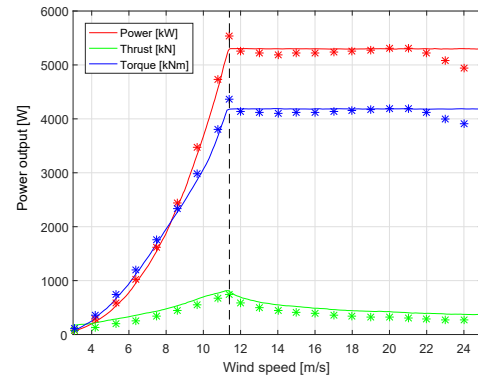
5.4 Validation of the analysis tool

The BladeOpt analysis tool, which contains the BEM and structural calculations is validated against the NREL 5MW reference turbine blade. The blade data and steady state results of the NREL 5MW reference turbine are from Jonkman et al. [2005].

The analyses are executed from cut in condition until cut out condition, see figure 5.9(a), using the originally defined control NREL control set up from Jonkman et al. [2005]. The loads are obtained by BEM analysis, presented in chapter 4 using the 17 aerodynamically defined cross sections, defined in chapter 2 table 2.2, and the control parameters presented in figure 5.9(a). The results of the BEM calculation can be seen in figure 5.9(b), marked with asterisks.



(a) Input for the BEM calculations.



(b) Operation results using BEM.

Figure 5.9: *BEM analysis results*

It can be seen, that the thrust results obtained by BEM are slightly under the published results, but the difference is equal within the whole operational condition interval. The power and torque results obtained by BEM analysis slightly deviate from the published results at rated wind speed. The reason for this behaviour might be that the NREL uses more advanced analysis tool to obtain the aerodynamic responses. After rated wind the difference becomes minor, then approaching the cut out wind speed the BEM results differ more. This phenomena can be explained by inaccuracy in the BEM calculations at high wind speed condition. It can be assumed that including additional correction factors to the BEM the results would be more accurate. In BladeOpt the implemented control strategies make it possible to evade the overshooting and undershooting problems at the region of rated condition and the cut out conditions, since it is assumed that after the rated power output is reached the power output and rotational speed become constant for the rest of the wind data. The load distribution for rated condition of the blade can be seen in appendix in table C.1.

Two sets of structural analyses are executed using 19 and 49 cross sections to define the

elements, where the last cross sections are used to define the end of the blade. The structural properties of the 49 and 19 cross sections are defined in appendix A, table A.1 and table A.2, respectively. For the analysis conducted with 19 cross sections, the cross sectional properties are linearly interpolated through the originally defined 49 cross sectional properties. For the analysis conducted with 49 cross sections, the loads are linearly interpolated from the BEM analysis. The out of plane (OoP) and in plane (IP) tip deflection results can be seen in figure 5.10, where the solid lines represent the NREL results while '*' show the analysis results using 19 cross sections and '+' shows the analysis results using 49 cross sections.

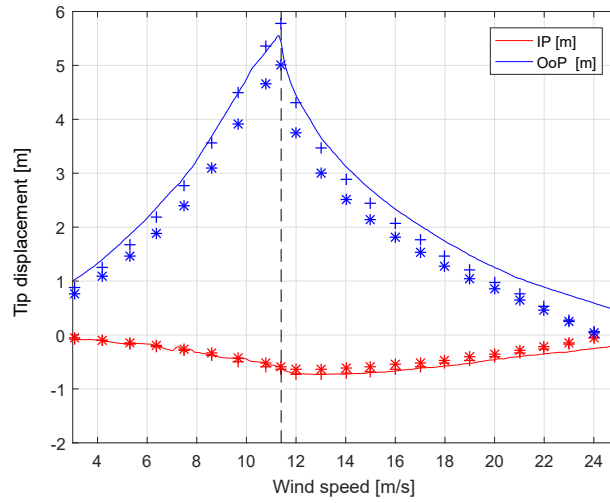


Figure 5.10: *FEM tip displacement results*

It can be seen in figure 5.10, that the overall shape of the tip deflection curves are similar. Using 19 elements to discretize the blade, the tip deflection deviates more from the NREL values than using 49 elements. This phenomena can be explained by the better discretization of the blade. The maximum deviation can be seen in both cases at cut out wind speed, where the BEM load calculations already show differences. The deflection results presented in figure 5.10 do show the same shape and behaviour as it is presented in Molnar and Albertsson [2016], hence changing the structural computation method over to FEM did not change the overall accuracy of the analysis tool. Although, it can be assumed, that having more accurate loads and more elements used for discretization, the tip displacement could be captured accurately, it is preferable for the optimization to have less design variable defined. In the wind turbine industry it is usual to describe a blade with only around 16 - 20 cross sections, hence for the optimization 18 element is implemented.

CHAPTER 6

SENSITIVITY CALCULATIONS

In the field of structural engineering most problems are not linear. Thus, to solve the optimization problems iterative optimization algorithms are usually used. These algorithms start with an initial guess, which is improved iteratively until the optimality conditions are satisfied [Arora, 2012]. Most iterative optimization methods compute the design change by solving a sub-problem in each iteration. Knowing the values and the derivatives of the criterion functions at the current point of the design space, Taylor series expansion can be used to approximate the optimization problem. Based on the order of accuracy of the approximation, different optimization methods can be distinguished such as zero, first and second order methods. Applying a zero order search algorithm can be advantageous, since it might converge to the global minimum of the problem without the need for evaluating gradients. The process is based only on the values of the involved functions. The zero order methods are applicable on any kind of problem, since it is not necessary for the functions to be differentiable or continuous. The drawbacks of the algorithms are, that, they are computationally expensive and do have slow convergence properties. Furthermore, the zero order methods are not suitable for problems with many design variables. If it is possible to evaluate the gradients of the problem efficiently, then deterministic first and second order algorithms might be used to solve the design optimization problem. Using a first or second order algorithm is advantageous, since; it has a low computational cost, it can handle a large amount of design variables, it has good convergence characteristics and it is possible to parallelize the sensitivity calculations. For first and second order algorithms, efficient evaluation of the gradients are necessary and the solver might find only the local optima of the problem. Hence, the optimum solution needs to be further investigated. In case of second order methods the evaluation of the second order derivatives is necessary, which can be impractical for structural optimization problems. Thus, second order derivatives are typically approximated from the first order derivatives.

Several numerical methods are available with different characteristic, for diverse type of optimization problems. Some algorithms work better for certain class of problem than others. Depending on the defined optimization problem, numerical methods for unconstrained and constrained optimization problem can be used.

For the optimization of the blade, a first order method is chosen, considering the large amount of design variables and the possibility to effectively obtaining the necessary gradients. The optimization problem is constrained, hence a numerical method for constrained optimum design is used. The choice of the optimization scheme is described in details in section 7.

6.1 Design Sensitivity Analysis

To find the derivatives of the objective and constraint functions of the optimization problem Design Sensitivity Analysis (DSA) is used. Finding a reliable and efficient method to compute sensitivities is a crucial step in case of first order numerical optimization. In a design optimization problem the state variables $\{U\}$, and design variables x_i , $i = 1, \dots, n$, are coupled through the state equations. This relation is expressed in residual form as:

$$\{R(\{U(\{X\})\}, \{X\})\} = \{0\} \quad (6.1)$$

where $\{R\}$ is the residual vector and $\{X\}$ is the vector of design variables defined, as:

$$\{X\} = \{x_i\}, \text{ where : } i = 1, \dots, N_{DesVar} \quad (6.2)$$

Please note, that the design variable vector is denoted as $\{X\}$ and the design variables as x_i , while the coordinate axis in chapter 5 and 4 is denoted as x . If the cost function or constraints of the optimization problem involve local criteria, then the criterion functions are implicitly depending on the state variables. The general response function \hat{f} can be expressed as:

$$\hat{f} = \hat{f}(\{U(\{X\})\}, \{X\}) \quad (6.3)$$

The aim of the DSA is to find the sensitivities $\frac{d\{U\}}{dx_i}$ efficiently. Here, the notation $\frac{d}{dx_i}$ denotes total derivatives.

The simplest DSA approach is the Finite Difference Method (FDM) [Lund, 2017b]. The FDM is approximating the gradients by executing additional analyses using perturbed design variables. In one hand, the FDM is independent of the implemented solver scheme and can be used on any kind of analysis. On the other hand, the method is computationally inefficient and the obtained gradients are strongly dependent on the perturbation size. Hence, extra studies are necessary to be conducted in order to find the right step size.

A computational more efficient, general approach to obtain the sensitivities in a reliable way is the continuum approach. In the continuum approach, the state equations are differentiated, then the problem is discretized and solved. This way of computing gradients is problem specific and can be difficult to apply on complex analysis problems. Another efficient DSA method is the discrete approach, which is based on differentiation of the discretized equations. FDM can be used to check the gradients obtained by these approaches.

To obtain the gradients of the AEP the FDM is used. The reason for that, is the aerodynamic loads along the blade are computed by an iterative algorithm, described in chapter 4. Although this iterative algorithm contains highly coupled non-linear equations, corrections and interpolation of lift and drag coefficients, it converges within few iteration, for each element of the blade. Hence, sensitivities can be obtained without significant increase in the computational time.

The DSA of the mass is done by simple analytical calculations, while the gradients of the structural constraints are evaluated using a discrete approach.

6.2 Finite Difference Method

FDM can be applied using the forward difference approximation or central difference approximation. The differences between the two methods are the following. The forward difference approximation is estimating the gradient of the response function $\frac{d\hat{f}}{dx_i}$ as:

$$\frac{d\hat{f}}{dx_i} = \frac{\hat{f}(\{U(\{X\} + \Delta x_i)\}, \{X\} + \Delta x_i) - \hat{f}(\{U(\{X\})\}, \{X\})}{\Delta x_i} + \mathcal{O}(\Delta x_i) \quad (6.4)$$

while, the central difference approximation:

$$\frac{d\hat{f}}{dx_i} = \frac{\hat{f}(\{U(\{X\} + \Delta x_i)\}, \{X\} + \Delta x_i) - \hat{f}(\{U(\{X\} - \Delta x_i)\}, \{X\} - \Delta x_i)}{2\Delta x_i} + \mathcal{O}(\Delta x_i^2) \quad (6.5)$$

In both formulas the Δx_i represents the perturbation and $\mathcal{O}(\Delta x_i)$ represents the truncation error. When the derivatives are approximated by any finite difference method, errors are introduced due to the neglected terms in the Taylor series expansion of the perturbed function (truncation error) and due to the computational round-off errors (condition error). Using higher order approximations, the truncation error can be reduced, but the time of evaluating the gradients will increase.

The blade optimization problem includes a large number of design variables and the central difference method requires two times more function evaluations than the forward difference method. Therefore the forward difference method is the chosen method to be used when computing gradients of the AEP due to superiority in computational efficiency.

6.2.1 Implementation of Forward Difference Approximation in BladeOpt

The gradients of the AEP with respect to the design variables are computed in every iteration of the optimization. The gradients are computed by a function that loops through every design variable and the gradient is computed using the appropriate perturbation size for the given design variable. Pseudo code of the procedure is the following.

Algorithm 7 ForwardDifferenceGradient.m

```

1: procedure CALCULATE THE SENSITIVITIES IN BEM USING FORWARD DIFFERENCE
   METHOD
2:   Compute current AEP value,  $AEP(\{X\})$ 
3:   Compute current allowable fatigue strain value,  $\epsilon_c(\{X\})$ 
4:   Compute current tip speed,  $V_{tip}(\{X\})$ 
5:   for  $i = 1 : N_{DesVar}$  do
6:     Compute AEP value for  $AEP(\{X\} + \Delta x_i)$ 
7:     Compute  $\frac{dAEP}{dx_i}$  by (6.4)
8:     Compute fatigue strain value for  $\epsilon_c(\{X\} + \Delta x_i)$ 
9:     Compute  $\frac{d\epsilon_c}{dx_i}$  by (6.4)
10:    Compute tip speed value for  $V_{tip}(\{X\} + \Delta x_i)$ 
11:    Compute  $\frac{dV_{tip}}{dx_i}$  by (6.4)
12:  end for
13: end procedure

```

To account for the change in the aerodynamic loads due to the change in the design variables, the sensitivity of the aerodynamic loads $\{r_{load}\}$ are obtained by forward difference approximations using algorithm 8 as:

Algorithm 8 ForwardDiffLoads.m

```

1: procedure CALCULATE THE SENSITIVITIES OF AERODYNAMIC LOADS USING FORWARD
  DIFFERENCE METHOD
2:   Compute tangential and axial force values  $\{r_{load}(\{X\})\}$ 
3:   for  $i = 1 : N_{DesVar}$  do
4:     Compute tangential and axial force components for  $\{r_{load}(\{X\} + \Delta x_i)\}$ 
5:     Compute  $\frac{d\{r_{load}\}}{dx_i}$  by (6.4)
6:   end for
7: end procedure

```

6.2.2 Perturbation size study

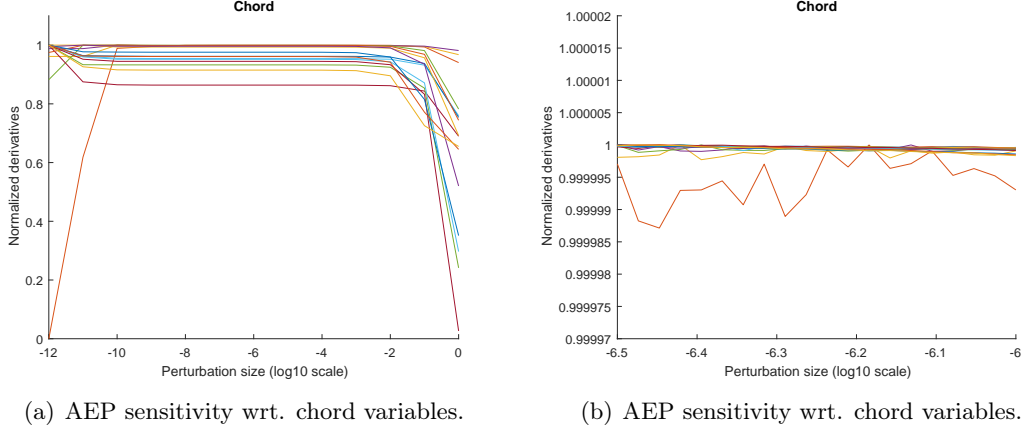
Using finite difference methods it is essential to investigate the choice of perturbation size. Choosing inappropriate perturbation size can result in two types of error as mentioned before, truncation error and condition error. The truncation error is the difference between the exact value and the computed value and is the result of a too large perturbation step, while the condition errors are round-off errors that are the results of a too small step size.

Performing a perturbation size study for the design variables is necessary to be able to identify a range of perturbation size where as accurate as possible gradients are achieved.

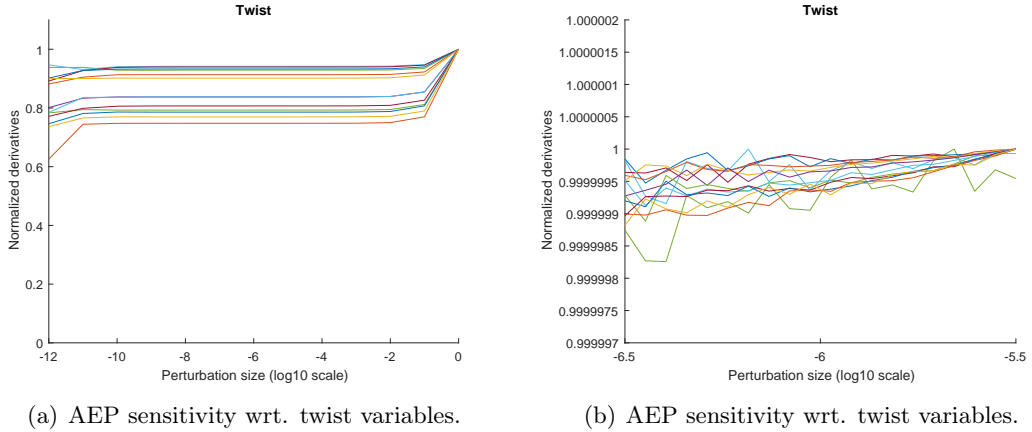
When computing the AEP gradients using forward difference there are three types of design variables involved, those are the chord, twist, and the element length. To find the appropriate perturbation range for each one of those design variables the gradients were initially computed in the interval of $10^{-12} - 1$ to see where the gradients are consistent. After a consistent range has been found the gradients are further analysed by reducing the interval with the aim of finding the range with as high accuracy as possible.

To present the results of the analysis, the gradients for each design variable are plotted as a function of perturbation size with each design variable type on separate figures. Furthermore the gradients of each design variable have been normalized with its largest value in the range being inspected and the perturbation size is displayed on a logarithmic scale.

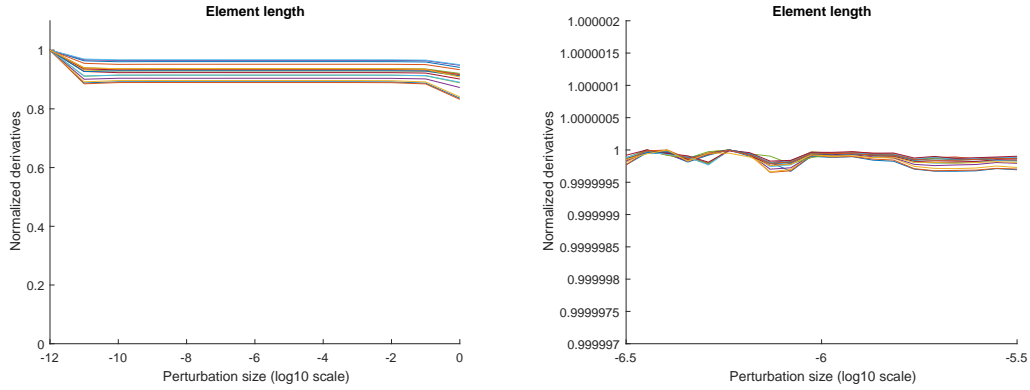
First design variable type to being investigated is the chord. Results from the full range of perturbation size can be seen in figure 6.1(a) where it can be seen that the gradient is rather consistent in the interval of $10^{-10} - 10^{-3}$. Analysing the gradients further it is found that the most consistent range is $3 \cdot 10^{-7} - 10^{-6}$ as is shown in figure 6.1(b).

Figure 6.1: *Sensitivity analysis for chord variables.*

Next design variable type to be investigated is the twist. Results from the full range of perturbation size can be seen in figure 6.2(a) where it can be seen that the gradient is rather consistent in the range of $10^{-10} - 10^{-2}$. Analysing the gradients further it is found that the most consistent interval is $3 \cdot 10^{-7} - 3 \cdot 10^{-6}$ as is shown in figure 6.2(b).

Figure 6.2: *Sensitivity analysis for twist variables.*

Final design variable type to be studied is the element length. The outcome from the full range of perturbation size can be seen in figure 6.3(a) where it can be seen that the gradient is relatively consistent in the range of $10^{-11} - 10^{-1}$. Analysing the gradients further it is found that the most consistent range is the same as for the chord or $3 \cdot 10^{-7} - 3 \cdot 10^{-6}$ as is shown in figure 6.3(b).



(a) AEP sensitivity wrt. element length variables. (b) AEP sensitivity wrt. element length variables.

Figure 6.3: *Sensitivity analysis for element length variables.*

The intervals that have been found to give the most consistent derivatives for the design variables are collected in table 6.1. Furthermore the biggest percentage deviation for each design variable type within the range is listed as well.

Design variable type	Perturbation interval	Biggest deviation [%]
Element length	$3 \cdot 10^{-7} - 3 \cdot 10^{-6}$	$3 \cdot 10^{-5}$
Chord	$3 \cdot 10^{-7} - 1 \cdot 10^{-6}$	$1 \cdot 10^{-4}$
Twist	$3 \cdot 10^{-7} - 3 \cdot 10^{-6}$	$1 \cdot 10^{-4}$

Table 6.1: *Perturbation intervals and accuracy*

All of the design variable types have a large range where the derivatives are relatively accurate. Additionally reduced ranges have been located where the gradients show great accuracy as is seen in table 6.1.

6.3 Discrete Approach

To obtain the gradients of the structural constraints the forward difference method would be computationally inefficient to apply. Implementing the finite element analysis to compute the structural responses of the blade, a computationally more efficient gradient calculation can be utilized. In BladeOpt, the gradients of the structural analysis are obtained by using the discrete approach. The discrete approach can be applied using either direct differentiation method or adjoint method. The direct differentiation method requires the solution of (6.1) for each design variable x_i , while the adjoint method eliminates the need for evaluating the derivative of $\frac{d\{U\}}{dx_i}$ for each design variable by involving the solution of an adjoint formulation for each general response function. The choice of the most efficient approach depends on the properties of the considered problem. When the number of criterion functions is less than the number of design variables, the adjoint method is more efficient to use [Lund, 2017b].

For the structural optimization of the blade, sensitivities of the constraints on the out of plane tip displacement $\frac{du_{tip}}{dx_i}$, cross sectional strains $\frac{d\epsilon_m}{dx_i}$, and eigenvalues $\frac{d\lambda_k}{dx_i}$ are necessary to compute. To obtain the strain gradients, first, the displacement gradients need to be evaluated at each cross section of the blade. Hence, the direct differentiation method is convenient to apply. To obtain the gradients of the displacements by direct differentiation method, the static linear equilibrium governed by (5.26) needs to be differentiated w.r.t. the design variables x_i as:

$$[K] \frac{d\{D\}}{dx_i} = -\frac{\partial [K]}{\partial x_i} \{D\} + \frac{\partial \{R\}}{\partial x_i} \quad (6.6)$$

The factorized stiffness matrix $[K]$ from the structural analysis can be reused for the DSA calculations of all displacement gradients. The right hand side of (6.6) is computed on element level as:

$$-\frac{\partial [K]}{\partial x_i} \{D\} + \frac{\partial \{R\}}{\partial x_i} = -\sum_{e=1}^{N_i^e} \frac{\partial [k_g]}{\partial x_i} \{d_g\} + \sum_{e=1}^{N_i^e} \frac{\partial \{r_g\}}{\partial x_i} \quad (6.7)$$

where $\frac{\partial [k_g]}{\partial x_i}$ is the gradient of the element stiffness matrix in global coordinate system, $\{d_g\}$ the element displacement vector in the element coordinate system and $\frac{\partial \{r_g\}}{\partial x_i}$ is the gradient of the element load vector in global coordinate system. N_i^e is the number of elements, which are affected by the design variable x_i . $\frac{\partial [k_g]}{\partial x_i}$ is calculated analytically, while $\frac{\partial \{r_g\}}{\partial x_i}$ is calculated as:

$$\frac{\partial \{r_g\}}{\partial x_i} = \frac{\partial \{r_{grav}\}}{\partial x_i} + \frac{\partial \{r_{aload}\}}{\partial x_i} \quad (6.8)$$

where $\frac{\partial \{r_{grav}\}}{\partial x_i}$ is the gradient of the load vector due to the gravitational loads, while $\frac{\partial \{r_{aload}\}}{\partial x_i}$ is the gradient of the load vector due the aerodynamic loads. The first term is calculated using analytical calculations, while the second is obtained by FDM described by algorithm 8. Once the right hand side of (6.6) is built, $\frac{d\{D\}}{dx_i}$ can be calculated by solving the linear system of equations where the factored stiffness matrix $[K]$ is reused. From $\frac{d\{D\}}{dx_i}$, the $\frac{du_{tip}}{dx_i}$ can be extracted. Based on the computed global displacement sensitivities, strain gradients can be determined for each cross section at each point of interest. To compute strain gradients, first the element displacement sensitivities need to be extracted from $\frac{d\{D\}}{dx_i}$ and transformed to the element local coordinate systems. To do that, (5.24) needs to be differentiated w.r.t the design variable x_i , as:

$$\frac{\partial \{d_e\}}{\partial x_i} = \frac{\partial \{d_g\}}{\partial x_i} [T] + \{d_g\} \frac{\partial [T]}{\partial x_i} \quad (6.9)$$

where $\frac{\partial \{d_e\}}{\partial x_i}$ is the sensitivity of the element displacement vector in the element coordinate system and $\frac{\partial [T]}{\partial x_i}$ is the gradient of the transformation matrix of the element. To obtain the strain field gradients, (5.11) needs to be differentiated w.r.t. the design variable x_i as:

$$\frac{\partial \{\tilde{\epsilon}\}}{\partial x_i} = \frac{\partial [B]}{\partial x_i} \{d_e\} + [B] \frac{\partial \{d_e\}}{\partial x_i} \quad (6.10)$$

where $\frac{\partial [B]}{\partial x_i}$ is the sensitivity of the corresponding element strain-displacement matrix. To compute the strain sensitivities at the maximum strain locations (5.32) need to be differentiated w.r.t. the design variable x_i as:

$$\frac{d\epsilon_{q_m}}{dx_i} = \frac{\partial \epsilon_{q_m}}{\partial x_i} + \frac{\partial}{\partial x_i} (\kappa_{z_{q_m}} y_{q_m}) + \frac{\partial}{\partial x_i} (\kappa_{y_{q_m}} z_{q_m}), \text{ where } m = (1, 2, 3, 4) \quad (6.11)$$

To obtain the eigenvalue sensitivities, (5.36) needs to be differentiated w.r.t. the design variable x_i . It is assumed, that all the eigenvalues are well separated i.e. distinct [Lund, 2017b].

$$\frac{d[K]}{dx_i} \{\phi_n\} + ([K] - \lambda_n [M]) \frac{d\{\phi_n\}}{dx_i} - \frac{d\lambda_n}{dx_i} [M] \{\phi_n\} - \lambda_n \frac{d[M]}{dx_i} \{\phi_n\} = \{0\} \quad (6.12)$$

Pre-multiplying (6.12) by $\{\phi_n\}^T$, making use of (5.38) and rearranging the equation, the following expression can be obtained:

$$\frac{d\lambda_n}{dx_i} = \{\phi_n\}^T \left(\frac{d[K]}{dx_i} - \lambda_n \frac{\partial [M]}{\partial x_i} \right) \{\phi_n\} \quad (6.13)$$

where the eigenvectors $\{\phi_n\}$ are $[M]$ orthonormalized as $\{\phi_n\}^T [M] \{\phi_n\} = 1$. The derivative of the mass matrix, $\frac{\partial [M]}{\partial x_i}$, is computed analytically on element level. The stiffness sensitivity, $\frac{\partial [K]}{\partial x_i}$, is reused from the displacement DSA calculations.

The gradient of the mass objective $\frac{dm}{dx_i}$ is calculated by simple analytical calculations as

$$\frac{dMass}{dx_i} = \frac{\partial}{\partial x_i} \left(\sum_{e=1}^{N_i^e} A \rho \right) \quad (6.14)$$

6.3.1 Implementation of Discrete DSA in BladeOpt

The structural gradient calculations in BladeOpt are based on the above presented theories. In the BladeOpt the analytical gradient calculations are coded using the Matlab symbolic tool, hence symbolic gradient matrices and vectors are computed outside of the optimization loop. Thus, the gradients are evaluated by substituting the corresponding values of the effected elements into the symbolic formulas. The implemented algorithms can be seen in algorithm 9 and algorithm 10.

Algorithm 10 DirectDiff.m

```

1: procedure CALCULATE THE SENSITIVITIES OF MASS
2:   for  $j = 1 : N_i^e$  do
3:     for  $i = 1 : N_{DesVar}$  do
4:       Evaluate  $\frac{dm}{dx_i}$ , by (6.14).
5:     end for
6:   end for
7: end procedure

```

6.3.2 Validation of Discrete DSA

To validate the gradients calculated by direct differentiation method, forward difference DSA is executed on the structural analysis, with 10^{-6} perturbation size for each design variables. The maximum absolute differences between the computed sensitivities are summarized in table 6.2.

Algorithm 9 DirectDiff.m

```

1: procedure CALCULATE THE SENSITIVITIES OF STRUCTURAL CONSTRAINTS
2:   Call symbolic gradient functions.
3:   for  $j = 1 : N_i^e$  do
4:     for  $i = 1 : N_{DesVar}$  do
5:       Evaluate  $\frac{\partial [k_g]^j}{\partial x_i}$ .
6:     end for
7:   end for
8:   Build  $\frac{\partial [K]}{\partial x_i}$ .
9:   for  $j = 1 : N_i^e$  do
10:    for  $i = 1 : N_{DesVar}$  do
11:      Evaluate  $\frac{\partial \{r_{grav}\}^j}{\partial x_i}$ , by (6.8).
12:    end for
13:  end for
14:  Build  $\frac{\partial \{R\}}{\partial x_i}$  by (6.8) and evaluate (6.7).
15:  Obtain displacement sensitivities,  $\frac{d\{D\}}{dx_i}$  by (6.6) and extract  $\frac{du_{tip}}{dx_i}$ .
16:  for  $j = 1 : N_i^e$  do
17:    for  $i = 1 : N_{DesVar}$  do
18:      Evaluate  $\frac{\partial [T]^j}{\partial x_i}$ .
19:    end for
20:  end for
21:  Compute element displacement sensitivities by (6.9).
22:  for  $j = 1 : N_i^e$  do
23:    for  $i = 1 : N_{DesVar}$  do
24:      Evaluate  $\frac{\partial [B]^j}{\partial x_i}$ .
25:    end for
26:  end for
27:  Compute  $\frac{\partial \{\tilde{\epsilon}\}}{\partial x_i}$  by (6.10), then  $\frac{d\epsilon_{qm}}{dx_i}$  by (6.11).
28:  for  $j = 1 : N_i^e$  do
29:    for  $i = 1 : N_{DesVar}$  do
30:      Evaluate  $\frac{\partial [m_g]^j}{\partial x_i}$ .
31:    end for
32:  end for
33:  Build  $\frac{\partial [M]}{\partial x_i}$ , then obtain  $\frac{d\lambda_n}{dx_i}$  by (6.13).
34: end procedure

```

Design variable type	Maximum absolute deviation %
$\frac{du_{tip}}{dx_i}$	$3.48 \cdot 10^{-5}$
$\frac{d\epsilon_{x1}}{dx_i}$	$9.79 \cdot 10^{-8}$
$\frac{d\epsilon_{x2}}{dx_i}$	$4.30 \cdot 10^{-7}$
$\frac{d\epsilon_{x3}}{dx_i}$	$9.79 \cdot 10^{-8}$
$\frac{d\epsilon_{x4}}{dx_i}$	$4.30 \cdot 10^{-7}$
$\frac{d\lambda_1}{dx_i}$	$1.06 \cdot 10^{-4}$
$\frac{d\lambda_2}{dx_i}$	$1.99 \cdot 10^{-4}$
$\frac{d\lambda_3}{dx_i}$	$9.32 \cdot 10^{-4}$
$\frac{dm}{dx_i}$	0

Table 6.2: *Maximum Absolute Differences*

CHAPTER 7

OPTIMIZATION SCHEME

To utilize the obtained gradients for solving the optimization problem a gradient based optimization strategy needs to be defined and implemented. Gradient based search methods start with an estimate for the optimum solution, which is improved in each iteration until the optimality condition is satisfied. The new design point in each iteration is computed, as:

$$\{X\}^{(k+1)} = \{X\}^{(k)} + \{\Delta X\}^{(k)}; \quad k = 0, 1, 2, \dots \quad (7.1)$$

where k denotes the iteration number, $\{X\}^{(k)}$ is the current design at iteration number k and $\{\Delta X\}^{(k)}$ represents the design change. Most of the gradient based methods compute the design change based on a search direction, $\{d\}^{(k)}$, and a step size, α_k , as:

$$\Delta \{X\}^{(k)} = \alpha_k \{d\}^{(k)}; \quad k = 0, 1, 2, \dots \quad (7.2)$$

For constrained optimization problems, the constraints must be considered when the search direction and the step size is determined. To compute the design change for a constrained problem, several numerical algorithm have been developed, for example Sequential Linear Programming (SLP), Sequential Quadratic Programming (SQP) and Constrained Steepest-Descent Method (CSDM). In this study, an SLP algorithm is implemented, because it is a simple and straightforward approach to solve constrained optimization problem, especially those having a large number of design variable [Arora, 2012].

7.1 Sequential Linear Programming

In SLP, the design change is computed by solving a sub-problem that is obtained by writing first order Taylor's expansions for the cost and constraint functions [Arora, 2012]. The cost and constraint functions of the optimization problem are linearised, around the design point $\{X\}^{(k)}$ by Taylor's expansion, as:

Minimize:

$$f(\{X\}^{(k+1)}) \cong f(\{X\}^{(k)}) + \{\nabla f\}^T(\{X\}^{(k)}) \{\Delta X\}^{(k)} \quad (7.3)$$

subjected to the equality constraints

$$h_j(\{X\}^{(k+1)}) \cong h_j(\{X\}^{(k)}) + \{\nabla h_j\}^T(\{X\}^{(k)}) \{\Delta X\}^{(k)} = H_j; \quad j = 1, \dots, p \quad (7.4)$$

and the inequality constraints

$$g_j(\{X\}^{(k+1)}) \cong g_j(\{X\}^{(k)}) + \{\nabla g_j\}^T(\{X\}^{(k)}) \{\Delta X\}^{(k)} \leq G_j; \quad j = 1, \dots, m \quad (7.5)$$

and bounds

$$\underline{x}_i \leq x_i^{(k+1)} \leq \bar{x}_i; \quad i = 1, \dots, n \quad (7.6)$$

where $\{\nabla f\}$, $\{\nabla h_j\}$ and $\{\nabla g_j\}$ are the gradient vector of the cost function, the j th equality constraint and the j th inequality constraint, respectively. H_j is the value of the equality constraint while G_j is the upper limit for inequality constraints. \underline{x}_i represents the lower bound while \overline{x}_i represents the upper bound on the i th design variable, x_i .

The linearisation of the problem, defined from (7.3) to (7.6), is only valid in case of small design changes, hence the optimization problem needs to be solved sequentially by linearising the problem around each design point at each iteration. The linearised blade optimization sub-problem can be defined as:

Minimize:

$$\bar{f} = \{c\}^T \{X\}^{k+1} \quad (7.7)$$

subjected to the equality constraints

$$[N]^T \{X\}^{k+1} = \{e\} \quad (7.8)$$

and the inequality constraints

$$[A]^T \{X\}^{k+1} \leq \{b\} \quad (7.9)$$

and bounds

$$\{\underline{X}\} \leq \{X\}^{k+1} \leq \{\overline{X}\} \quad (7.10)$$

where $\{c\}$ is the derivative of the cost function, defined as:

$$\{c\} = \left\{ \nabla f \left(\{X\}^k \right) \right\} \quad (7.11)$$

$[N]$ is the matrix of the equality constraint derivatives,

$$[N] = \begin{bmatrix} \left\{ \nabla h_1 \left(\{X\}^{(k)} \right) \right\}^T \\ \left\{ \nabla h_2 \left(\{X\}^{(k)} \right) \right\}^T \\ \vdots \\ \left\{ \nabla h_p \left(\{X\}^{(k)} \right) \right\}^T \end{bmatrix} \quad (7.12)$$

$\{e\}$ is the vector of equality constraint function values, defined as:

$$\{e\} = \begin{bmatrix} H_1 + \left\{ \nabla h_1 \left(\{X\}^{(k)} \right) \right\}^T \{X\}^{(k)} - h_1 \left(\{X\}^{(k)} \right) \\ H_2 + \left\{ \nabla h_2 \left(\{X\}^{(k)} \right) \right\}^T \{X\}^{(k)} - h_2 \left(\{X\}^{(k)} \right) \\ \vdots \\ H_p + \left\{ \nabla h_p \left(\{X\}^{(k)} \right) \right\}^T \{X\}^{(k)} - h_p \left(\{X\}^{(k)} \right) \end{bmatrix} \quad (7.13)$$

$[A]$ is the matrix of the inequality constraint derivatives,

$$[A] = \begin{bmatrix} \left\{ \nabla g_1 \left(\{X\}^{(k)} \right) \right\}^T \\ \left\{ \nabla g_2 \left(\{X\}^{(k)} \right) \right\}^T \\ \vdots \\ \left\{ \nabla g_m \left(\{X\}^{(k)} \right) \right\}^T \end{bmatrix} \quad (7.14)$$

$\{b\}$ is the vector of inequality constraint function values, defined as:

$$\{b\} = \begin{bmatrix} G_1 + \left\{ \nabla g_1 \left(\{X\}^{(k)} \right) \right\}^T \{X\}^{(k)} - g_1 \left(\{X\}^{(k)} \right) \\ G_2 + \left\{ \nabla g_2 \left(\{X\}^{(k)} \right) \right\}^T \{X\}^{(k)} - g_2 \left(\{X\}^{(k)} \right) \\ \vdots \\ G_m + \left\{ \nabla g_m \left(\{X\}^{(k)} \right) \right\}^T \{X\}^{(k)} - g_m \left(\{X\}^{(k)} \right) \end{bmatrix} \quad (7.15)$$

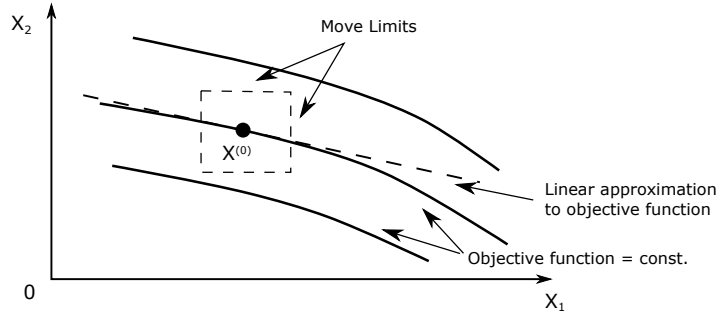
This linearised sub-problem can be solved for $\{X\}^{k+1}$, using Linear Programming (LP) methods, i.e Simplex Method. Drawbacks of the algorithm are that, there is no descent function defined, thus the progress can not be monitored and the problem may become unbounded or oscillating, moreover the method may not converge to the precise minimum.

7.1.1 Move Limit Strategy

In the SLP algorithm, move limits δ_i are defined to restrict the size of the design change. Hence, the linear approximation stays valid and the linearised sub-problem becomes bounded. The move limits define the allowable step size for each iteration, as

$$x_i^k - \delta_i \leq x_i^{k+1} \leq x_i^k + \delta_i \quad (7.16)$$

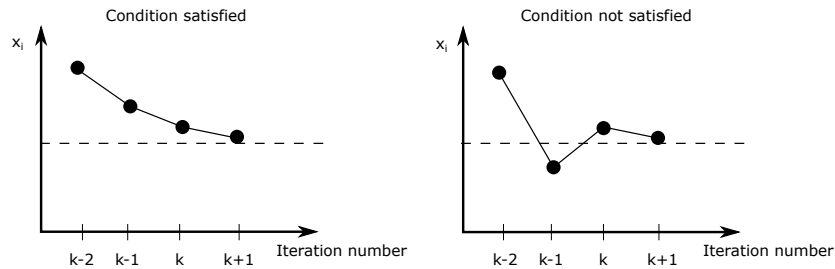
thus there is no need to perform line search calculations. The move limits are defined as a fraction of the current design variable values.


 Figure 7.1: *Move Limits*

Setting the appropriate size for the move limits is crucial for the SLP algorithm. Poor choice of move limits can lead to inaccuracies and may prevent convergence, or increase the time of convergence. Moreover, the method can alter between two vertices, if the solution does not lie at a vertex of a constraint set [Lund, 2017a]. Thus, it is desired to apply a robust move limit strategy to control the behaviour of the optimization. To monitor the progress of the optimization a condition is defined as:

$$cond = \frac{x_i^{k-2} - x_i^{k-1}}{x_i^{k-1} - x_i^k} \geq 0 \quad (7.17)$$

When (7.17) is satisfied, the process behaves well, thus the move limits can be extended or kept constant. Otherwise, oscillation arises, hence the limits need to be reduced. The different condition scenarios are illustrated in figure 7.2.


 Figure 7.2: *Optimization progress*

This method is implemented in a function called `AdaptiveMovelimt`, which has been developed at Aalborg University Lund [2017a]. In the `AdaptiveMovelimt` function, the fraction of the design variable is defined, as *MoveLimit* and a reduction factor is defined as, *Reduction*. The reduction factor is used to relax or tighten the move limits. The `AdaptiveMovelimt` strategy can be seen in algorithm 11.

Algorithm 11 AdaptiveMoveLimit.m

```
1: procedure ADAPTIVEMOVELIMIT
2:   Apply the adaptive move limit strategy
3:   if  $k > 1$  then
4:     for  $i = 1:N_{DesVar}$  do
5:       Compute previously allowable change, by  $\delta_i = (xU_i - xL_i)/2$ 
6:       if  $|x_i^k - x_i^{k-1}| > 10^{-10}$  then
7:         Compute condition by (7.17)
8:         if  $cond < 0$  then
9:           Reduce  $\delta_i$ , as  $\delta_i = \delta_i \cdot Reduction^2$ 
10:        else
11:          Relax  $\delta_i$ , as  $\delta_i = \delta_i / Reduction$ 
12:        end if
13:      end if
14:      Compute  $\delta_{i_{max}} = (\bar{x}_i - \underline{x}_i) \cdot MoveLimit$ 
15:      if  $\delta_i > \delta_{i_{max}}$  then
16:         $\delta_i = \delta_{i_{max}}$ 
17:      end if
18:      Estimate new lower bounds  $xL_i$  and upper bounds  $xU_i$ .
19:      Make sure that  $xL_i \geq \underline{x}_i$  and  $xU_i \leq \bar{x}_i$ .
20:    end for
21:  else
22:    for  $i = 1:N_{DesVar}$  do
23:      Start with  $\delta_i = (\bar{x}_i - \underline{x}_i) \cdot MoveLimit/2$ 
24:    end for
25:    Estimate new lower bounds  $xL_i$  and upper bounds  $xU_i$ .
26:    Make sure that  $xL_i \geq \underline{x}_i$  and  $xU_i \leq \bar{x}_i$ .
27:  end if
28: end procedure
```

For the optimization studies the move limit parameters are defined with numbers in chapter 8.

7.1.2 Convergence requirements

In order to determine if the optimization algorithm has converged to a local minimum, it is necessary to define convergence criteria. In BladeOpt the optimization is converged, when fulfilling the following three convergence criteria. At first, the relative change, *RelChange*, of the design variables must be sufficiently small, which can be calculated, as:

$$RelChange [\%] \leq ConvCrit_1 [\%], \quad \text{where} \quad (7.18)$$

$$RelChange = 100 \cdot \sqrt{\frac{\sum_{i=1}^{N_{DesVar}} ((\{x_i\}^{k+1} - \{x_i\}^k)^2)}{\sum_{i=1}^{N_{DesVar}} ((\{\bar{x}_i\} - \{\underline{x}_i\})^2)}} \quad (7.19)$$

Secondly, the feasibility needs to be at acceptable level. To ensure that, convergence factor, $ConvCrit_2$ is defined. This factor is used to calculate a fraction of the allowable constraint values. To fulfil the second criterion, the following inequalities need to be satisfied for all the constrained values:

$$(1 - ConvCrit_2) \cdot H_j \leq h_j \left(\{X\}^{(k)} \right) \leq (1 + ConvCrit_2) \cdot H_j; \quad j = 1, \dots, p \quad (7.20)$$

$$g_j \left(\{X\}^{(k)} \right) \leq (1 + ConvCrit_2) \cdot G_j; \quad j = 1, \dots, m \quad (7.21)$$

It was necessary to introduce the second criterion, since during the development of BladeOpt it was experienced that the first criteria can be satisfied even in the non feasible region.

The third criterion implies that, the BEM calculations need to be converged at all cross sections along the blade. As stated in chapter 4, the applied BEM solution algorithm does not always converge due to infeasible parameters in the blade design. During the development of the BladeOpt it has been experienced, that this problem can arise in the optimization process. This non-convergence is handled by setting the tangential forces at the non-converging element to zero, hence resulting in zero power output, while the normal forces are set to a very high value, hence resulting in large strains. Thus, it will not be desirable for the optimizer to stay at the non converging region. Even implementing this strategy, it has been seen that the first and second criteria can be satisfied while there is BEM non convergence. To make sure that the finalized design has only converged elements the following criteria is implemented in BladeOpt: whenever the non-convergence occurs the BEM code sends a Boolean parameter, which is monitored through the optimization. If the signal value is 1, the convergence requirement is not satisfied and if it is 0 then the third convergence criterion is fulfilled.

For the optimization studies the convergence parameters are defined with numbers in chapter 8.

7.2 Implementation

Now all necessary building blocks for implementation of the complete optimization scheme are readily available. The optimization problem was formulated in chapter 3, the theory and algorithms to compute the aerodynamic part were defined in chapter 4 and the theory and algorithms to compute the structural part were defined in chapter 5. Furthermore the methods for sensitivity computation were defined in chapter 6 and finally, the formulation of the SLP problem is defined in this current chapter.

The final product is the BladeOpt HAWT optimization program, where all of the previously mentioned theory and methods are used to built up the optimization scheme. The main execution script for the program is shown in Algorithm 12.

Algorithm 12 BladeOpt.m

```
1: procedure MAIN EXECUTION SCRIPT FOR BLADEOPT
  ▷ Preprocessing of the optimization problem
2:   Load user input (initial guess, Weibull parameters, optimization setup etc.)
3:   Load data for material properties and lift and drag coefficients
4:   Set up the design variable (DV) vector
5:   Set upper and lower bounds for DV's as well as perturbation size for forward difference
6:   Check if initial guess is within defined boundaries, notify user if outside boundaries
7:   Define constraints between design variables
8:   Symbolically compute gradients for structural part
  ▷ Start the optimization process
9:   while Convergence criteria is not satisfied do
10:    Find the rotor speed controls by Algorithm 1 or 2
11:    Compute values and gradients of objective and constraints for aerodynamic part,
    loads computed by Algorithm 4, power by Algorithm 5, AEP by Algorithm 3 and
    gradients by Algorithm 7
12:    Compute loads to apply on structural model, using  $\omega_{rated}$  and  $V_{rated} + V_{gust}$  in
    Algorithm 4
13:    Compute gradients of loads by Algorithm 8
14:    Compute values and gradients of objective and constraints for structural part,
    structural responses are computed by Algorithm 6, sensitivities of constraints by
    Algorithm 9 and sensitivities of mass by Algorithm 10
15:    Determine upper and lower bounds using adaptive move limits by Algorithm 11
16:    Define the linear programming problem according to section 7.1
17:    Solve the linear programming problem with linprog Matlab function
18:    Refresh convergence criteria
19:   end for
  ▷ Postprocessing
20:   Plot the blade design
21:   Save the results
22: end procedure
```

CHAPTER 8

STUDIES

In this chapter a baseline design is defined that is used for the optimization studies, moreover the implemented constraints and bounds are summarized numerically. The capabilities of the BladeOpt are presented through five different case studies. In each study the optimization set up is changed. In the first two studies, analyses are conducted using a range of weight factors and the outcomes of the analyses are examined comparing the different results with respect to the weight factors. The third case study is used to present results about purely *AEP* optimization for different power curve set ups. The fourth case study presents a purely aerodynamic and a purely structural optimization where the mass and length of the blade is set to be equal with NREL 5MW turbine blade.

8.1 Baseline Turbine

In this section the steps of developing a feasible baseline design are presented. The constraints for the baseline design are presented symbolically in section 3.9, and with numbers in table 8.3 for the constraints that are not design independent. The baseline turbine is defined utilizing the published data on the NREL 5 MW wind turbine blade from Jonkman et al. [2005]. The baseline turbine is described with 18 cross sections and 18 elements along the length of the blade, with element length L_e . The outer geometry of each cross section is described with 2 design variables Tw and c , while the inner geometry is described with 2 design variables TC_e and TF_e for the circular cross sections in the root region and 8 design variables for the ellipse cross sections in the other regions of the blade. The 8 design variables of the ellipse cross section are presented again for convenience in figure 8.1. In total, the baseline design deals with 174 design variables.

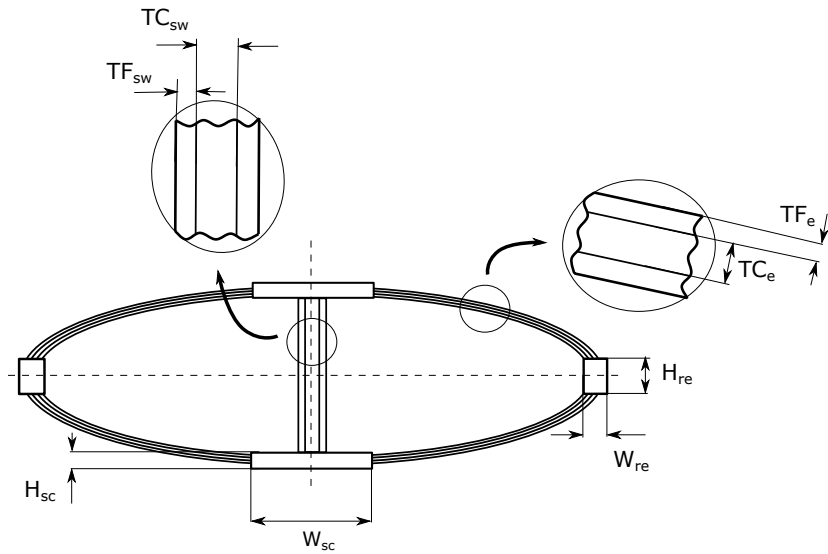


Figure 8.1: *Inner geometry of ellipse cross sections*

The outer geometry parameters of the 18 cross sections and the length of the elements are set to be the same as the 17 defined cross section in table 2.2. Additionally, one circular cross section is defined at the root assuming that the root cross section has the same parameters as the first defined value in table 2.2 only its location is at the root of the blade.

The NREL blade publication does not contain data about the inner cross sectional geometry or the design constraints neither additional information about the used material properties or safety factors. Thus, the following steps have been taken to achieve a feasible baseline design for the optimization studies. Firstly, strict bounds have been set on the outer design parameters $\pm 1\%$ of the NREL blade, then the inner geometry has been defined based on initial guesses. In the faces of the sandwich materials biaxial (biax) glass fibre - epoxy material is used, while in the spar caps unidirectional (UD) carbon fibre - epoxy material is implemented, moreover the edge reinforcements are chosen to be UD glass fibre - epoxy material. The core of the sandwich materials are made from balsa wood. The choice of materials and their locations are based on the selection of materials in the phase one of this project. The properties of the aforementioned materials are taken from ESAComp material database. The implemented materials and their properties are summarized in table 8.1.

Material	E GPa	G GPa	ρ kg/m^3	ϵ_{ult_t} [—]	ϵ_{ult_c} [—]
Biax glass - epoxy	13.66	8.6	2000	not used	n.u.
UD glass - epoxy	45	5	2000	0.0245	-0.015
UD carbon - epoxy	125	15	1220	0.0125	-0.008
Balsa wood	0.0685	0.0270	220	n.u.	n.u.

Table 8.1: *Material properties of the baseline design*

Safety factors are implemented to ensure that the obtained design is on the safety side. For the baseline design and through the case studies the following safety factors are used, and implemented according to (3.13) - (3.15) on the corresponding parameters.

	γ_f	γ_m	γ_n
Defined safety factors	1.25	1.5	1.1

Table 8.2: *Safety factors for the case studies and baseline design*

Secondly, to obtain feasible design a purely structural optimization has been executed. The optimization problem has been symbolically defined in section 3.9. In table 8.3 only the values of the constraints are presented which do not depend on the design.

Parameter	Value
\bar{u}_{tip}	6 m
\bar{V}_{tip}	110 m/s

Table 8.3: *Design independent constraints*

For the baseline design, the weight factors presented in table 8.4 have been implemented. To ensure that the *AEP* does not change constraints are set on the initial *AEP*.

Parameter	Value
w_1	0
w_2	1

Table 8.4: *Weight factors for the baseline design*

For the baseline blade design optimization the power curve set up 2 has been used to ensure that the rated rotor speed is the same as the NREL rated rotor speed. In BladeOpt, constraints between any design variables can be set. The design variable constraints applied for the baseline design and for the case studies are set to ensure feasible design and are based on published planform blade designs and studies found where the planform of the wind turbine is plotted. The design variable constraints are presented in table 8.5.

Design variable	Expression between cross sections
c_q	$c_1 \leq \dots \leq c_6$
c_q	$c_6 \geq \dots \geq c_{18}$
Tw_q	$Tw_1 = \dots = Tw_5$
Tw_q	$Tw_5 \geq \dots \geq Tw_{13}$
W_{sc_q}	$W_{sc_q} \leq 0.3 \cdot c_q$
H_{sc_q}	$H_{sc_q} \leq 0.3 \cdot \frac{c_q}{2} \cdot ratio_q$

Table 8.5: *Design variable constraints*

The chord c of the first 6 cross sections are constrained to ensure a smooth increase from the chord of root to the maximum chord. The maximum chord of the blades are usually between the first two airfoil sections. After the maximum chord is reached the constraints are set between chord design variables to ensure that the chord is continuously decreasing.

The twist Tw of the first 5 cross sections are constrained to be equal. The reason is that the circular cross sections at the root do not contribute to the AEP, hence the twist at the first 4 circular cross section would become zero which is unseen behaviour in the published blade design plots. The reason why the twist is set to equal in root of the seen blade designs can be to ensure a same coordinate system when the fibre materials are placed. Along the middle section of the blade the twist is set to be continuously decreasing. The tip region is not constrained, since it has been seen that the twist at the tip region can have a slight increase towards the tip.

The spar cap W_{sc} and H_{sc} parameters are constrained, to ensure that the spar caps do not grow out from the ellipse in width and that the spar caps do not grow over the small axes of the ellipses.

The parameters of the adaptive move limit and the convergence criteria used during the development of the baseline turbine and in the case studies are summarized in table 8.6 and 8.7.

<i>MoveLimit</i>	<i>Reduction</i>
0.01	0.8

Table 8.6: *Move limit parameters*

The *MoveLimit* has been defined to be 0.01, because it has been seen that the optimization becomes fluctuating for larger move limit values, while using smaller *MoveLimit* the optimization either converges very slow or does not converge.

<i>ConvCrit₁</i>	<i>ConvCrit₂</i>
6%	0.01

Table 8.7: *Convergence parameters*

The baseline design optimization has been terminated as soon as the first feasible design were achieved. The reason for that is through the optimization case studies various constraints on the length of the blade have been implemented and a range of weight factors have been used, hence the aim of the baseline design was neither to have a purely structural optimized structure or to match with the NREL design, but to have a feasible initial design. The general results of the baseline design are summarized in table 8.8.

Design	Rated (MW)	AEP (GWh)	Mass power output (ton)	Rated wind speed (m/s)	Rated rotational speed (rpm)
NREL 5MW blade	5	17.84	17.74	11.4	12.1
Baseline blade	5	18.20	21.16	10.9	12.1

Table 8.8: *Comparison of the baseline design with NREL 5MW design*

It can be seen that the main difference between the overall properties of the NREL 5MW blade and the baseline blade is the mass. Although the mass of the baseline blade is higher than the mass of the NREL blade the design is feasible and can be used to present the capabilities of the BladeOpt through the different optimization case studies. Through the case studies it is presented that the BladeOpt can generate results comparable with the NREL 5MW baseline turbine. The mass, and stiffness distributions of the NREL and baseline blades are plotted in appendix E figure E.1 - E.2. The first three blade eigen frequencies are compared in appendix E table E.1.

The above presented baseline design is used for the all of the optimization studies as starting point or initial guess. Every case study has different aim with the intention to imitate real design situations where the BladeOpt can be used in the future. The studies are named by capital Roman numbers and are the following:

In case study I. it is examined what are the effects of the different weight factors on the design if the length of the blade is constrained and the rated rotational speed is kept constant during the optimization. The outcome is Pareto front that the blade manufacturer can use to pick up a design based on the wanted *AEP* or *Mass*, where all design along the front fulfill the length and rotational speed constraints.

In case study II. it is examined what are the effects of the different weight factors on the design if the length of the blade is not constrained and the rated rotational speed is kept constant during the optimization. The outcome is a Pareto front similar to the one from case study one apart from allowing the change in blade length.

In case study III. it is examined what is the maximum AEP that can be achieved knowing the mass of the blade, using both power curve set up. Thus, this case study presents a fully aerodynamic optimization, that is achieved by setting additional constraint on the mass of the blade. Through this optimization the length of the blade is unconstrained. This case study represent a situation where the allowable load generated by the weight of the blade on the hub and the nacelle of the turbine is known and the blades need to be designed with maximizing the AEP.

In case study IV. it is examined what maximum AEP can be achieved by setting constraint on the mass and the length of the blade to match with the NREL 5MW blade. Moreover what is the minimum mass that can be achieved while the turbine still providing the same AEP as the NREL 5MW blade.

8.2 Design Variable Bounds

To ensure feasible design and bound the design space the values of design variables need to be restricted. To perform that bounds are set on the design variables. In this section the design variable bounds are presented that are used for the optimization studies. These restrictions are set based on gained experience through the development of BladeOpt and the general knowledge summarized through this report.

8.2.1 Bounds on the design variables of the outer geometry

The following bounds are set on the design variables of the outer geometry:

Design variable	Lower bound	Upper bound	Cross section
c_q	0.4 m	6.2 m	q=4,...,18
c_q	0.4 m	3.5 m	q=1
c_q	0.4 m	3.5 m	q=2
c_q	0.4 m	3.8 m	q=3
c_q	0.4 m	4.1 m	q=4
L_e	1 m	6.5 m	e = 1,...,18
Tw_q	-10 °	40 °	q =1,...,18

Table 8.9: *Bounds on the design variables of the outer geometry*

The chord c : is bounded to ensure that the blade can be transported and the chord of the cross sections is not reduced to zero. Upper bounds are set to be 6.2 m on the chord, which is a usual transportation boundary and have been used as boundary in other optimization studies as Zahle et al. [2015]. During the development of BladeOpt it has been experienced that the chord of the root segment grows to the maximum. The reason for that is that second moment of inertia grows in a quartic manner with the radius of the circular cross section, while the mass grows quadratically. Hence, the weight of the root section can be reduced by increasing the radius to be as large as possible while reducing the thickness to be as thin as possible, thus it is necessary to put different upper bounds on the chord at the root region. The upper bounds on the chord of the root segment are defined to match with the chord of the NREL blade root segment. In some optimization cases the chord of the last element converged to zero hence lower bound is set on the corresponding design variable.

The element length L_e : is bounded to ensure that the differences between the smallest and the longest elements are not extremely large. In many optimization cases the elements of the mid region in the blade has converged to the upper bound, which can cause inaccuracy in the results.

The twist Tw : of the cross sections have very wide range of bounds, since during the optimizations the twist did not show any extreme behaviour.

8.2.2 Bounds on the inner geometry design parameters

The following bounds are set on the design variables of the inner geometry:

Design variable	Lower bound [m]	Upper bound [m]
TF_{eq}	0.05	0.6
TC_{eq}	0.02	0.3
W_{scq}	0.01	2
H_{scq}	0.01	0.8
TF_{swq}	0.05	0.1
TC_{swq}	0.02	0.3
H_{req}	0.005	0.2
W_{req}	0.03	0.1

Table 8.10: *Bounds on the design variables of the inner geometry*

The lower bounds on the inner geometry design parameters are set to ensure that all the building blocks of the cross section are presented in all sections. Without setting constraints on the buckling of the sandwich panels the thickness of the core material would be reduced to zero through the optimization, thus minimum bounds need to be set on TC_{swq} and TC_{eq} .

The upper bounds on the inner geometry design parameters are set to ensure that all the building blocks of the cross section are within the boundaries of the ellipse.

8.3 Case Study I.

The purpose of this study is to illustrate the capabilities of BladeOpt of producing a set of results as options for a design with certain constraints. In this case the constraints are all the previously described constraints that apply to all of the studies and also adding a length restriction on the blade. The length of the blade is constraint to the NREL 5 MW blade length of 63m. Furthermore, the rated rotational speed is fixed to the same 12.1 rpm as the NREL 5 MW. To fix the rated rotational speed requires the use of control set up 2. The study is conducted for a range of weight factor w_1 for AEP. The lower bound for the weight factor was limited to 1.4 as lowering the weight factor more resulted in infeasible designs. This occurred as the design went in a direction to try to reduce the loads as much as possible which caused the twist to become really large at the tip and more strict bounds would have been needed to get feasible design. The upper bounds of the weight factor where considered as the point when the weight started to increase to much for little increase in AEP. Figure 8.2 shows a pareto front for varying weight factor w_1 where AEP and $Mass$ have been normalized with the baseline design.

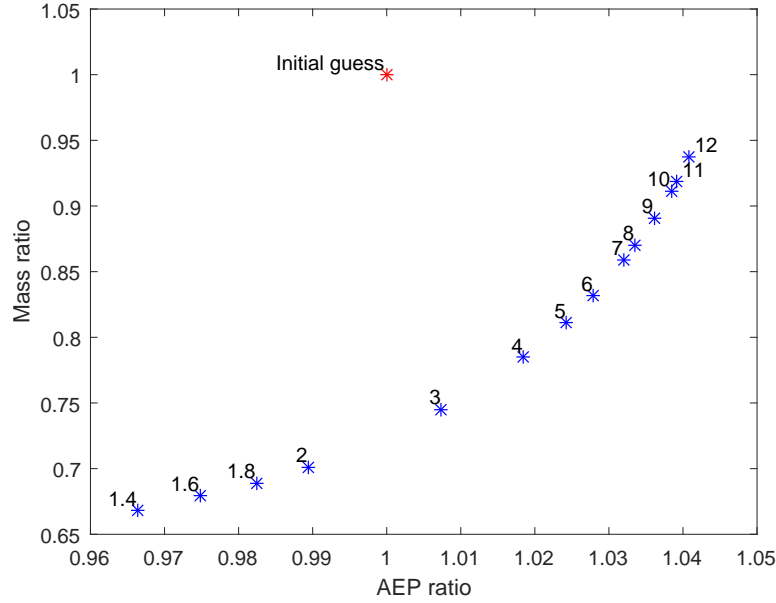


Figure 8.2: *Pareto front with normalized AEP and Mass. The factors associated with each result are the weight factors w_1*

The pareto front on the figure above is as expected as the AEP increases by adding weight on it in the optimization. Furthermore, results from a same purpose study by Zahle et al. [2015] show comparable behaviour where a small increase in AEP requires a much bigger increase in mass at the same time. To take a closer look at how those two performance measures change it is convenient to take a look at the ratio between the AEP and the mass. The AEP/Mass ratio as a function of the weight factor w_1 is presented in figure 8.3.

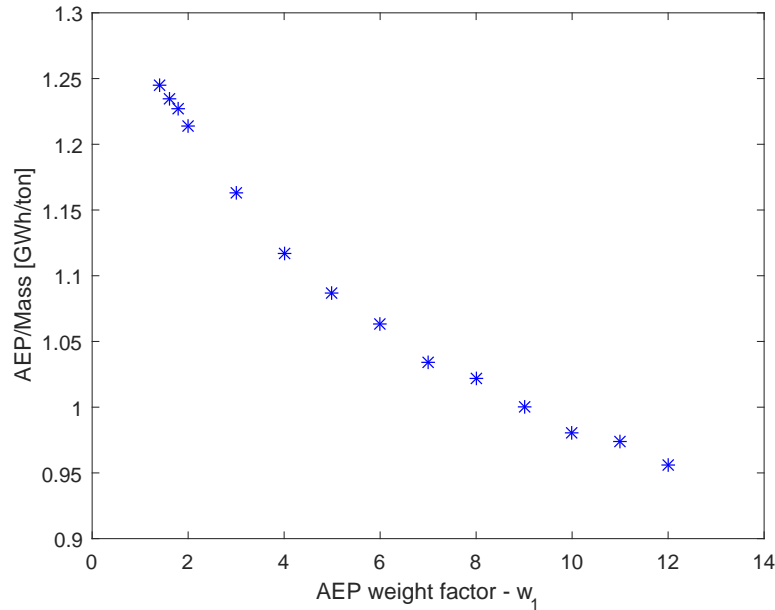


Figure 8.3: *Pareto front for AEP/Mass as a function of the weight factor w_1*

The highest AEP/Mass ratio is achieved by the lowest weight factor as can be seen on the figure above. Furthermore, the slope between the weight factors is steepest for low weight factors and flattens out for higher weight factor due to the more rapid increase in weight. The rated conditions for the designs as a function of the weight factor w_1 are presented in figure 8.4. It can be seen that the rated rotational speed is constant as it is constraint at 12.1

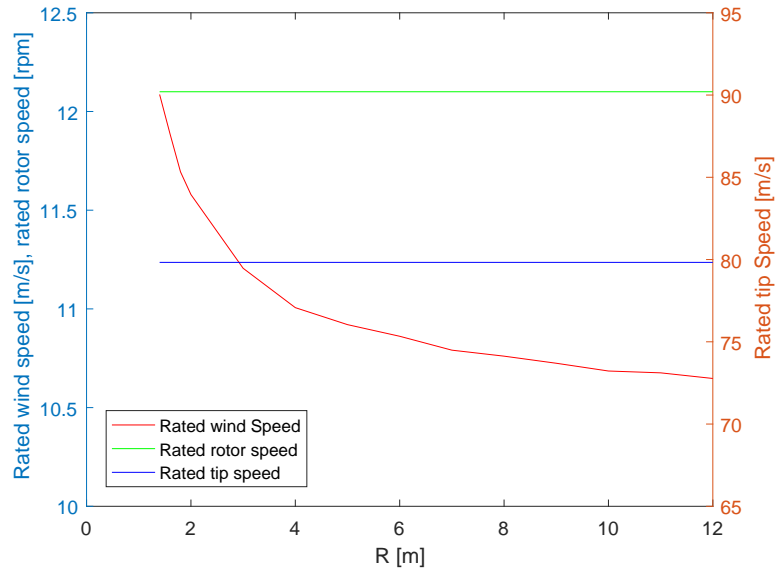


Figure 8.4: *Rated wind speed as a function of the weight factor w_1*

RPM. Furthermore, the rated tip speed is constant as well since both the rated rotational speed and the blade length are fixed. The rated wind speed does on the other hand change as expected. The rated wind speed decreases with higher weight factor as the rated power is achieved earlier with designs that are more driven towards high AEP.

Blade planform for the optimization study is presented in figure 8.5, where chord distribution is shown in figure 8.5(a), twist distribution in figure 8.5(b), ratio distribution in figure 8.5(c) and mass distribution in figure 8.5(d).

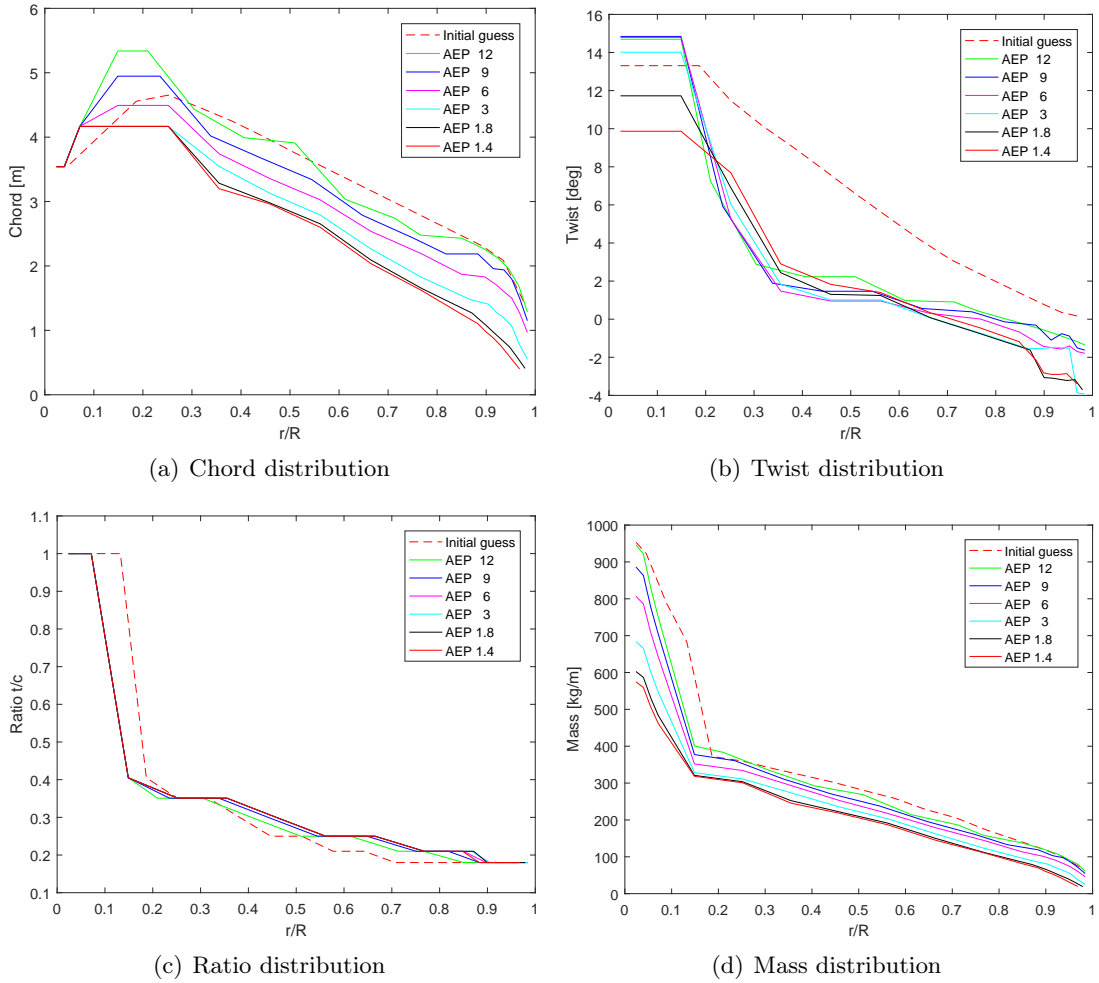


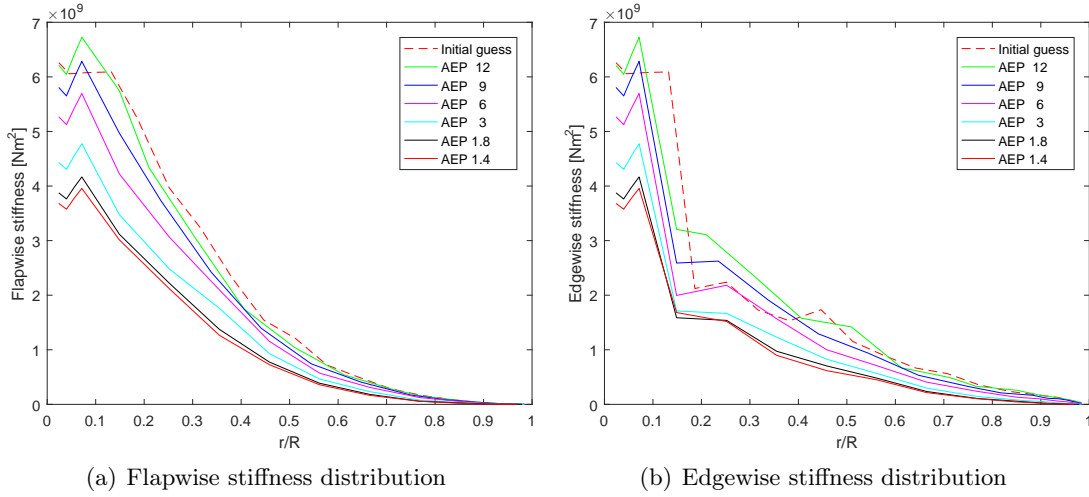
Figure 8.5: *Blade planform for case study I*

Looking at the blade planform plots there are obvious differences seen between design for the chord, twist and mass while the ratio distribution is relatively unchanged between designs. The chord distribution increases for the whole blade for higher weight factor as expected since higher loads are achieved with larger cord which results in increased AEP. The biggest difference in twist can be seen in the root region as the tendency for AEP driven designs is to increase the twist to obtain more power for a greater range of wind speeds. Finally the mass increases dramatically for higher AEP as previously mentioned as the AEP becomes so dominant that the mass has little effect on the objective during optimization.

The final properties to be presented in the study are the flapwise and edgewise stiffness distribution of the designs, they are shown in figures 8.6(a) and 8.6(b) respectively.

The both flapwise and edgewise stiffness increases with increased weight on AEP as expected since chord and mass are higher for those cases. Furthermore, a drop in stiffness is seen at the root which is expected as well since the upper bounds in the root region are always active for all designs.

To get a better idea of some of the behaviour in the design a closer look is taken at the

Figure 8.6: *Stiffness distribution for case study I*

constraints and bounds for the case study. Following is an overview of what bounds and constraints were active during the study.

Constraints: Flapwise strains were always active in the circular root section as the chord narrows towards the rotor and mass is reduced during optimization. The flapwise strains were never active in any other sections of the blade. The edgewise strains were always active in cross section seven and sometimes in the cross sections five and six. The spar cap was constrained so that it would not result in infeasible design. The constraint on the spar cap width was always active in the mid section in the blade for between three to ten cross sections were the constraint was more commonly active for low AEP weight as those are the cases where mass reduction has more effect. The spar cap height constraint became active just at a single cross section at the tip for high weight factor. Finally, 3P frequency constraint and tip speed constraint were never active.

Bounds: The bounds on the twist never became active during the case study. The element length always had some bounds active. Upper bounds of the element length were usually active in the mid region of the blade and more commonly for lower weight factors while lower bounds were always active in the circular cross sections at the root as there is no additional AEP gained from those. Furthermore, upper bound of the chord were always active at the root as well as more stiffness for lower mass can be obtained that way. Lower bounds for the core material in the ellipse were always active as expected since those bounds are used as a penalty parameter to prevent buckling of the outer shell. The thickness of the ellipse faces was always at the lower bound except at the circular cross section as it is the only way that can be used to increase stiffness there while the spar cap is usually increased in other regions to increase stiffness. The spar cap bounds were never active neither the upper or lower bounds, that behaviour is as expected as the bounds on the spar cap are greater than the previously mentioned constraints that have been enforced on them to prevent the design from becoming infeasible. Additionally, the lower bounds of both the core and the face sheets of the shear

web were always active as expected since the bounds were introduced to take the shear load, support the shape of the airfoils and prevent buckling which are things that are not captured with the modelling methods being used. Finally, the lower bounds on the edge reinforcements were always active apart from occasionally single cross section in mid region. That indicates that the edgewise fatigue is not sufficiently taken into account.

Violation of constraints and bounds: During the optimization process it occurs that constraints or bounds are violated for one and one iteration but it was not the case for well behaved optimizations. None of the final designs included violated bounds or constraints which is as expected since it is part of the convergence criteria to ensure that they are not violated.

8.4 Case Study II.

Case study II has a similar aim as case study I. Possible designs for a turbine with a set of constraints are explored by varying the weight of the performance measures for the design. This time the designs are given the freedom of varying the length of the blade while still being constrained to the rated rotor speed of 12.1 rpm as well as the previously listed constraints for the baseline turbine. The outcome of the study gives valuable information about what designs are achievable while still fulfilling the bounds and requirements of the design so that a design can be chosen based on the importance of performance measures. Control set up 2 is used in this study.

The first results to be presented is a pareto front of all of the designs. Figure 8.7 shows a pareto front for varying weight factor w_1 where AEP and $Mass$ have been normalized with the baseline design.

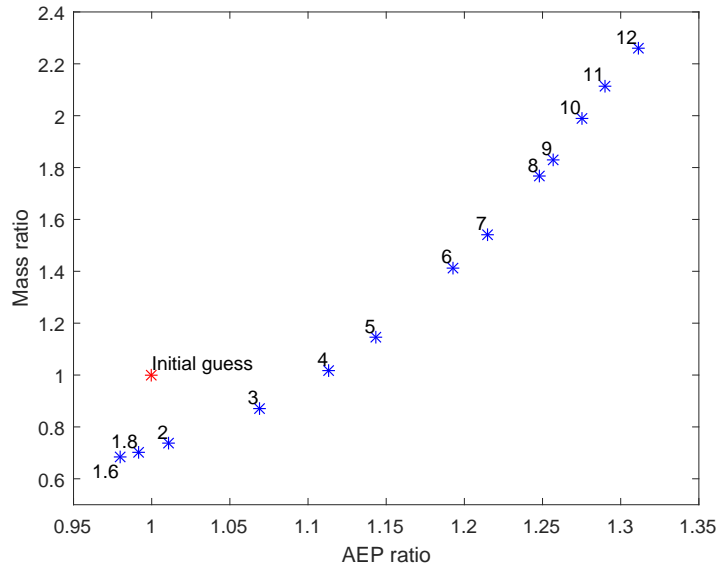


Figure 8.7: *Pareto front with normalized AEP and Mass. The factors associated with each result are the weight factors w_1*

From the pareto front it can be seen right away that allowing the blade length to vary results in a greater range of achievable AEP then seen in case study I. The increased achievable AEP is as expected since the obtainable growth in AEP grows quadratically with blade length as previously mentioned. The increased blade length comes with the price of increased mass as well, where the mass increases faster then the AEP as seen before.

The pareto front for the $AEP/Mass$ ratio as a function of blade length is shown in figure 8.8 to get a clearer picture of what the effect the weight factors have on the blade length and the ratio. It is seen that the highest ratios are obtained for the lowest weight factors as before

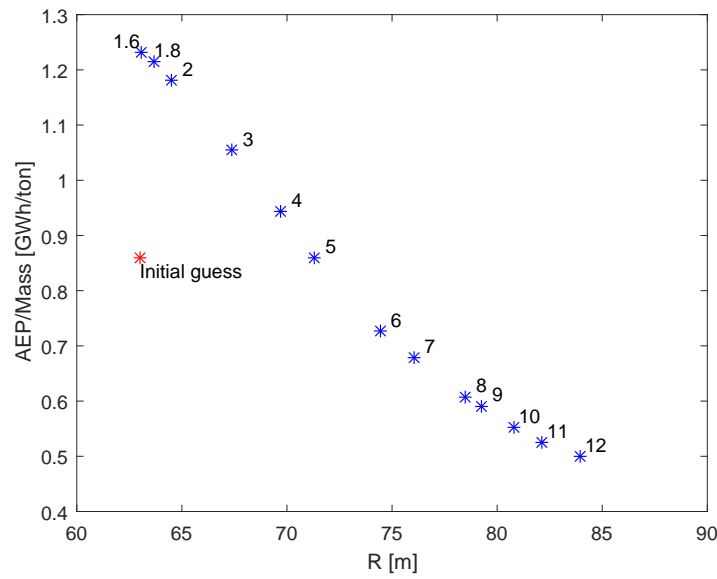


Figure 8.8: *Pareto front for $AEP/Mass$ as a function of blade length. The factors associated with each result are the weight factors w_1*

since the mass reduction contribution becomes more evident. Furthermore, way higher AEP can be obtained but for low ratio as the mass increases so fast with increased length.

Rated conditions, as a function of blade length, for the optimization study are presented in figure 8.9. The rated conditions show much more variability then in case study I as the blade length can vary. The rated wind speed decreases with increased eight factor and increased blade length as the turbine manages to achieve rates power at lower wind speeds then for design with shorter blades. The rated tip speed consequently increases as blade length increases and rated rotational speed is constant but when the blade length gets over 80 m long there is a sudden decrease in rated rotor speed and rated tip speed. This decrease is caused by the fact that the rated power output is actually achieved before the rated rotor speed.

Blade planform for the optimization study is presented in figure 8.10, where chord distribution is shown in figure 8.10(a), twist distribution in figure 8.10(b), ratio distribution in figure 8.10(c) and mass distribution in figure 8.10(d).

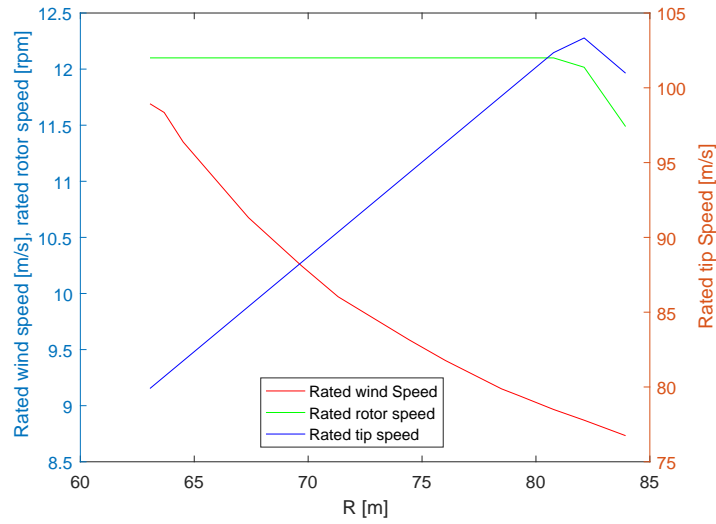


Figure 8.9: *Rated conditions as a function of blade length*

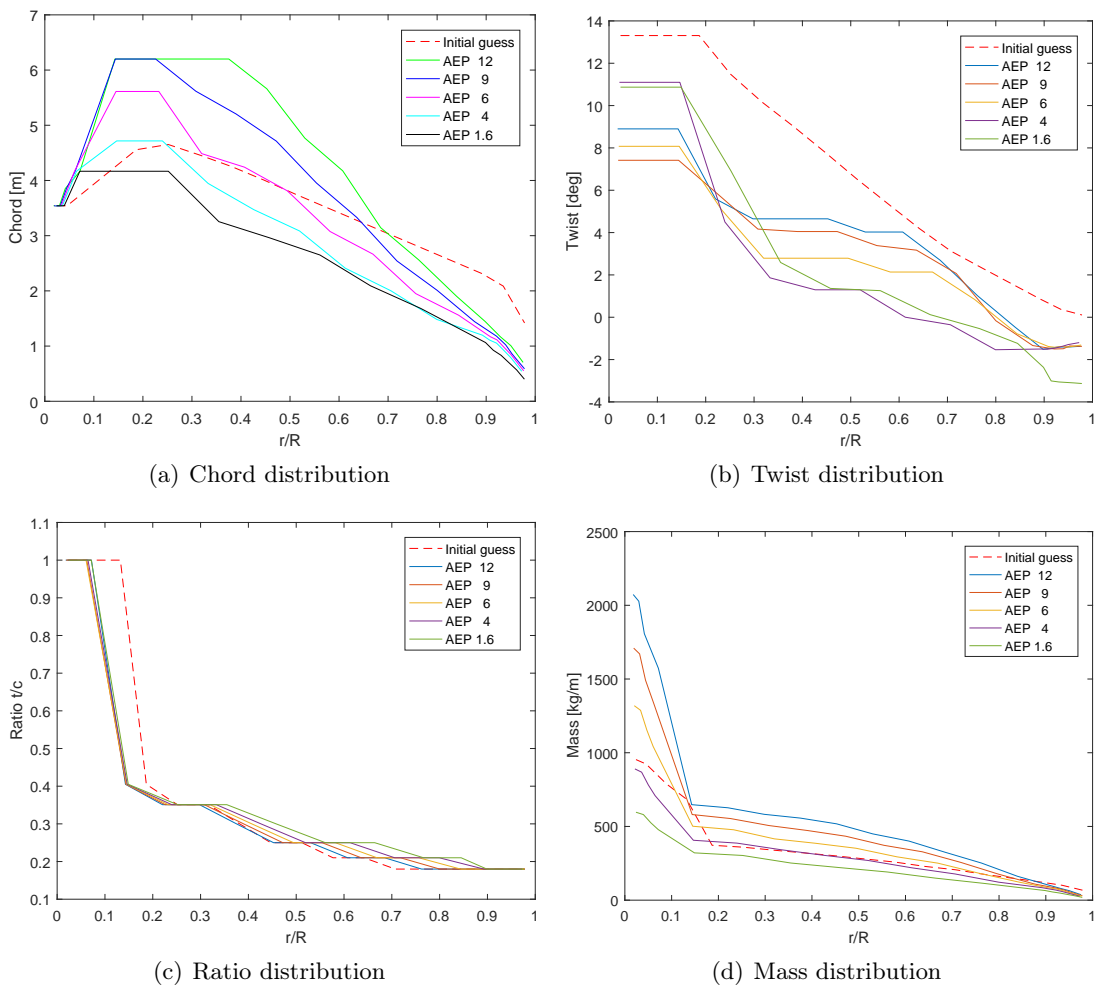


Figure 8.10: *Blade planform for case study II*

Examining the blade planform reveals in most cases the same behaviour as previously seen from case study I. The chord increases dramatically with increased weight factor and blade length as expected. The twist on the other hand shows a behaviour that is not fully understood as the twist at the root is not in a sequential order with the weight factors as seen before. The twist at the root is higher for the shorter blades than the longer blades which might just be a result of the blade length. The ratio shows very comparable behaviour for all cases. Finally, the mass shows the expected tendency as the blade mass is drastically bigger for the longer blades.

The stiffness distribution for the optimization study is presented in figure 8.11, where flapwise stiffness and edgewise stiffness are shown in figures 8.11(a) and 8.11(b) respectively.

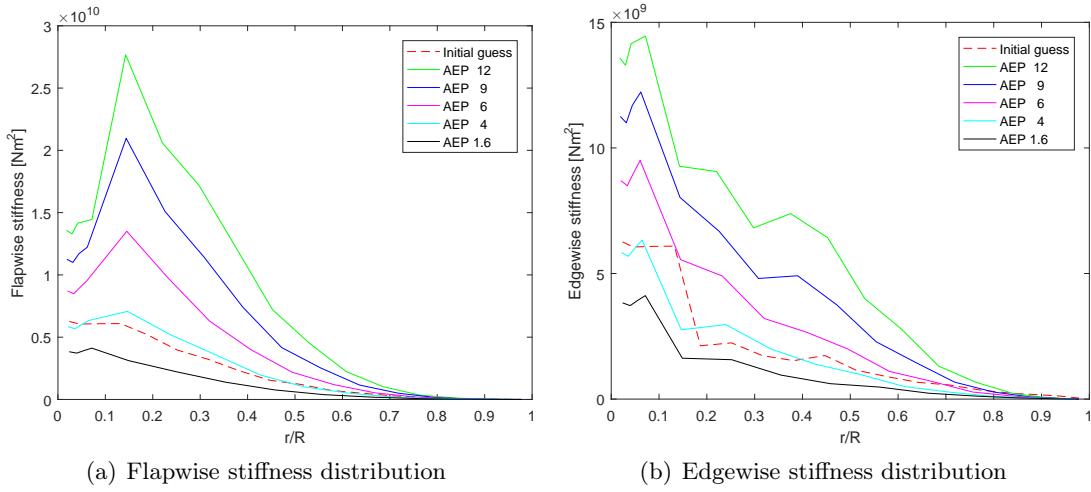


Figure 8.11: *Stiffness distribution for case study II*

The stiffness grows rapidly with increased length for the high weight factor. This effect can especially be seen for the flapwise stiffness as a lot of stiffness is needed to fulfill the displacement requirement which is the same for all of the designs. Consequently, the blades grow dramatically in weight as seen on figure 8.10(d).

Constraints and bounds: The majority of the active bounds and constraints presented in case study I are also active for case study II but there are few additional active in this study. The upper bounds of both the spar cap width and the element length are much more frequently active around the mid region of the blade. The edgewise strain constraint is always active in at least one cross section around the mid range of the blade. The chord upper bound are as previously always active for the circular cross section and additionally are the upper bounds active at max chord for the two highest weight factors.

8.5 Case Study III.

The aim of this case study is to present a purely *AEP* driven optimization of a blade. Thus, this case study imitate a design situation where the maximum allowable weight of the blade is

known, and the AEP needs to be maximized. In order to perform this additional constraint on the mass of the blade is set to be equal with the initial design, while the length of the blade is set to be unconstrained. Two optimizations have been executed using the control setup 1 and control setup 2. Comparison of main performance measures and rated conditions for the optimization study is presented in table 8.11.

	Initial guess	Control setup 2	Control setup 1
Length [m]	63.000	69.499	63.974
AEP [GWh]	18.209	20.202	19.332
Mass [ton]	21.162	21.163	21.163
AEP/Mass [GWh/ton]	0.860	0.954	0.914
Rated rotor speed [RPM]	12.100	12.100	16.419
Rated wind speed [m/s]	10.891	10.284	10.335
Rated tip speed [m/s]	79.828	88.063	109.997

Table 8.11: *Comparison of performance measures and rated conditions for case study III*

It can be seen that the total length of the blades increase using both control set up for the optimization. Using control set up 2 the blade length increases with 6.5 meters while using for control setup 1 the blade length increases with 1 meter. The AEP in both cases are increased significantly. In case of control set up 2 the increase is more than in case of the set up 1, hence the $AEP/Mass$ is increased for set up 2 is more, as well. The rated rotor speed became 16.419 rpm by using the control set up 1 thus the rated tip speed constraint became active. The reason for the big difference between the two optimization result is believed to be that using control setup1 the rotational speed becomes uncontrolled, and purely design dependent. Other studies that have been conducted by using control setup 1 this unboundedness became a problem and the optimization behaved chaotic. Hence, it is concluded that it is necessary to have a good initial design for the optimization using set up 1.

Blade planform for the optimization study is presented in figure 8.12, where chord distribution is shown in figure 8.12(a), twist distribution in figure 8.12(b), ratio distribution in figure 8.12(c) and mass distribution in figure 8.12(d).

Looking at the blade planform plots in figure 8.12 there are obvious differences seen between the design for the chord and the twist while the mass and the ratio distribution is relatively unchanged between designs. The chord distribution in the first third of the blade increases for the blade using set up 1. The reason for that is by having large chord at the root the blade can capture the lower wind speeds. For set up 2 the chord distribution decreases hence the length of the blade can increase, by having longer blade the swept area becomes larger hence the AEP increases. The biggest difference can be seen in the twist of the different results at the root region. For set up 1 the upper bounds of the twist at the root are active. As the tendency for AEP driven designs is to increase the twist to obtain more power for a greater range of wind speeds.

The stiffness distribution for the optimization study is presented in figure 8.13, where flapwise stiffness and edgewise stiffness are shown in figures 8.13(a) and 8.13(b) respectively.

It can be seen in figure 8.13 that for set up 2 design both flapwise and edgewise stiffnesses are distributed along the length similarly to the initial design. For set up 1 both flapwise

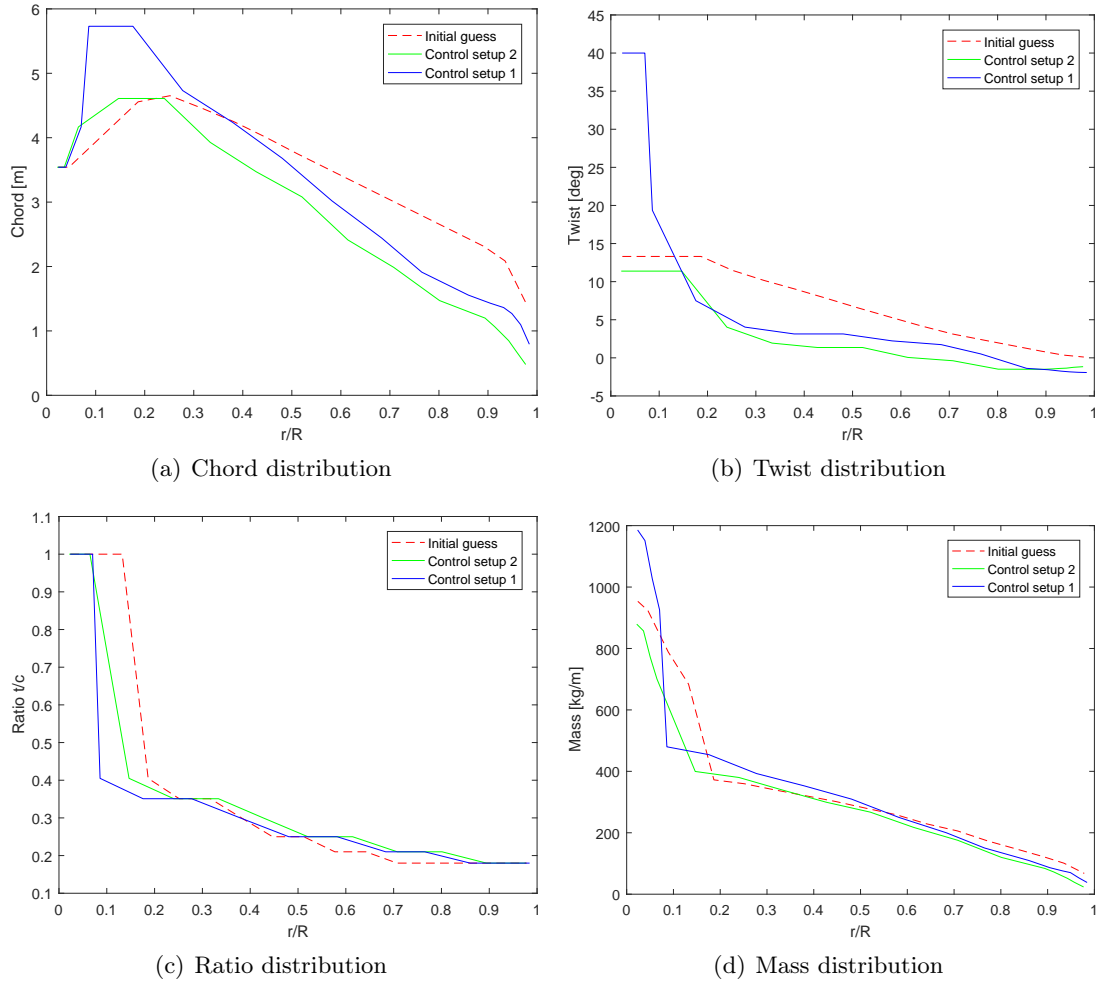


Figure 8.12: Blade planform for case study III

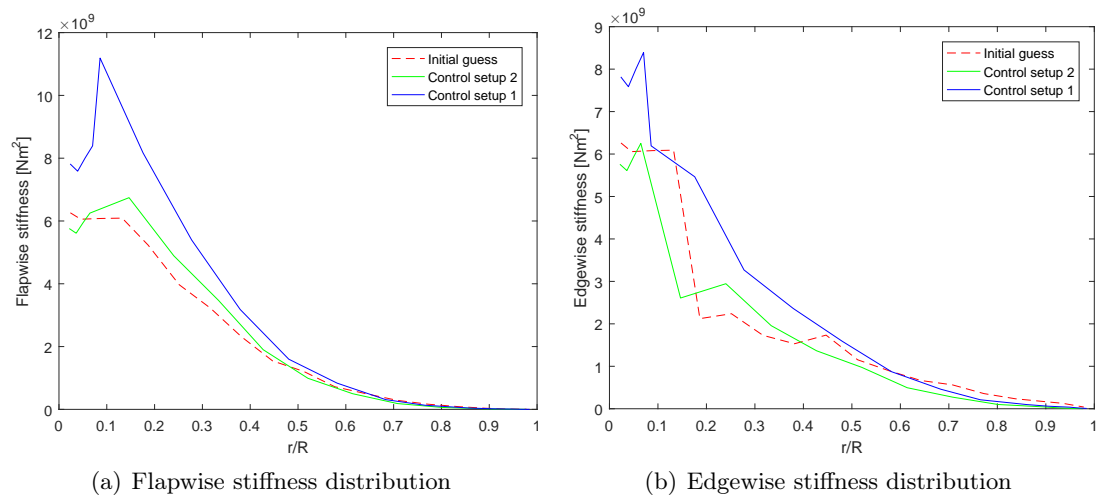


Figure 8.13: Stiffness distribution for case study III

and edgewise stiffnesses are higher and the first 4 root cross sections are strain driven. The constraints of the width and height of the spar caps are active in every cross section except the last one.

8.6 Case Study IV.

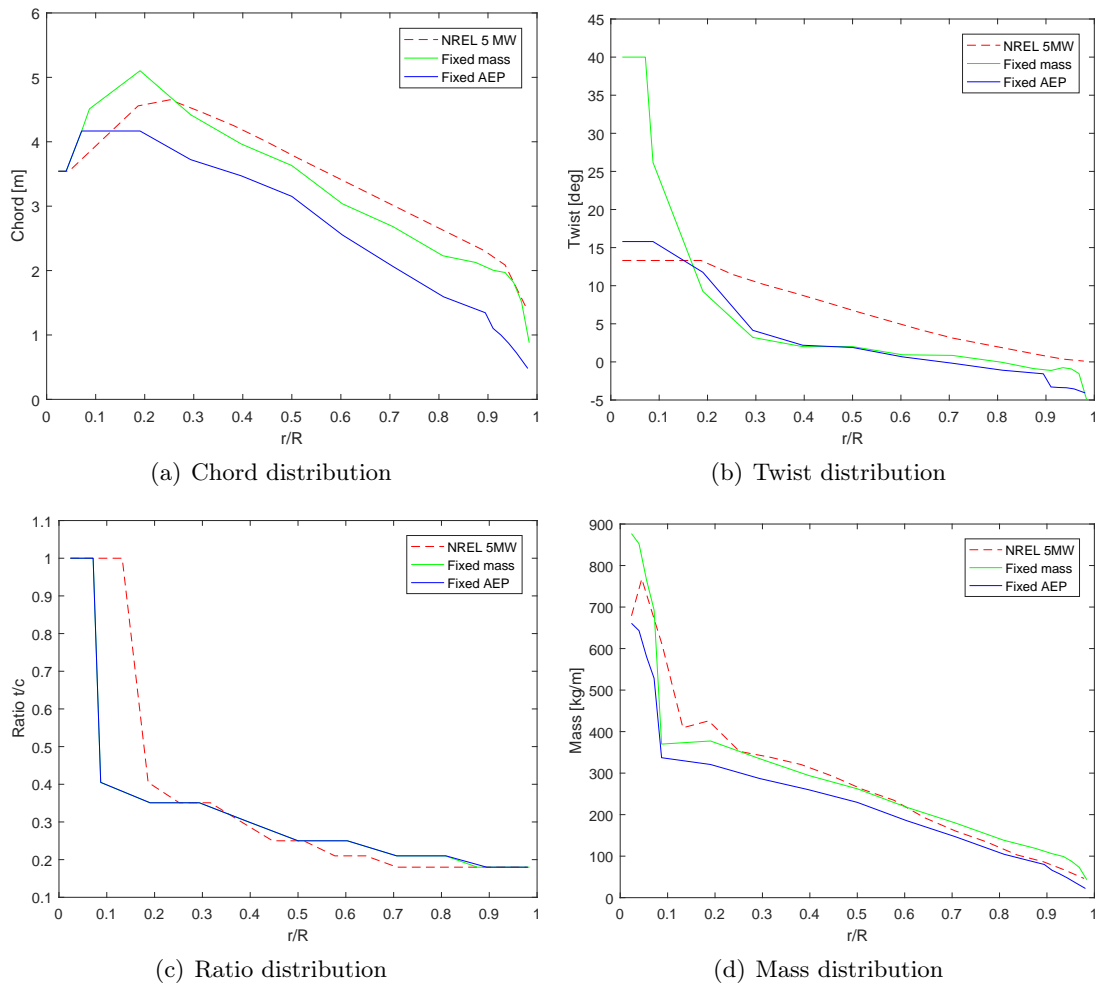
The aim of this study is to make a comparison with the NREL 5MW turbine for two different cases. In the first case the *Mass* is constraint to be the same as the 17.74 ton NREL 5 MW blade. Thus, pure aerodynamic optimization is performed for this given *Mass*. In the second case the *AEP* is constraint to be 18.209 GWh as the NREL 5 MW turbine. Thus, pure structural optimization is conducted for the given *AEP*. The designs are also constraint to have the same blade length as the NREL blade as well as fulfilling the previously defined bounds and constraints as defined by the baseline turbine. It is worth mentioning again that detailed design of inner geometry, materials, safety factors and constraints was not available for the NREL 5 MW which makes this comparison more difficult. Comparison of main performance measures and rated conditions for the optimization study are presented in table 8.12.

	NREL 5 MW	Fixed <i>Mass</i>	Fixed <i>AEP</i>
Length [m]	63.000	63.000	63.000
AEP [GWh]	18.209	18.927	18.209
Mass [ton]	17.740	17.740	14.795
AEP/Mass [GWh/ton]	1.006	1.067	1.231
Rated rotor speed [RPM]	12.100	12.100	12.100
Rated wind speed [m/s]	11.400	10.696	11.386
Rated tip speed [m/s]	79.828	79.828	79.828

Table 8.12: *Comparison of performance measures and rated conditions for case study IV*

From table 8.12 it is seen that a 4% increase of *AEP* was achieved for the fixed mass case while 17% reduction *Mass* of mass was achieved for the fixed *AEP* case. Blade planform for the optimization study is presented in figure 8.14, where chord distribution is shown in figure 8.14(a), twist distribution in figure 8.14(b), ratio distribution in figure 8.14(c) and mass distribution in figure 8.14(d).

Looking at the chord distribution it can be seen that the chord in the root region deviates for both the fixed *Mass* case and the fixed *AEP* study. This is the same behaviour as has been seen before as the circular elements are reduced to the lower bounds as they do not contribute anything to the *AEP*. The root could have been more strictly bounded to match with the root of the NREL blade. Furthermore, the upper bounds of the chord of the circular cross sections are also active for both cases. The fixed *Mass* case shows a very good correlation during the mid section while the fixed *AEP* case has considerably chord values as it is driven towards *Mass* minimization. The twist for the fixed *Mass* case shows a huge variation in the root region and the upper bound of the twist is active as it tries to capture more power at lower wind speeds as well. The fixed *AEP* case shows much more similarity for the twist but has rather big deviation in the mid region. The ratio for both cases are identical and

Figure 8.14: *Blade planform for case study IV*

do mainly deviate from the NREL ratio as the circular elements at the root are on the lower boundary of the element length. The mass shows remarkably good correlation between all cases though the fixed *AEP* case has the obviously lowest mass.

The stiffness distribution for the optimization study is presented in figure 8.15, where flapwise stiffness and edgewise stiffness are shown in figures 8.15(a) and 8.15(b) respectively.

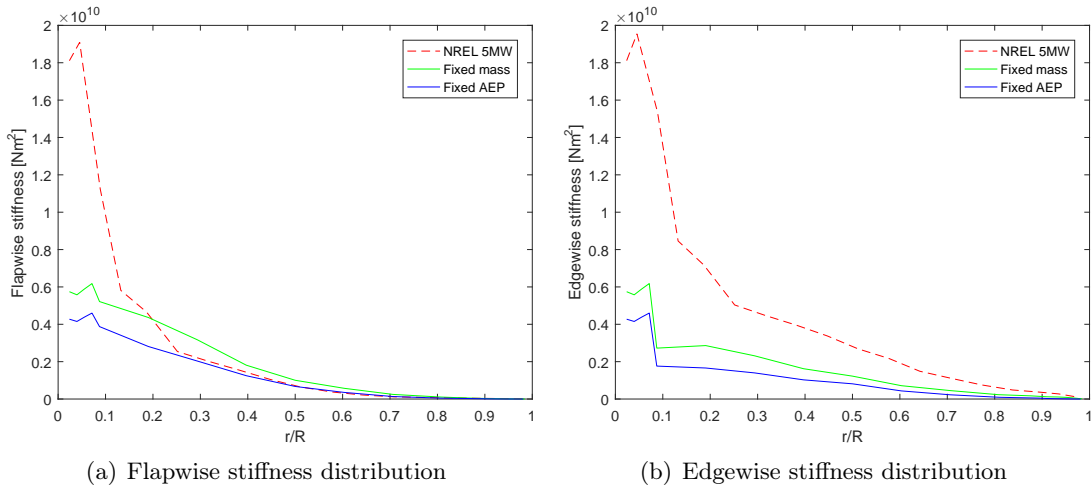
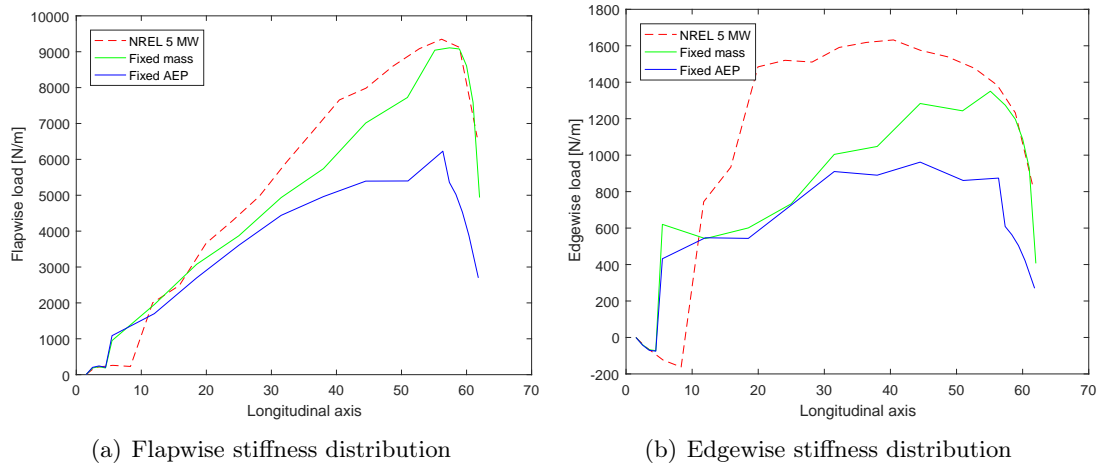


Figure 8.15: *Stiffness distribution for case study IV*

It can be seen from the stiffness comparison that the NREL 5 MW has way larger stiffness for both flapwise and edgewise stiffness. This difference can originate from few reasons. One possible reason might originate from the fact that the material properties are unknown so the NREL blade might be using materials with higher elastic modulus then implemented in BladeOpt. Another possibility is that the ellipsoidal cross sections in BladeOpt are not capable of accurately capturing the true airfoil stiffness properties but it is part of future work to develop scaling methods between the ellipsoidal cross sections and true airfoils. It can also be seen that the difference is bigger for the edgewise stiffness. Possible reason for that is that the implemented method of taking edgewise strains into account was not performing as expected as has been seen from the previous study cases where the edge reinforcements are always on the allowable lower boundaries and not really driving anything in the design. The flapwise stiffness has less deviation as it is driven by the deflection design. Loads on the blades in this study are shown in figure 8.16, where flapwise loads are shown in figure 8.16(a) and edgewise loads in figure 8.16(b).

The loads on the blades are lower for both of the BladeOpt designs. Those lower loads might partially account for the lower required stiffness of the design and especially in the fixed *AEP* case where the loads are considerably lower. The results for the overall comparison between the BladeOpt designs and the NREL 5 MW blade are considered acceptable based the amount of unknowns with regards to the detailed NREL design and constraints enforced on it in the design phase to be able to more accurately.

Figure 8.16: *Load distribution distribution for case study IV*

CHAPTER 9

CONCLUSION

This report has presented the second phase of a one year project which aimed to automate the initial design phase for horizontal axis wind turbines. Through this report the development of a multi objective blade optimization tool, called BladeOpt has been presented. This program lies on the foundation of the IMHAWT initial modelling of HAWT tool, which has been developed in the first phase of the project.

To improve and generalize the analysis tool two control strategies have been implemented and the structural computations have been changed towards to finite element method. Validation studies have been conducted to validate the new analyses. The implemented analyses have been validated against the published 5MW wind turbine from National Renewable Energy Laboratory. The results obtained by the general control methods have shown good correlation with the published results. The finite element computations have been validated through an example study, where the deflection, strain and eigen frequencies obtained by the BladeOpt structural analysis tool have been compared with the results obtained by ANSYS. Even though the results did show some large differences, the finite element calculations have been assumed to be valid, knowing the beam elements used in BladeOpt and ANSYS are based on different assumptions. To validate the aerodynamic and structural computations the NREL 5MW wind turbine have been implemented and the tip displacements have been compared with published information for different operational conditions. For 18 implemented elements the displacement results have shown slightly stiff. Using more elements to discretize the blade the displacements converged to the published results. The over and under shooting at rated and high wind conditions still presented as it has been experienced in the validation of the IMHAWT.

Moving over to finite element formulations have made it possible to utilize direct differentiation method to obtain the gradients of the structural analysis. The gradients of the aerodynamic calculations have been obtained by forward difference method. The obtained structural gradients have been validated against finite difference method, while studies have been conducted to ensure the perturbation size is appropriate for the forward difference gradients. To execute the optimization an SLP algorithm has been implemented.

The objective of the blade optimization has been defined from two component, the mass of the blade and the annual energy production of the turbine. The two objectives have been combined such that different weight factors can be set on the each component. Several constraints have been implemented both on the structural responses and the design variables of the blade. The capabilities of BladeOpt have been presented through four case studies with the aim to imitate real life design problems.

From the results obtained through the different case studies it can be concluded that setting different weight factors on the *AEP* and the *Mass* the direction of the optimization can be controlled. As it was expected having large weight factor on *AEP* leads to *AEP* driven optimization while using low weight factor leads to structural driven optimization. The control strategy one did not provide stable optimization process, hence most of the results have been generated by using the control strategy 2.

It can be generally concluded that the BladeOpt is capable to handle the multi objective

optimization of a wind turbine blade subjected to several various constraints. To conclude the accuracy of the optimization tool the obtained results needs to be further analysed and compared to existing wind turbine blades. It is believed that introducing more constraints on both response functions and design variables the results obtained by BladeOpt can be used as initial models of horizontal axis wind turbines.

CHAPTER 10

FUTURE WORK

This report concludes the second phase of a one year university project, where an initial blade optimization and design tool has been developed. During the first phase a design tool has been developed that utilizes simple computational methods to capture the overall behaviour of wind turbines. In the second phase an optimization tool has been developed, that utilizes gradient based optimization method to optimize wind turbine blades with respect to various implemented constraints. Although many studies has been conducted to present the capabilities of the optimization tool, there are several opportunities for improvements before the tool can be used as an initial step of wind turbine blade designs. The following main areas are suggested as future improvements:

Implementing flapwise fatigue: To get optimized results that are closer to a final blade design flapwise fatigue analysis needs to be implemented in the optimization. For gradient based optimization, the frequency based method presented in [Tibaldi et al., 2016] could be a good direction to look further into.

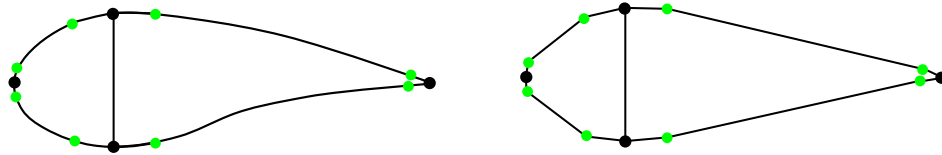
Dealing with BEM non-convergence: Introducing the third convergence criteria the optimization will not converge for some cases. To deal with this problem, whenever only the third criteria is not satisfied, the bounds on the corresponding design variables could be automatically relaxed, hence providing wider design space.

Airfoil selection Apart from the chosen design variables it would also be a possibility to implement airfoil types and material types as design variables. That would require the work of collecting a selection of airfoils and materials to make available to BladeOpt to choose from and do some sort of mapping of the properties being used such that the gradients of altering those variables can be computed during optimization.

Improving cross sectional analyses: To get optimized results that are closer to a final blade design the ellipsoid cross sections needs to be "translated" to airfoil sections.

This can be done by e.g. using pre-defined correction factors within the optimization algorithm which would correct for the differences in cross sectional properties between ellipsoids and airfoils. This would potentially lead to an optimization result which can be easily adapted to real cross sections during the next steps in blade design.

Other possibility is to directly implement a polygon cross section in the optimization which is closer to an airfoil. The outer shape of the airfoil section can be defined by equations, depending on the type of the airfoil and the chord length, which can be represented by lines see figure 10.1. In figure 10.1 the black dots are automatically defined by the equations. The lines could be further divided into small segments (marked by green dots). The segments could be approximated by straight lines. In the optimization segments could have different material thickness. The cross sectional properties could be approximated by adding the rectangular parts defined by the line segments and the thickness of the materials.

Figure 10.1: *A possible cross section*

Implementing the cost of the blade: A possible development is to include estimations for the cost of the blade, which would be dependent on the mass and on other parameters such as, surface area, cost of materials etc. Including estimations for other parts of the turbine would be a step in the direction of reducing the levelized cost of energy produced by wind turbines.

Refining element length: Some study results show that the length of the elements can often exceed the defined upper or lower boundaries. Modifying the boundaries of the element length could lead non convergence in the BEM or highly distorted elements in the FEM analysis, hence refinement of the elements could be necessary. An idea is to stop the optimization whenever the upper or lower boundaries are exceeded and refine the too long elements or remove the too short once. After interpolation of the new design variables of the newly introduced cross sections the optimization could be restarted using the last iteration as an initial design.

Implementing merit functions: Based on Sørensen et al. [2014] and Sørensen and Lund [2015] merit function approach could be implemented to establish a more robust SLP implementation. Using this approach the linearized problem presented to the optimizer would be feasible at all times. In the aforementioned research works the objective and constraint functions are reformulated into merit functions, furthermore a convergence filter is defined and the adaptive move limit strategy is utilized. The convergence filter is described as a line search method which utilizes the current design value, a linear prediction, and possible constraint violations in determining if a new design update should be accepted Lund [2017a].

In one hand all the aforementioned development directions would improve the capabilities of BladeOpt and would lead to a more realistic optimized design. On the other hand these improvements would lead to significantly increasing computational time, hence this trade-off need to be investigated. Obtaining additional results and comparing them to existing designs could show other areas for improvements of BladeOpt.

BIBLIOGRAPHY

- Arora, J. S. (2012). *Introduction to Optimum Design*. Elsevier. ISBN 978-0-12-381375-6. 61, 73
- Bitsche, D. R. (2014). Airfoil2becas: A preprocessor for the cross-section analysis software becas. Technical report, DTU Wind Energy. 6, 115
- Blasques, J. P. (2014). Multi-material topology optimization of laminated composite beams with eigenfrequency constraints. *Composite Structures* 111, 45–55. 6, 115
- Blasques, J. P. and R. D. Bitsche (2014). An efficient and accurate method for computation of energy release rates in beam structures with longitudinal cracks. *Engineering Fracture Mechanics* 133, 56–69. 6, 115
- Blasques, J. P., R. D. Bitsche, V. Fedorov, and B. S. Lazarov (2014). Accuracy of an efficient framework for structural analysis of wind turbine blades. *Wind Energy* 19, 1603–1621. 6, 115
- Blasques, J. P. and M. Stolpe (2012). Multi-material topology optimization of laminated composite beam cross sections. *Composite Structures* 94, 3278–3289. 6, 115
- Cai, X., J. Zhu, P. Pan, and R. Gu (2012). Structural optimization design of horizontal-axis wind turbine blades using a particle swarm optimization algorithm and finite element method. *Energies* 5, 4683–4696. 2
- Choi, K. K. and N.-H. Kim (2005). *Structural Sensitivity Analysis and Optimization* 2. Springer-Verlag New York. ISBN: 978-0-387-23336-9. 27
- Cook, R. D., D. S. Malkus, M. E. Plesha, and R. J. Witt (2002). *Concepts and applications of finite element analysis*. John Wiley & Sons. ISBN 978-81-265-1336-9. 45, 51, 123, 125, 127
- Domnica, S. M., C. Ioan, and T. Ionut (2016). Structural optimization of composite from wind turbine blades with horizontal axis using finite element analysis. *Procedia Technology* 22, 726–733. 2
- Dykes, K., A. Platt, Y. Guo, A. Ning, R. King, T. Parsons, D. Petch, P. Veers, and B. Resor (2014). Effect of tip-speed constraints on the optimized design of a wind turbine. Technical report, National Renewable Energy Laboratory. 33
- Fuglsang, P., C. Bak, J. G. Schepers, B. Bulder, T. T. Cockerill, P. Claiden, A. Olesen, and R. van Rossen (2002). Site-specific design optimization of wind turbines. *Wind Energy* 5, 261–279. 32
- GWEC (2017). Global wind report - annual market update 2016. Technical report, Global Wind Energy Council. 3

BIBLIOGRAPHY

- Hansen, M. O. L. (2008). *Aerodynamics of wind turbines* (Second ed.). Earthscan. ISBN: 978-1-84407-438-9. 5, 9, 13, 14, 17, 24, 37, 40, 41
- Harman, J. (2013). Capital expenditure must be reduced in offshore wind. Technical report, Wind Energy Update. 13
- Haselbach, P. U., R. D. Bitsche, and K. Branner (2016). The effects of delaminations on local buckling in wind turbine blades. *Renewable Energy* 85, 295–305. 33
- IEC (2005). *International Standard - IEC 61400-1* (Third ed.). International Electrotechnical Commission. 24, 34, 35
- IRENA (2012). Renewable energy technologies: Cost analysis series. Technical report, International Renewable Energy Agency. 13
- James, A. B. and D. G. Seamus (2015). Redefining the design objectives of large offshore wind turbine rotors. *Wind Energy* 18, 835–850. 13
- Johansen, J., H. Aa. Madsen, M. Gaunaa, C. Bak, and N. N. Sørensen (2009). Design of a wind turbine rotor for maximum aerodynamic efficiency. *Wind Energy* 12, 261–273. 2
- Jonkman, J., S. Butterfield, W. Musial, and G. Scott (2005). Definition of a 5-mw reference wind turbine for offshore system development. Technical report, National Renewable Energy Laboratory. 4, 6, 10, 11, 24, 25, 37, 42, 59, 81, 111, 112
- Krohn, S., P.-E. Morthorst, and S. Awerbuch (2009). The economics of wind energy. Technical report, European Wind Energy Association. 13
- Lund, E. (2017a). SLP with matlab examples. Additional Lecture Notes for Optimization Course, Aalborg University. 76, 106
- Lund, E. (2017b). Structural optimization. Lecture Notes for Optimization Course, Aalborg University. 62, 66, 68
- Maalawi, K. Y. and M. A. Badr (2003). A practical approach for selecting optimum wind rotors. *Renewable Energy* 28, 803–822. 2
- Mandell, J. F. and D. D. Samborsky (1997). Doe/msu composite material fatigue database: Test methods, materials, and analysis. Technical report, Sandia National Laboratories. 32
- Matlab (2017). Matlab documentation eigs. <https://se.mathworks.com/help/matlab/ref/eigs.html>. Accessed:07-05-2017. 54
- Molnar, D. and H. Albertsson (2016). *Initial Modelling of Horizontal Axis Wind Turbines*. Semester project at the Department of Mechanical and Manufacturing Engineering, Aalborg University. 1, 4, 41, 42, 60, 113, 115, 116, 117, 118
- Moriarty, P. J. and A. C. Hansen (2005). Aerodyn theory manual. Technical report, National Renewable Energy Laboratory. 6, 37, 40, 44
- Munson, B. R., T. H. Okiishi, W. W. Huebsch, and A. P. Rothmayer (2015). *Fluid Mechanics* (Seventh ed.). John Wiley & Sons. ISBN: 978-81-265-5343-3. 37

- Ning, A., R. Damiani, and P. Moriarty (2013). Objectives and constraints for wind turbine optimization. Technical report, American Institute of Aeronautics and Astronautics. 32
- NREL (2010). Harp-opt user's guide. Technical report, National Renewable Energy Laboratory. 2
- Olesen, J. F. (2009). FEM for civil engineering. Lecture material from DTU Department of Civil Engineering. 45, 46
- Overgaard, L. (2016). Failure modes in composite materials. Lecture Notes for Mechanics of Composite Materials and Structures, Aalborg University. 31
- Resor, R. B. (2013). Definition of a 5mw/61.5m wind turbine blade reference model. Technical report, Sandia National Laboratories. 6
- Sandia (2003). Cost study for large wind turbine blades: Windpact blade system design studies. Technical report, Sandia National Laboratories. SAND2003-1428. 2
- Siemens (2012). Siemens unveils 75m wind turbine blade. *Reinforced Plastics* 56, 30–31. 26
- Sieros, G., P. Chaviaropoulos, J. D. Sørensen, B. H. Bulder, and P. Jamieson (2012). Upscaling wind turbines: theoretical and practical aspects and their impact on the cost of energy. *Wind Energy* 15, 3–17. 13
- Sørensen, J. N. (2016). *General Momentum Theory for Horizontal Axis Wind Turbines*. Springer. ISBN: 978-3-319-22113-7. 2, 13, 41
- Sørensen, R. and E. Lund (2015). Thickness filters for gradient based multi-material and thickness optimization of laminated composite structures. *Structural and Multidisciplinary Optimization* 52, 227–250. 106
- Sørensen, S. N., R. Sørensen, and E. Lund (2014). DMTO – a method for discrete material and thickness optimization of laminated composite structures. *Structural and Multidisciplinary Optimization* 50, 25–47. 106
- Thomsen, O. T. (2009). Sandwich materials for wind turbine blades — present and future. *Journal of Sandwich Structures and Materials* 11, 7–26. 24, 25
- Tibaldi, C., L. C. Henriksen, M. H. Hansen, and C. Bak (2016). Wind turbine fatigue damage evaluation based on a linear model and a spectral method. *Wind Energy* 19, 1289–1306. 32, 105
- Troen, I. and E. L. Petersen (1989). *European Wind Atlas*. Risø National Laboratory. ISBN: 87-550-1482-8. 14, 16, 42
- Zahle, F., C. Tibaldi, D. R. Verelst, C. Bak, R. Bitsche, and J. P. Blasques (2015). Aeroelastic optimization of a 10 MW wind turbine. *American Institute of Aeronautics and Astronautics* 1, 201–223. 32, 33, 86, 88
- Zhu, J., X. Cai, R. Gu, and J. Zhu (2017). Multi-objective aerodynamic and structural optimization of horizontal-axis wind turbine blades. *Energies* 10, 101. 2

APPENDIX A

NREL 5 MW WIND TURBINE

This chapter contains additional information about the NREL 5MW wind turbine blade, being presented in chapter 2.

A.1 NREL Blade Cross Sectional Properties

In Jonkman et al. [2005], the blade structural properties are defined by distributed parameters in 49 cross sections. The 49 cross sectional properties are presented in table A.1.

For validation of the analysis module, 17 airfoils presented in chapter 2 table 2.2 are used to obtain the aerodynamic loads and power output of the blade. To obtain the structural responses the same 17 cross sections are used plus the first and the last defined cross sections from table A.1. To obtain the cross sectional properties of the 19 cross section from the 49 defined cross section linear interpolation is used. The interpolated structural properties of the 19 cross sections are summarized in table A.2.

Rotor Radius (m)	Mass (kg/m)	Flappwise stiffness ($10^6 Nm^2$)	Edgewise stiffness ($10^6 Nm^2$)	Torsional stiffness ($10^6 Nm^2$)	Axial stiffness ($10^6 N$)
0	678.935	18110.00	18113.60	5564.40	9729.48
2.87	767.8931	19096.66	19548.46	5358.64	10669.09
5.60	607.2506	11232.90	15351.53	3593.89	7833.85
8.33	409.2246	5814.81	8459.76	1694.12	4668.99
11.75	425.8460	4654.55	7172.87	846.71	4165.35
15.85	352.3202	2541.91	5033.88	332.23	3127.33
19.95	338.1669	2022.32	4469.23	256.97	2581.90
24.05	320.5603	1549.02	3952.48	196.13	2111.37
28.15	293.0209	1051.39	3377.82	138.95	1587.63
32.25	260.5556	640.99	2684.91	77.86	1135.39
36.35	234.8319	378.23	2169.80	53.70	870.25
40.45	192.4596	215.09	1486.32	32.77	607.40
44.55	160.5537	118.04	1114.18	19.89	500.91
48.65	134.4795	83.95	755.91	15.44	353.49
52.75	102.8078	54.97	484.94	8.53	227.00
56.17	86.8658	37.17	375.79	6.61	171.59
58.90	67.7688	25.44	273.53	5.17	96.94
61.63	46.2577	7.88	87.27	2.23	30.85
63.00	10.319	0.17	5.01	0.19	3.53

Table A.2: *NREL blade 19 distributed cross sectional properties*

APPENDIX A. NREL 5 MW WIND TURBINE

Radius [m]	StrcTwst [°]	BMassDen [kg/m^3]	FlpStff [Nm^2]	EdgStff [Nm^2]	GJStff [Nm^2]	EASStff [N]
1.5	13.308	678.935	1.81E+10	1.81E+10	5.56E+09	9.73E+09
1.7	13.308	678.935	1.81E+10	1.81E+10	5.56E+09	9.73E+09
2.7	13.308	773.363	1.94E+10	1.96E+10	5.43E+09	1.08E+10
3.7	13.308	740.55	1.75E+10	1.95E+10	4.99E+09	1.01E+10
4.7	13.308	740.042	1.53E+10	1.98E+10	4.67E+09	9.87E+09
5.7	13.308	592.496	1.08E+10	1.49E+10	3.47E+09	7.61E+09
6.7	13.308	450.275	7.23E+09	1.02E+10	2.32E+09	5.49E+09
7.7	13.308	424.054	6.31E+09	9.14E+09	1.91E+09	4.97E+09
8.7	13.308	400.638	5.53E+09	8.06E+09	1.57E+09	4.49E+09
9.7	13.308	382.062	4.98E+09	6.88E+09	1.16E+09	4.03E+09
10.7	13.308	399.655	4.94E+09	7.01E+09	1.00E+09	4.04E+09
11.7	13.308	426.321	4.69E+09	7.17E+09	8.56E+08	4.17E+09
12.7	13.181	416.82	3.95E+09	7.27E+09	6.72E+08	4.08E+09
13.7	12.848	406.186	3.39E+09	7.08E+09	5.47E+08	4.09E+09
14.7	12.192	381.42	2.93E+09	6.24E+09	4.49E+08	3.67E+09
15.7	11.561	352.822	2.57E+09	5.05E+09	3.36E+08	3.15E+09
16.7	11.072	349.477	2.39E+09	4.95E+09	3.11E+08	3.01E+09
17.7	10.792	346.538	2.27E+09	4.81E+09	2.92E+08	2.88E+09
19.7	10.232	339.333	2.05E+09	4.50E+09	2.61E+08	2.61E+09
21.7	9.672	330.004	1.83E+09	4.24E+09	2.29E+08	2.36E+09
23.7	9.11	321.99	1.59E+09	4.00E+09	2.01E+08	2.15E+09
25.7	8.534	313.82	1.36E+09	3.75E+09	1.74E+08	1.94E+09
27.7	7.932	294.734	1.10E+09	3.45E+09	1.44E+08	1.63E+09
29.7	7.321	287.12	8.76E+08	3.14E+09	1.20E+08	1.43E+09
31.7	6.711	263.343	6.81E+08	2.73E+09	8.12E+07	1.17E+09
33.7	6.122	253.207	5.35E+08	2.55E+09	6.91E+07	1.05E+09
35.7	5.546	241.666	4.09E+08	2.33E+09	5.75E+07	9.23E+08
37.7	4.971	220.638	3.15E+08	1.83E+09	4.59E+07	7.61E+08
39.7	4.401	200.293	2.39E+08	1.58E+09	3.60E+07	6.48E+08
41.7	3.834	179.404	1.76E+08	1.32E+09	2.74E+07	5.40E+08
43.7	3.332	165.094	1.26E+08	1.18E+09	2.09E+07	5.31E+08
45.7	2.89	154.411	1.07E+08	1.02E+09	1.85E+07	4.60E+08
47.7	2.503	138.935	9.09E+07	7.98E+08	1.63E+07	3.76E+08
49.7	2.116	129.555	7.63E+07	7.10E+08	1.45E+07	3.29E+08
51.7	1.73	107.264	6.11E+07	5.18E+08	9.07E+06	2.44E+08
53.7	1.342	98.776	4.95E+07	4.55E+08	8.06E+06	2.12E+08
55.7	0.954	90.248	3.94E+07	3.95E+08	7.08E+06	1.82E+08
56.7	0.76	83.001	3.47E+07	3.54E+08	6.09E+06	1.60E+08
57.7	0.574	72.906	3.04E+07	3.05E+08	5.75E+06	1.09E+08
58.7	0.404	68.772	2.65E+07	2.81E+08	5.33E+06	1.00E+08
59.2	0.319	66.264	2.38E+07	2.62E+08	4.94E+06	9.22E+07
59.7	0.253	59.34	1.96E+07	1.59E+08	4.24E+06	6.32E+07
60.2	0.216	55.914	1.60E+07	1.38E+08	3.66E+06	5.33E+07
60.7	0.178	52.484	1.28E+07	1.19E+08	3.13E+06	4.45E+07
61.2	0.14	49.114	1.01E+07	1.02E+08	2.64E+06	3.69E+07
61.7	0.101	45.818	7.55E+06	8.51E+07	2.17E+06	2.99E+07
62.2	0.062	41.669	4.60E+06	6.43E+07	1.58E+06	2.13E+07
62.7	0.023	11.453	2.50E+05	6.61E+06	2.50E+05	4.85E+06
63	0	10.319	1.70E+05	5.01E+06	1.90E+05	3.53E+06

Table A.1: *NREL 5 MW blade distributed structural properties [Jonkman et al., 2005]*

APPENDIX B

CROSS SECTIONAL ANALYSES

This appendix chapter presents the calculation of the cross sectional properties and contains the cross sectional validation material.

B.1 Cross sectional calculation

This section presents the summary of the cross sectional calculations implemented in BladeOpt. The main computations have been developed in the phase one of this project and presented by Molnar and Albertsson [2016]. In phase two of the project the cross sectional calculations have been slightly modified in order to fit more to an actual wind turbine blade cross section. In figure B.1, the cross section implemented in BladeOpt is presented with the parameters used for describing the inner geometry of a cross section. Beside the 8 inner geometry parameters the chord C and the (t/c) ratio is necessary to be known to obtain the cross sectional parameters.

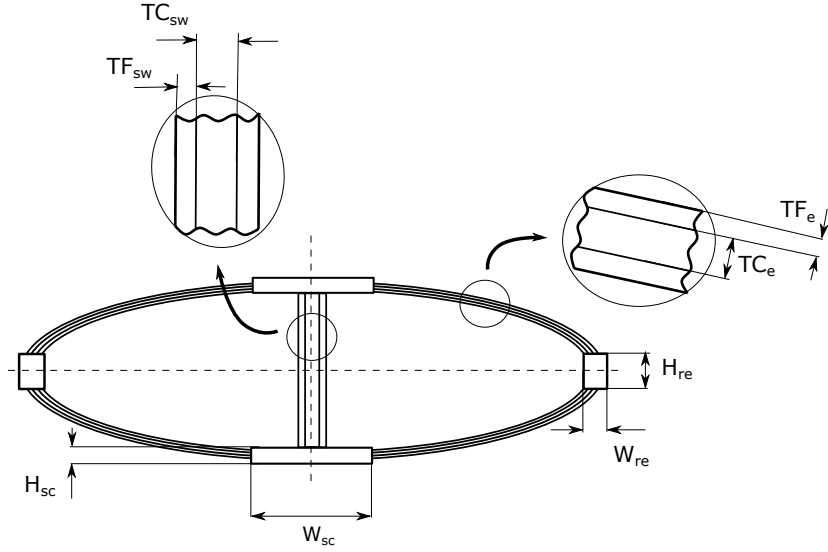


Figure B.1: *Inner geometry of cross sections*

To utilize simple computational methods, the cross section is built from 3 elliptical and 7 rectangular parts. The main difference in this cross section compared to the one used in Molnar and Albertsson [2016] is that the spar caps and edge reinforcements are moved further away from the center, hence the rectangular parts cover parts from ellipses. Hence extra mass and extra stiffness is introduced in the cross section, this needs to take into account when translating the above presented cross section to an actual airfoil with composite lay ups in the further steps of the development.

The cross sectional calculations are presented by two example computations, one for the spar caps and one for the outer ellipse. In this study it is assumed that only the ellipses contribute to the torsional stiffness, hence the torsional stiffness computation is only shown

to the ellipse.

B.1.1 Cross sectional computation of the spar caps

The area of the spar caps are calculated as:

$$A_{SparCap} = 2W_{SC}H_{SC} \quad (B.1)$$

The flapwise moment of inertia is calculated as:

$$I_{SparCap_z} = 2 \left(\frac{W_{SC}H_{SC}^3}{12} + W_{SC} \cdot H_{SC} \left(\frac{c}{2}ratio - \frac{H_{SC}}{2} \right)^2 \right) \quad (B.2)$$

where ratio presents the thickness chord ratio of the airfoil. The edgewise moment of inertia is calculated as:

$$I_{SparCap_y} = 2 \left(\frac{W_{SC}^3H_{SC}}{12} \right) \quad (B.3)$$

To calculate the mass, axial and flapwise and the edgewise stiffness (B.1), (B.1) - (B.3) need to be multiplied by the density ρ and the Youngs modulus E , respectively. The same methodology is applied to calculate the stiffness and mass of the edge reinforcements.

B.1.2 Cross sectional computation of the ellipse

The area of the outer ellipse is calculated as:

$$A_{Ellipse1} = \pi \frac{c}{4}ratio \quad (B.4)$$

The flapwise moment of inertia is calculated as:

$$I_{Ellipse_z} = \frac{\pi}{4} \frac{c}{2} \left(\frac{c}{2}ratio \right)^3 - \frac{\pi}{4} \left(\frac{c}{2} - TF_e \right) \left(\frac{c}{2}ratio - TF_e \right)^3 \quad (B.5)$$

The edgewise moment of inertia is calculated as:

$$I_{Ellipse_y} = \frac{\pi}{4} \left(\frac{c}{2} \right)^3 \frac{c}{2}ratio - \frac{\pi}{4} \left(\frac{c}{2} - TF_e \right)^3 \left(\frac{c}{2}ratio - TF_e \right) \quad (B.6)$$

The torsional moment of inertia is calculated as:

$$I_{Ellipse_x} = \frac{\pi \left(\frac{c}{2}\right)^3 \left(\frac{c}{2}ratio\right)^3}{\left(\frac{c}{2}\right)^2 + \left(\frac{c}{2}ratio\right)^2} - \frac{\pi \left(\frac{c}{2} - TF_e\right)^3 \left(\frac{c}{2}ratio - TF_e\right)^3}{\left(\frac{c}{2} - TF_e\right)^2 + \left(\frac{c}{2}ratio - TF_e\right)^2} \quad (B.7)$$

To calculate the mass, axial and flapwise and the edgewise stiffness moreover the torsional stiffness (B.4), (B.4) - (B.6) and (B.7) need to be multiplied by the density ρ , Youngs modulus E and torsional modulus G of the used material.

The same methodology is used to obtain the cross sectional parameters of the other ellipses. To obtain the final cross sectional properties the corresponding part results are summed.

B.2 Cross sectional stiffness validation

This section summarizes the results of validation of cross sectional stiffness computation, performed during phase one of this project and presented by Molnar and Albertsson [2016]. The cross sectional analysis tool within IMHAWT is referred to as ECSAT. Validation of the results from ECSAT is performed against stiffness computation obtained by the advanced cross sectional analysis tool BECAS [Blasques and Stolpe, 2012], [Blasques, 2014], [Blasques and Bitsche, 2014], [Blasques et al., 2014] and [Bitsche, 2014]. BECAS computes the full 6x6 stiffness matrix for the cross sections while ECSAT only computes the flapwise and edgewise stiffness. Therefore, validation is performed on flapwise and edgewise stiffness, referred to as EI_y and EI_z respectively, in the tables below. The material properties used for the validation are listed in table B.1. Those material properties along with laminate layup and fibre orientation are used to build up the cross sections in BECAS, since it is capable of handling laminate layup and fibre orientation.

	UD glass - epoxy	Balsa	Biax glass - epoxy
E1	45 GPa	0.0685 GPa	24 GPa
E2	10 GPa	0.0685 GPa	24 GPa
E3	10 GPa	0.005199 GPa	9 GPa
G12	5 Gpa	0.027845 Gpa	3.6 Gpa
G31	5 Gpa	0.206 Gpa	3.6 Gpa
G23	3.84615 Gpa	0.206 Gpa	3.5 Gpa
nu 12	0.3	0.23	0.11
nu 13	0.3	0.014	0.3
nu23	0.3	0.014	0.3
Rho	2000	220	1870 kg/m ³

Table B.1: *Material properties used for the validation [Molnar and Albertsson, 2016]*

ECSAT only uses the spanwise Young's modulus, E_x , for the computation, which in case of 0 deg fibre orientation is equal to $E1$. Both the UD glass and the Balsa are only used at 0 deg fibre orientation in the four validation cases while the Biax glass is used at 45 deg fibre orientation. Therefore, $E1$ from table B.1 can be used for both the UD glass and the Balsa.

On the other hand, the equivalent spanwise elastic modulus is needed to be computed for the Biax glass. The equivalent material properties for the Biax glass can be seen in table B.2.

Biax glass - epoxy	
Equivalent material properties at $\pm 45^\circ$	
E_x	11.37 Gpa
E_y	11.37 GPa
G_{xy}	10.81 Gpa
G_{zx}	2.92 Gpa
G_{yz}	2.92 Gpa
nu_{xy}	0.579
nu_{yx}	0.579

Table B.2: *Biax - equivalent material properties [Molnar and Albertsson, 2016]*

Four cases are validated, starting with a simple case and gradually increasing the complexity to make sure that all of the included building blocks of the ellipse are correctly computed.

Case 1 is an ellipse with only UD glass material. The validation is conducted for four geometries that are listed in table B.3.

		<i>Ellipse thickness</i> (mm)	166.67			276.67		
<i>c</i> (m)	<i>t</i> (m)	Stiffness (GPa)	ECSAT	BECAS	Diff (%)	ECSAT	BECAS	Diff (%)
5	3.75	EI_y	171.29	171.32	0.02	262.41	262.42	0.01
		EI_z	268.42	268.47	0.02	415.95	415.98	0.01
5	1.25	EI_y	13.63	13.63	0.01	18.28	18.28	0.00
		EI_z	139.36	139.38	0.01	210.48	210.49	0.01

Table B.3: *Results from ellipsoid cross section using UD composite material [Molnar and Albertsson, 2016]*

Case 2 is an ellipse with sandwich material with UD glass material in the face sheets and balsa core. The validation is conducted for four geometries that are listed in table B.4.

B.2. CROSS SECTIONAL STIFFNESS VALIDATION

		TF_e (mm)	41.67			69.44		
		TC_e (mm)	83.33			138.89		
c (m)	t (m)	Stiffness (GPa)	ECSAT	BECAS	Diff (%)	ECSAT	BECAS	Diff (%)
5	3.75	EI_y	85.89	85.89	0.00	131.94	131.94	0.01
		EI_z	134.55	134.55	0.00	208.92	208.92	0.01
5	1.25	EI_y	6.89	6.89	0.00	9.43	9.43	0.00
		EI_z	69.91	69.91	0.00	105.93	105.93	0.01

Table B.4: Results from ellipsoid sandwich structure using UD composite face material and Balsa core[Molnar and Albertsson, 2016]

Case 3 is an ellipse with sandwich material with Biax glass material at 45 deg fibre orientation in the face sheets and balsa core. The validation is conducted for four geometries that are listed in table B.5.

		TF_e (mm)	41.67			69.44		
		TC_e (mm)	83.33			138.89		
c (m)	t (m)	Stiffness (GPa)	ECSAT	BECAS	Diff (%)	ECSAT	BECAS	Diff (%)
5	5	EI_y	42.32	42.00	0.75	66.04	65.55	0.74
		EI_z	42.32	42.00	0.75	66.04	65.55	0.74
5	3.75	EI_y	21.78	21.72	0.28	33.46	33.36	0.29
		EI_z	34.12	34.04	0.24	52.98	52.86	0.23

Table B.5: Results from ellipsoid sandwich structure using $\pm 45^\circ$ biax composite material and Balsa core [Molnar and Albertsson, 2016]

Case 4 is an ellipse with sandwich material with Biax glass material at 45 deg fibre orientation in the face sheets and balsa core. Furthermore, spar caps and edge reinforcements with UD glass material have been added to the model. Finally, shear web from sandwich material has been added, with UD glass in the face sheets and balsa in the core. The validation was only validated for one geometry as it brought complications to built this cross section with BECAS. The geometry for the validation is seen in table B.6 and the results in B.7.

Ellipse	c	5 m
	t	2.5 m
	TF_e	0.01 m
	TC_e	0.02 m
Spar cap	W_{sc}	0.78 m
	H_{sc}	0.04 m
Shear web	TF_{sw}	0.02 m
	TC_{sw}	0.04 m
Edge Reinf.	H_{re}	0.39 m
	W_{re}	0.06 m

Table B.6: *The parameters of the geometry for case 4 [Molnar and Albertsson, 2016]*

	El _y (GPa)	El _z (GPa)
ECSAT	8.3	19.4
BECAS	8.7	19.1
Diff (%)	5	2

Table B.7: *Cross sectional stiffness results case 4 [Molnar and Albertsson, 2016]*

Final Conclusion from the examples above is that for all of the four test cases there was excellent agreement between the BECAS and the ECSAT results. The first three cases had close to zero percentage deviation between the two but in case 4 the deviation went up to 4%. This deviation has been explained by Molnar and Albertsson [2016] and is due to a slight difference of the geometry as the programs use different methods to make the cross sections. The bottom line is that the results show close to no deviation if the exact same geometries are being modelled.

APPENDIX C

BEM CORRECTIONS

The aim of this appendix chapter is to present the BEM correction factors that are implemented in BladeOpt.

C.1 BEM Correction Factors

In the past two decades many researches have been conducted to develop simple methods, that can correct the limitations of the BEM theory. These limitations mainly originate from the assumptions of the BEM. The correction factors are developed based on empirical and analytical approaches, hence to understand their effects the flow around a real wind turbine needs investigated.

The classical BEM theory assumes that the forces generated by the blades are constant within each annular element, which can be related to a turbine with infinite number of blades. For real wind turbines this assumption is invalid. As the flow passes the rotor plane the blades modify the direction and speed of the flow, generating vortices at the tip of the blade and in the wake. The vortices reduce the force at the tip region of the blade, hence the contribution to the power output from this region decreases. To consider these effects tip loss correction factor F_{tip} can be defined as:

$$F_{tip} = \frac{2}{\pi} \arccos \left(e^{-f} \right) \quad (C.1)$$

where exponent f :

$$f = \frac{B}{2} \frac{R - r}{r \sin \phi} \quad (C.2)$$

and R is the total length of the blade, while r is the radial position of the element. F_{tip} approaches zero as the radial position along the blade gets in the tip region. As the correction factor tends to zero the induced velocity raises, which results decreasing relative wind speed and angle of attack.

Similarly to the tip region of the blade, the flow direction and speed varies at the root region. This phenomenon originates from the flow passing the hub of the turbine. To consider the effects of hub shading hub loss correction factor F_{hub} can be defined as:

$$F_{hub} = \frac{2}{\pi} \arccos \left(e^{-f} \right) \quad (C.3)$$

where exponent f :

$$f = \frac{B}{2} \frac{r - R_{hub}}{r \sin \phi} \quad (C.4)$$

and R_{hub} denotes the radius of the hub. Similarly to the tip correction, F_{hub} tends to zero as the radial position along the blade approaches the root.

The total correction factor F can be obtained multiplying the tip correction factor F_{tip} by the hub correction factor F_{hub} , the total correction factor is implemented in the BladeOpt BEM algorithm using (4.8) and (4.9).

The classical BEM theory assumes that there is no flow between the annular elements. For highly loaded turbines $a \gtrsim a_c$, turbulence is generated in the wake. The free shear layer at the boundaries of the wake becomes unstable, hence eddies are formed, which transform more flow into the wake. Due to the entering flow, the turbulence further increases and the flow behind the rotor slows down. Resulting in continuous increase of the thrust on the rotor disk. In this case, the classical BEM theory becomes inaccurate, hence correction needs to be applied. a_c is defined as the induction factor where the turbine becomes highly loaded, the value of a_c depends on the chosen correction approach. In BladeOpt the value of a_c is equal with 0.2. For $a \leq a_c$ correction does not necessary to be applied, hence the a is calculated as until now. In case of $a \leq a_c$, the correction can be applied as:

$$a = \frac{1}{2} \left[2 + K(1 - 2a_c) - \sqrt{(K(1 - 2a_c))^2 + 4(Ka_c^2 - 1)} \right] \quad (C.5)$$

where

$$K = \frac{4F \sin^2 \phi}{\sigma C_n} \quad (C.6)$$

In BladeOpt the corrections for tip loss and hub loss correction factors, moreover the correction for highly loaded turbines are implemented. Other correction factors can be easily implemented in the further development process.

In figure C.1 the axial and tangential load distribution can be seen along the length of the blade for rated conditions of the turbine using 19 aerodynamically defined cross sections.

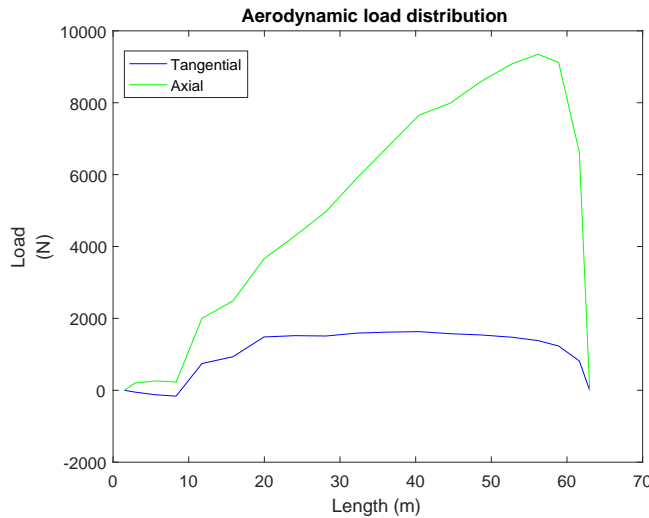


Figure C.1: *Aerodynamic load distribution*

It can be seen that the at the tip of the blade both the tangential and axial forces are zero, due to the applied tip correction. This phenomena can result small chord neat to the tip of the blade, in the optimization.

APPENDIX D

FEM FORMULATIONS

In this appendix chapter additional information is presented about the development of the beam finite elements.

D.1 Additional FEM formulation

The principle of virtual work states, that for any quasi static and admissible virtual displacement $\{\delta u\}$ from an equilibrium configuration, the increment of strain energy stored is equal to the increment of work done by body forces $\{F\}$ in the volume and surface tractions $\{\Phi\}$ on surface S [Cook et al., 2002].

$$\int \{\delta \epsilon\}^T \{\sigma\} dV = \int \{\delta u\}^T \{F\} dV + \int \{\delta u\}^T \{\Phi\} dS \quad (\text{D.1})$$

The displacements, $\{u\}$, hence the virtual displacements, $\{\delta u\}$, can be interpolated over an element as:

$$\{\tilde{u}\} = [N] \{d\} \quad (\text{D.2})$$

where $\{\tilde{u}\} = \{u_1 \ u_2 \ u_3 \ \theta_1 \ \theta_2 \ \theta_3\}^T$ and $\{d_e\} = [d_1 \ d_2 \ d_3 \ d_4 \ d_5 \ d_6 \ d_7 \ d_8 \ d_9 \ d_{10} \ d_{11} \ d_{12}]^T$. The shape functions $[N]$ are expressed for the 3-D beam element as follows:

$$N_1 = \frac{L-x}{L} \quad (\text{D.3})$$

$$N_2 = \frac{x}{L} \quad (\text{D.4})$$

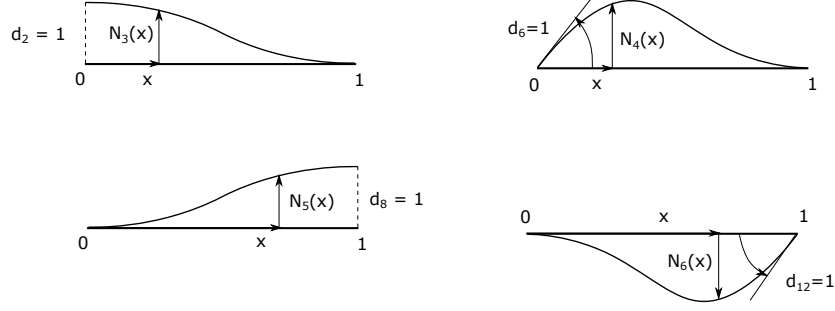
$$N_3 = 1 - 3\frac{x^2}{L^2} + 2\frac{x^3}{L^3} \quad (\text{D.5})$$

$$N_4 = x - \frac{2x^2}{L} + \frac{x^3}{L^2} \quad (\text{D.6})$$

$$N_5 = \frac{3x^2}{L^2} - \frac{2x^3}{L^3} \quad (\text{D.7})$$

$$N_6 = -\frac{x^2}{L} + \frac{x^3}{L^2} \quad (\text{D.8})$$

where x is the position within the element. The graphic representation of the deflection fields can be seen D.1.


 Figure D.1: *Interpolation shape functions for deflection modes*

The matrix form of the shape functions is constructed as:

$$[N] = \begin{bmatrix} N_1 & 0 & 0 & 0 & 0 & 0 & N_2 & 0 & 0 & 0 & 0 & 0 \\ 0 & N_3 & 0 & 0 & 0 & N_4 & 0 & N_5 & 0 & 0 & 0 & N_6 \\ 0 & 0 & N_3 & 0 & -N_4 & 0 & 0 & 0 & N_5 & 0 & -N_6 & 0 \\ 0 & 0 & 0 & N_1 & 0 & 0 & 0 & 0 & 0 & N_2 & 0 & 0 \\ -\frac{d}{dx}[0 & N_3 & 0 & 0 & 0 & N_4 & 0 & N_5 & 0 & 0 & 0 & N_6] \\ \frac{d}{dx}[0 & 0 & N_3 & 0 & -N_4 & 0 & 0 & 0 & N_5 & 0 & -N_6 & 0] \end{bmatrix} = \begin{bmatrix} [N_{u_x}] \\ [N_{u_y}] \\ [N_{u_z}] \\ [N_{\theta_x}] \\ [N_{\theta_y}] \\ [N_{\theta_z}] \end{bmatrix} \quad (D.9)$$

The strains $\{\epsilon\}$, hence the virtual strains $\{\delta\epsilon\}$, can be obtained as:

$$\{\tilde{\epsilon}\} = \begin{Bmatrix} \frac{du_1}{dx_1} \\ \frac{d\theta_1}{dx_1} \\ \frac{dx_1}{d^2u_3} \\ -\frac{dx_1^2}{d^2u_2} \\ \frac{d^2u_2}{dx_1^2} \end{Bmatrix} = \begin{bmatrix} \frac{d}{dx} [N_{u_x}] \\ \frac{d}{dx} [N_{\theta_x}] \\ \frac{dx}{d^2} [N_{u_z}] \\ -\frac{dx^2}{d^2} [N_{u_z}] \\ \frac{dx^2}{d^2} [N_{u_y}] \end{bmatrix} \{d_e\} = [B] \{d_e\} \quad (D.10)$$

where $[B]$ is the strain-displacement matrix. The strain-displacement functions are expressed as:

$$B_1 = \frac{1}{L} \quad (D.11)$$

$$B_2 = \frac{-6}{L^2} + \frac{12x}{L^3} \quad (D.12)$$

$$B_3 = \frac{4}{L} - \frac{6x}{L^2} \quad (D.13)$$

$$B_4 = \frac{2}{L} - \frac{6x}{L^2} \quad (D.14)$$

The $[B]$ matrix is constructed as:

$$[B] = \begin{bmatrix} -B_1 & 0 & 0 & 0 & 0 & 0 & B_1 & 0 & 0 & 0 & 0 & 0 \\ 0 & 0 & 0 & -B_1 & 0 & 0 & 0 & 0 & 0 & B_1 & 0 & 0 \\ 0 & 0 & -B_2 & 0 & -B_3 & 0 & 0 & 0 & B_2 & 0 & -B_4 & 0 \\ 0 & B_2 & 0 & 0 & 0 & -B_3 & 0 & -B_2 & 0 & 0 & 0 & -B_4 \end{bmatrix} \quad (D.15)$$

Substituting (D.2) and (D.10) into (D.1), the following expression is obtained:

$$\{\delta d\}^T \left(\int [B]^T [E] [B] dV \{d\} - \int [N]^T \{F\} dV - \int [N]^T \{\Phi\} dS \right) = 0 \quad (D.16)$$

where $\{F\}$ and $\{\Phi\}$ can be defined, as:

$$\{F\}_{6 \times 1} = \begin{Bmatrix} \{\tilde{q}\} \\ 0 \\ 0 \end{Bmatrix} \quad (D.17)$$

and

$$\{\Phi\}_{6 \times 1} = \begin{Bmatrix} \{\tilde{\sigma}\} \\ 0 \\ 0 \end{Bmatrix} \quad (D.18)$$

(D.16) is true for any admissible virtual displacement, for the equilibrium configuration. The element stiffness matrix $[k_e]$ can be defined as:

$$[k_e] = \int [B]^T [E] [B] dV \quad (D.19)$$

and the consistent element load vector, $\{r_e\}$, as:

$$\{r_e\} = \int [N]^T \{F\} dV + \int [N]^T \{\Phi\} dS \quad (D.20)$$

(D.16) yields to the governing equation of the static problem for a single element:

$$[k_e] \{d_e\} = \{r_e\} \quad (D.21)$$

The dynamic equilibrium equation is obtained by applying the equation of motion, which states that work done by externally applied loads must be equal to the sum of work absorbed by inertial, dissipative and internal forces for any admissible virtual displacement [Cook et al., 2002].

$$\int \{\delta \epsilon\}^T \{\sigma\} dV + \int \{\delta u\}^T \rho \{\ddot{u}\} dV + \int \{\delta u\}^T c \{\dot{u}\} dV \quad (D.22)$$

$$= \int \{\delta u\}^T \{F\} dV + \int \{\delta u\}^T \{\Phi\} dS + \int \{\delta u\}_i^T \{p\}_i \quad (D.23)$$

where $\{p\}_i$ and $\{\delta u\}_i$ represent prescribed concentrated loads and their corresponding virtual displacements at a total of n points, ρ represents mass density, and c is the damping parameter analogous to viscosity. Using FE discretization on the time and spatial variables, the following expressions are obtained:

$$\{u(x, t)\} = [N(x)] \{d(t)\} \quad (D.24)$$

$$\{\dot{u}(x, t)\} = [N(x)] \{\dot{d}(t)\} \quad (D.25)$$

$$\{\ddot{u}(x, t)\} = [N(x)] \{\ddot{d}(t)\} \quad (D.26)$$

Substituting (D.24) - (D.26), (D.2) and (D.10) into (D.23), the equilibrium equation is expressed as:

$$\begin{aligned} \{\delta d\}^T \left(\int \rho [N]^T [N] dV \{\ddot{d}\} + \int c [N]^T [N] dV \{\dot{d}\} + \right. \\ \left. \int [B]^T [E] [B] dV \{d\} - \int [N]^T \{F\} dV - \int [N]^T \{\Phi\} dS - \sigma \{p\}_i \right) = 0 \end{aligned} \quad (D.27)$$

The consistent element mass matrix $[m_e]$ can be defined as:

$$[m_e] = \int \rho [N]^T [N] dV \quad (D.28)$$

and the element damping matrix $[c_e]$ as:

$$[c_e] = \int c [N]^T [N] dV \quad (D.29)$$

(D.16) yields to the governing equation of the dynamic problem, for a single element in FE form:

$$[m_e] \{\ddot{d}_e\} + [c_e] \{\dot{d}_e\} + [k_e] \{d_e\} = \{r^{ext}\} \quad (D.30)$$

For an undamped, free vibration problem (D.30) can be simplified to:

$$[m_e] \{\ddot{d}_e\} + [k_e] \{d_e\} = \{0\} \quad (D.31)$$

D.1.1 Assembly of the Elements

To represent the whole structure, it is necessary to appropriately assemble the element matrices and vectors, taking into account that each node is a connector to which elements are attached. Assembly of element stiffness matrices and load terms produces a set of equations, stating that each node within the structure is in equilibrium [Cook et al., 2002]. Considering, that the nodes connected to more elements are represented in all of the corresponding element matrices, hence overlapping of the related coefficients will occur in the assembled matrices and vectors. The place of the element coefficients, in the global matrix, are determined based on the structure numbers of element nodes [Cook et al., 2002].

In case of a structure formed by two 3-D beam elements, the stiffness matrices for each element are 12x12 matrices. The global degrees of freedom is 18, thus the size of the global stiffness matrix needs to be 18x18. Since, the node 2 is represented in both elements, the global stiffness matrix is constructed by placing the element corresponding matrices in the diagonal positions of the global matrix and summing the coefficients of the common nodes, see figure D.2.

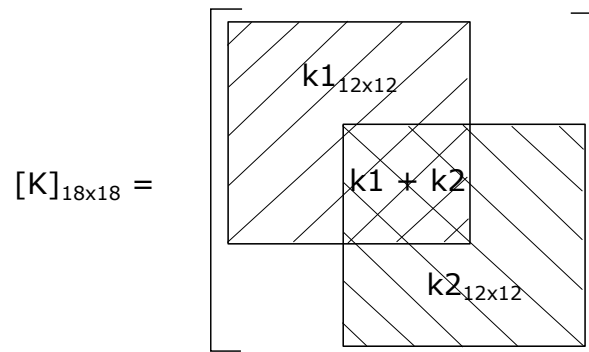


Figure D.2: *Assembly of global stiffness matrix*

The global mass matrix can be assembled similarly to the stiffness matrix. The global load vector is assembled by adding the consistent element load vectors for the corresponding nodes and the external loads applied directly to structure nodes.

APPENDIX E

BASELINE TURBINE

The aim of this chapter is to present additional information about the baseline design compare with the NREL 5MW wind turbine.

E.1 Mass

The mass of the NREL 5MW blade and the baseline design can be seen in figure E.1.

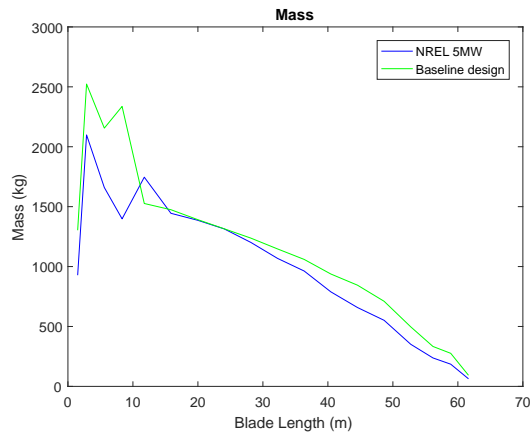


Figure E.1

E.2 Stiffness

The flapwise and edgewise stiffness of the NREL 5MW blade and the baseline design can be seen in figure E.2.

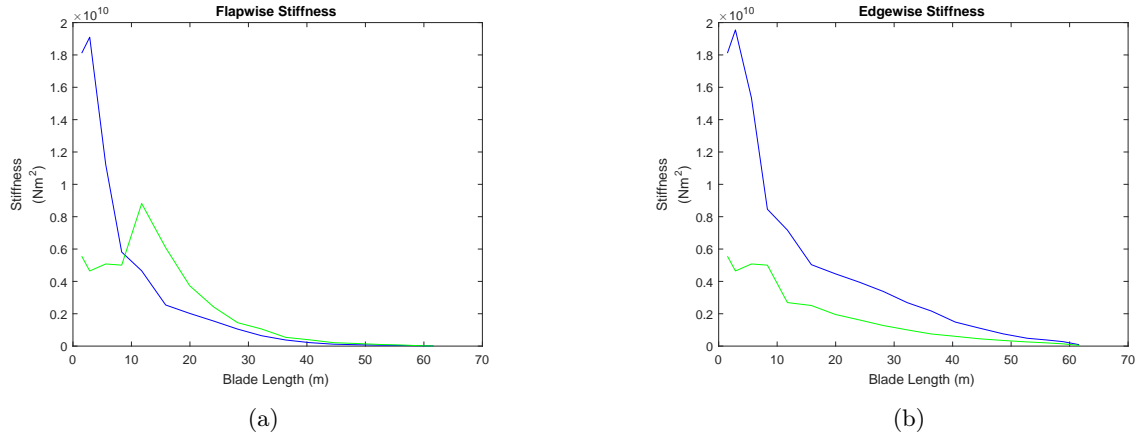


Figure E.2: *Stiffness comparison of the baseline and NREL designs*

E.3 Eigen Frequency

Comparison of the first three eigen frequencies of the baseline blade and the NREL 5MW blade.

Design	Eigen frequency 1 (Hz)	Eigen frequency 2 (Hz)	Eigen frequency 3 (Hz)
NREL 5MW blade	0.6993	1.0740	2.0205
Baseline blade	0.6219	0.7078	2.2386

Table E.1: *Comparison of the baseline design with NREL 5MW design*

APPENDIX F

CROSS SECTIONAL PLOTS

The aim of this chapter is to present the cross sections obtained in the case study IV set up b.

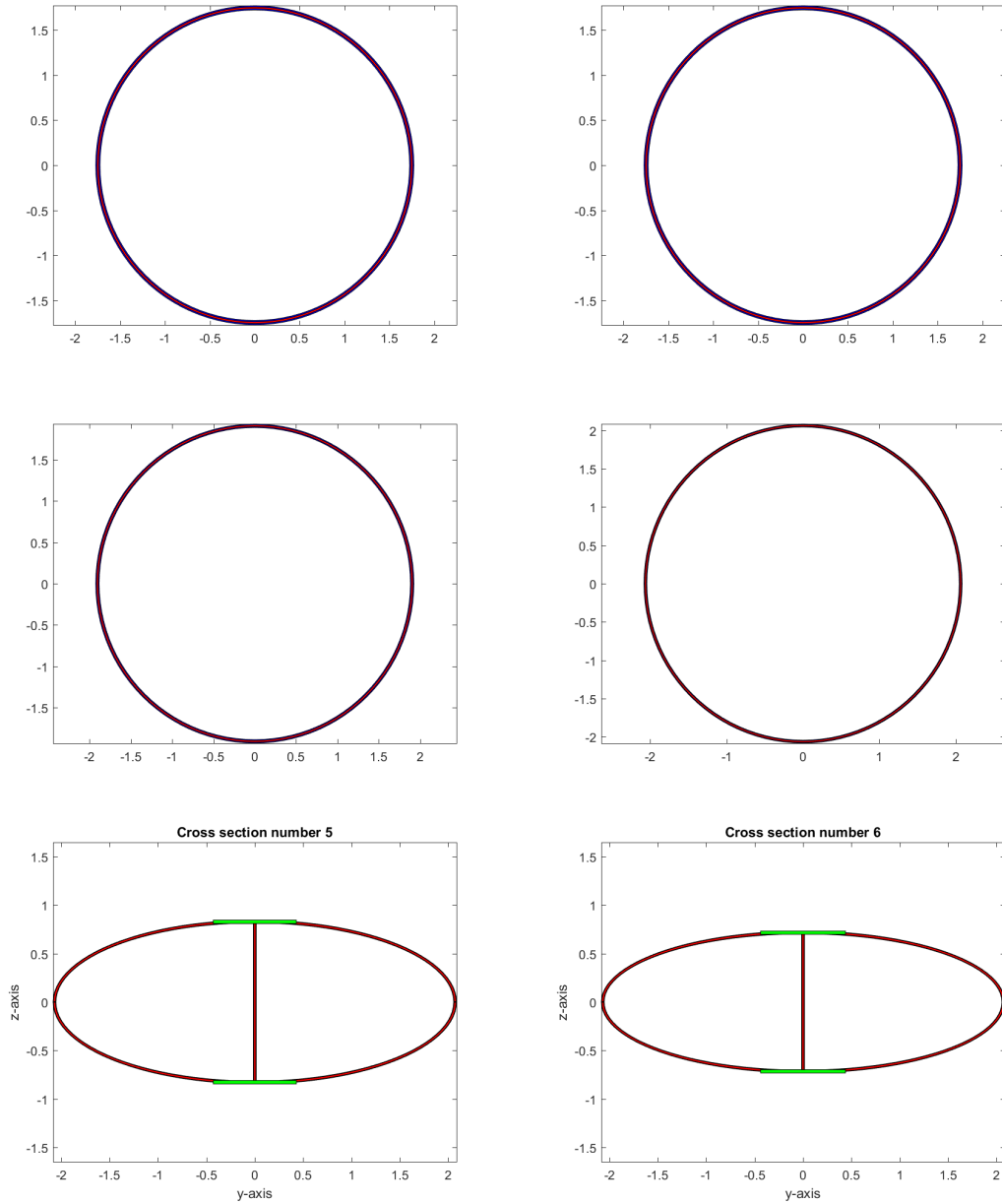


Figure F.1: *Cross section 1 - 6*

APPENDIX F. CROSS SECTIONAL PLOTS

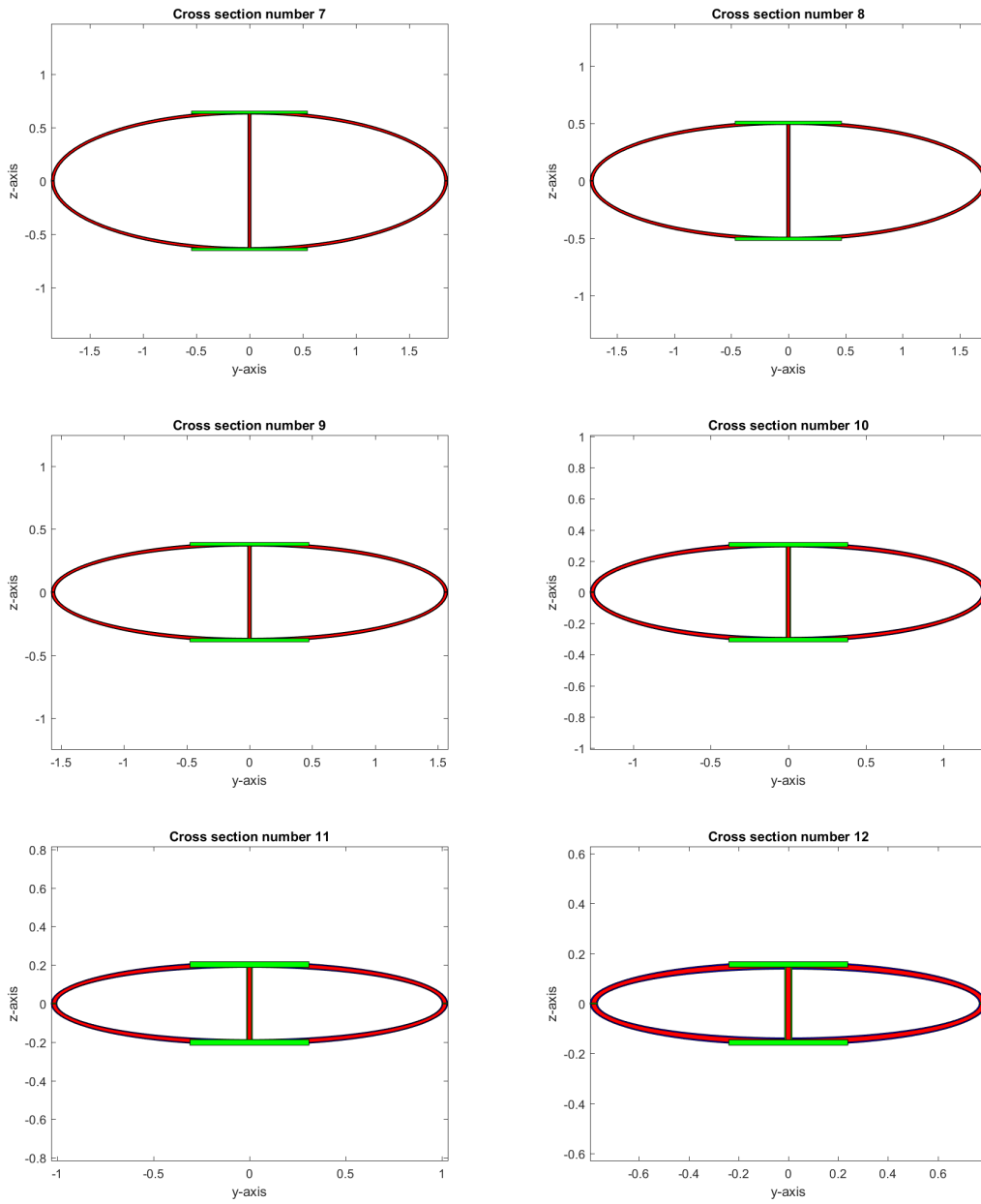


Figure F.2: *Cross section 7 - 12*

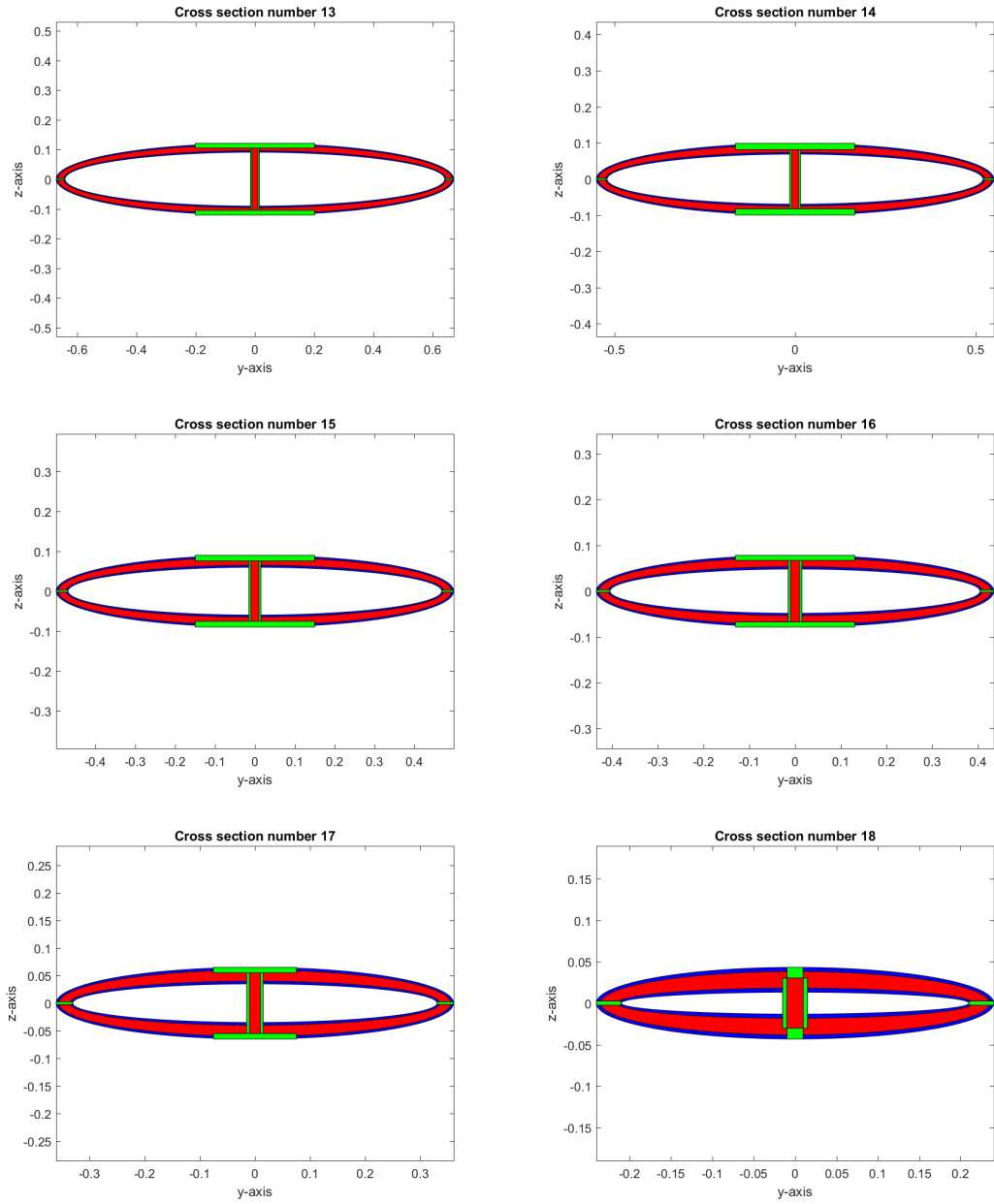


Figure F.3: *Cross section 13 - 18*